

**Plasma technology for lignocellulosic biomass conversion
toward an electrified biorefinery**

Journal:	<i>Green Chemistry</i>
Manuscript ID	GC-CRV-09-2021-003436.R2
Article Type:	Critical Review
Date Submitted by the Author:	05-Mar-2022
Complete List of Authors:	Dimitrakellis, Panagiotis; Univ. of Delaware, Chemical and Biomolecular Engineering Delikonstantis, Evangelos; University of Ghent, Chemical Engineering Stefanidis, Georgios; Ghent University Faculty of Engineering and Architecture, Chemical Engineering ; National Technical University of Athens, Chemical Engineering Vlachos, Dion; Univ. of Delaware, Chemical and Biomolecular Engineering

Plasma technology for lignocellulosic biomass conversion toward an electrified biorefinery

P. Dimitrakellis^{1,2†}, E. Delikonstantis^{3†}, G. D. Stefanidis^{3,4} and D. G. Vlachos^{1,2*}*

¹ Department of Chemical and Biomolecular Engineering, University of Delaware, Newark, DE 19716, USA

² Catalysis Center for Energy Innovation, Newark, DE 19716, USA

³ Laboratory for Chemical Technology, Ghent University; Tech Lane Ghent Science Park 125, Ghent, B-9052, Belgium

⁴ School of Chemical Engineering, National Technical University of Athens, Iroon Polytechniou 9, Athens, 15780, Greece

[†]These authors have equally contributed to this work

*Corresponding author. E-mail: vlachos@udel.edu ; gstefani@mail.ntua.gr

Abstract

Lignocellulosic biomass conversion to renewable, carbon-neutral materials, fuels, and chemicals is the cornerstone of the transition to a sustainable future bioeconomy. Green energy in the form of electricity needs to be coupled with or substitute conventional thermally driven processes to realize small-scale, economically viable and environmentally friendly biorefineries. Gas discharge plasmas enable the conversion of renewable electric energy, supplied in the form of an electric field, to chemical energy through the formation of a highly reactive environment that can induce several transformations related to agricultural waste valorization processes. Herein, we review the application of plasma technology to lignocellulosic biomass upgrade, aiming to provide the scientific background and technical challenges in this rapidly emerging research field. To bridge the gap between plasma science and biomass valorization technologies, we initially present the technical aspects of plasma reactors related to biomass processing and further discuss the advances in plasma processing for each biomass conversion technology, providing insights into the related plasma chemistry and interaction mechanisms. We first focus on the low and medium-temperature biomass conversion processes, including biomass pretreatment and delignification to promote enzyme or acid-catalyzed hydrolysis to sugars and biomass liquefaction using plasma electrolysis. Then we discuss the high and very high-temperature conversion processes, such as plasma-assisted pyrolysis and gasification to syngas and plasma application to tar removal, combustion, and vitrification. Overall, this review provides knowledge at the interface of plasma science and biomass conversion technology to promote the interaction between the individual communities, which is crucial for the further advancement of the field.

1. Introduction

Biomass holds promise as a widely available, inexpensive, and CO₂-neutral resource, suited for modern processes that supply power and fuels/chemicals.^{1–6} The term “biomass” refers to crops, residues, and other biological materials, which can serve as substitutes for fossil feedstock. Biomass feedstocks are highly diverse and can be classified to forest products (wood, logging residues, trees, and sawdust), biorenewable wastes (agricultural wastes, crop residues, and municipal organic wastes), industrial organic wastes (wastewater treatment sludge and waste cooking oil), energy crops (woody crops, grasses, starch crops, sugar crops, and oilseed crops), food crops (grains and oil crops), aquatic plants (algae and water weed), and animal byproducts (tallow, fish oil, and manure).

The lignocellulose structure comprises three organic polymers: cellulose (38-50%), hemicellulose (23-32%), and lignin (15-30%). Added to these are lipids, proteins, simple sugars, starches, inorganic substances, and water in different proportions. Biomass feedstocks significantly vary in physical and chemical properties, such as bulk density, moisture content, ash content, volatiles fraction, heating value, and chemical composition. These variations determine the sustainability of biomass as an energy and/or chemical building block. Various processes suitable for biomass valorization have been proposed, developed, and optimized.^{7,8} An overview of the up-to-date reported processes, ranging from trifling combustion to complex and advanced chemical routes, is given elsewhere.⁹ Advanced catalytic technologies are currently the spearhead of biomass conversion strategies.^{10,11,12,13,14,15,16}

The application of plasma technology for sustainable agriculture and bioeconomy has attracted significant interest during the last decade.^{17,18} In particular, non-thermal plasmas are currently investigated for the treatment of seeds to promote germination, watering of plants as alternative nitrogen-rich fertilizers, food disinfection, removal of pesticides, as well as waste water and soil remediation.^{19,20,21,22,23} Plasma technologies could be employed in both pre- and post-harvesting, with the processing of edible products attracting the most attention. In contrast, plasma processing of non-edible biomass from agricultural post-harvesting by-products or even food waste is often overlooked. Recently, plasma-assisted biomass valorization processes have been introduced as an alternative to the conventional thermally driven ones, featuring feedstock flexibility²⁴ due to the electricity-based heat source that is independent of the process chemistry, and the highly reactive environment,^{25,26} comprising charged species, chemically active molecules and radicals, heat, highly energetic photons and strong electric fields.^{27,28} Plasmas can be applied directly for biomass combustion for heat and/or electricity generation and thermochemical conversion to chemicals and fuels.²⁹ In the former case, plasma improves the flame characteristics, as further discussed in Section 3.2.4. In the latter case, plasma is placed upstream (plasma biomass pre-treatment) to enhance the formation of primary species and intermediates, which serve as precursors to other chemicals through conventional (bio)chemical downstream processing. Furthermore, it can facilitate the direct biomass conversion to targeted products, usually in a single step – this constitutes the core of biomass valorization (plasma biomass decomposition). Sometimes, plasma is also used downstream to upgrade biomass processing side-streams or destruct undesirable biomass residuals (plasma biomass post-treatment).

Collectively, plasma biomass valorization could be a promising alternative to converting lignocellulosic, non-edible biomass toward renewable added-value products. Plasma can enable gasification of biomass to syngas and hydrogen (very high-temperature process), pyrolysis and liquefaction to bio-oil and other products (high and medium-temperature processes), and pretreatment to promote enzymatic or chemical hydrolysis (low or ambient temperature processes), as depicted in Figure 1. Plasma is attractive only when the product value compensates for the actual costs, including the electricity price.^{30,31}

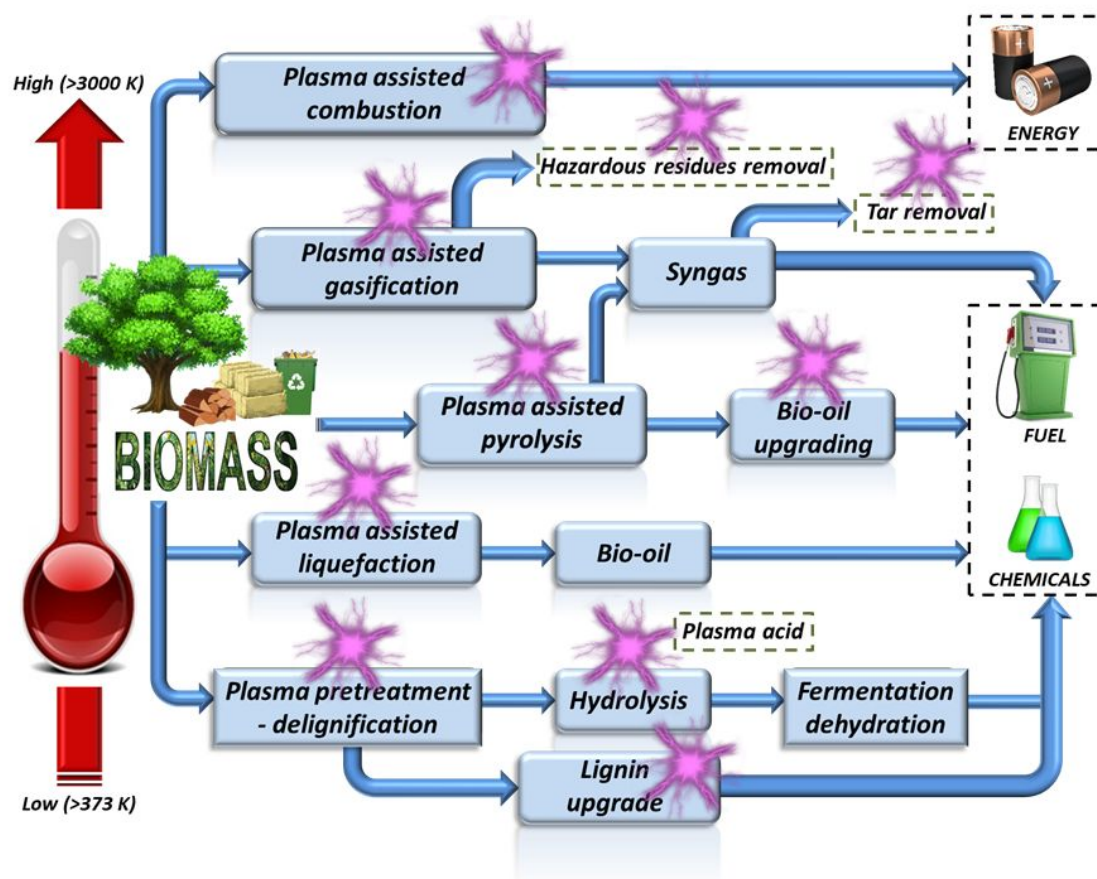


Figure 1: Plasma technology for biomass conversion to value-added products. The plasma cartoons signify the individual processes where plasma technology has been reported so far.

In this review, we aim to bridge the gap between plasma science and biomass conversion technologies to promote further research in the field. We provide an overview of the status and recent advances on plasma technologies proposed for biomass upgrading and shed light on the various plasma sources and reactor designs for such applications. Notably, we present the technical challenges and process characteristics of all plasma reactor configurations and power sources employed in relevant applications. Finally, we provide an empirical correlation for the capital investment-plasma gasifier capacity for preliminary techno-economic analysis for this emerging technology and propose future developments.

2. Plasma reactors

Plasma is widely known as the “fourth state of matter”. It is a partially ionized gas comprising electrons, ions, radicals, excited species, and neutral molecules. Although it is electrically conductive, its collective behavior is neutral (quasi-neutrality). Plasma is a gas discharge initiated when sufficient energy in the form of a strong electric field is applied to ionize the gas.³² The electrical energy may be supplied in the form of direct (DC) or alternative current (AC), radiofrequency (RF), and microwave power (MW).³³ Upon plasma initiation, numerous electron impact-induced chemical reactions occur

which, combined with secondary reactions among ions and neutral particles, form a mixture of highly reactive species in the plasma region.

Plasmas can be classified as thermal or non-thermal, based on the plasma species temperature. Thermal plasmas are close to thermodynamic equilibrium as the neutral gas and “heavy” particle temperatures approach the temperature of electrons, being as high as a few thousand degrees Kelvin ($T_e \approx T_g$). On the contrary, non-thermal plasmas are far from thermodynamic equilibrium as the energetic electrons exhibit temperatures greater than the neutral gas that can be even ambient temperature ($T_e \gg T_g$). Both plasmas are industrially relevant; however, their applications differ substantially. Another distinction is between low or atmospheric pressure plasmas, with the latter being more promising for “low-value” applications due to the lower equipment cost and potential for continuous processing.^{34,35,36}

Plasma exhibits specific characteristics (mean electron energy and density) and temperatures to promote the desirable chemistry. In view of low-power plasma ignition and stable operation, as well as fine tuning of plasma characteristics, different reactor configurations have been proposed. Furthermore, power supplies also play a key role in plasma properties and drive the process global energy efficiency. Herein, a detailed description of the main plasma reactor concepts and power supplies employed for biomass valorization is firstly presented, followed by a relative comparison of all (technically) possible combinations, with respect to operating conditions, energy efficiency and technical advantages and limitations.

2.1 Plasma reactor configurations

Although various plasma-based reactors have been developed to handle the biomass feedstock diversity (some already realized at industrial scale; discussed in Section 4), all plasma reactors can be electrode-based or electrodeless; however, a strict distinction with reference to reactor configuration is not always straightforward as hybrid configurations have been proposed as well.

Electrode-based plasma reactors

In electrode-based configurations targeted for elevated temperature applications, e.g., pyrolysis and gasification, the discharge is initially ignited between two metallic electrodes; one is in high-voltage (HV), while the other is grounded. When the gas flow is high, the plasma projects outwards as a plume, typically known as a jet or torch. The operating gas can be argon, helium, oxygen, nitrogen, air, or hydrogen. The plasma generated in electrode-based reactors can be non-transferred or transferred plasma jet, as shown in Figure 2a and Figure 2b, respectively. In non-transferred plasma jets, the electrodes are housed in the main reactor body where the plasma jet is initiated. In transferred plasma jets, only one electrode is hosted in the main reactor body (preferably the HV electrode) while the ground electrode, holding the biomass material, is placed outside, allowing the plume to elongate over a long distance.

In general, non-transferred plasma jets operate at lower gas flow rates and voltages as compared to the transferred ones. Moreover, they can be employed for any feedstock, irrespective of its characteristics (i.e., conductivity), unlike transferred ones. However, non-transferred plasma jets demand higher operating currents and attain comparatively a lower energy efficiency of 40-50%. In contrast, in transferred plasma jets, energy efficiency of 70-80% is normally reached and can be significantly higher should optimum conditions be applied.³⁷ Herein, energy efficiency is defined as

heating the plasma gas over the input power. Given high energy efficiencies, plasma jets are preferred for high-temperature processes. High-temperature plasma jets (torches), provide high heat fluxes and operate either in DC or AC mode. The flexible operation of plasma torches, which allows for ramping up or down the input electric power or the gas flow rate, enables the processing of diverse feedstock quantities and composition at a given temperature and pressure conditions.

Dielectric barrier discharges (DBDs) constitute a special configuration of electrode-based plasma reactors, targeted mostly for low-temperature processing in atmospheric pressure. DBDs comprise two electrodes, one in HV and one grounded, separated by at least one dielectric (barrier) material, e.g., quartz or alumina, in co-axial (Figure 2c), co-planar (Figure 4a) or hybrid geometries (Figure 5). The discharge is typically powered by an AC power unit and ignited between the electrodes in the form of multiple micro-discharges over the surface of the dielectric barrier, resulting in a more diffusive plasma regime. The high energy consumption along with low plasma energy densities lead to significantly low energy efficiencies, which is the most considerable drawback and the reason why DBD-like plasma jets (Figure 2d) have not been widely employed for high-temperature biomass conversion processes. Nonetheless, DBDs are suitable for low-temperature biomass treatment, such as delignification and hydrolysis, due to the highly reactive plasma medium. A detailed discussion on the working principle and specific reactor designs for low-temperature biomass treatment is given in Section 3.1.

In general, electrode-based plasma reactors allow operation in a wide range of gas flow rates and scale-up potential. However, the high voltage electrode vulnerability to moisture and other corrosive contaminants,³⁸ the impurities produced by the electrode erosion,³⁹ and the high parasitic load associated with low energy efficiency (only ~50% of the power input is utilized for the reaction)⁴⁰ are considered major technical limitations for broad utilization of the technology at commercial scale. Nevertheless, commercial applications have been released as reported in Section 4.

Electrodeless plasma reactors

In this configuration, the plasma is initiated upon applying an external electromagnetic field, either in radio-frequency (RF-driven plasma; Figure 2e) or microwaves (MW-imposed plasma; Figure 2f).⁴¹ Although no electrodes are required, nozzle-type injectors, through which the carrier gas is fed into the reactor volume, are employed to assist plasma ignition. The plasma is ignited at the edge (tip) of the nozzle, where the field is enhanced. Coaxially arranged injectors are usually used to co-feed auxiliary gases, serving either as plasma agents (i.e., noble gases) or plasma shielding; in the former case, easier plasma ignition is promoted through Penning ionization, while in the latter one, the plasma is limited in a confined core zone away from the reactor wall, preventing possible reactor failure. In an RF-driven configuration, an induction coil is placed around the reactor body, inducing an electric field. In MW-induced configuration, an electromagnetic field travels towards the reactor volume through the waveguide. In both cases, the applied field forces the free electrons to move and collide with the gas molecules, resulting in plasma ignition.

Electrodeless plasma reactors feature longer operating periods and require less maintenance due to the absence of electrodes. The latter also promotes higher process stability as plasma is not affected by contamination or erosion of the electrodes, and flexibility, i.e., biomass feedstock with diverse moisture content, whereas no intensive feedstock pretreatment, e.g., drying, is required. Also, less heat is dissipated in the surroundings by radiation and conduction, and plasmas of high energy and

active species densities are ignited⁴². Therefore, they are employed for high temperature biomass treatment.

On the downside, sub-atmospheric pressures and narrow gas flow operating windows are mostly preferred for stable plasma ignition and non-equilibrium operation,⁴³ while the design of such plasma reactors for solid organic material is rather complicated and challenging.

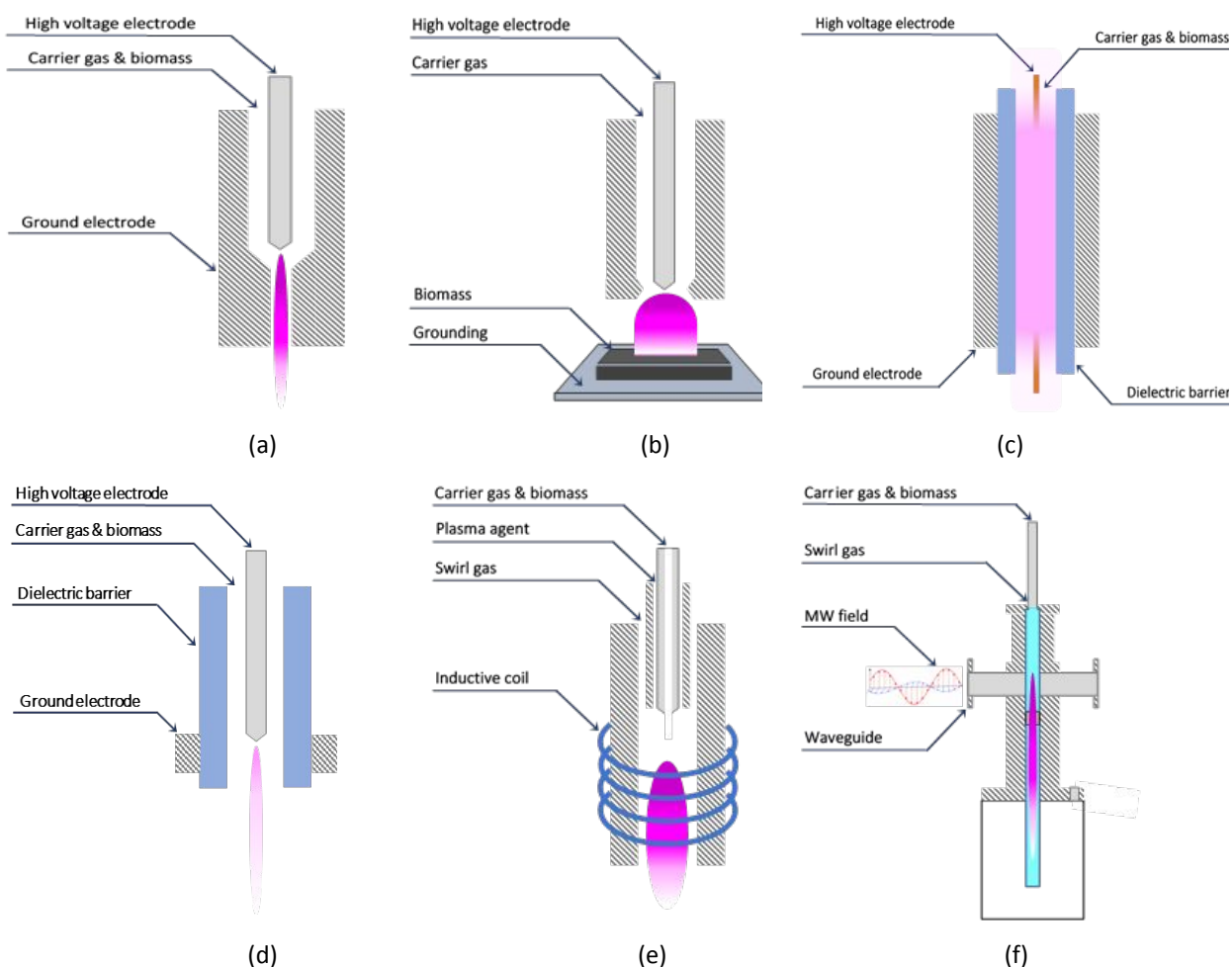


Figure 2: Characteristic plasma reactor designs implemented in biomass valorization to value-added products. Electrode-based configurations: (a) non-transferred plasma jet; (b) transferred plasma jet; (c) co-axial DBD and (d) DBD-like plasma jet. Electrodeless configurations: (e) RF-driven plasma and (f) MW-imposed plasma.

2.2 Plasma power supplies

Plasmas can be ignited over a wide range of frequencies. The frequency is directly associated with the energy channeled into the plasma, which subsequently determines the plasma characteristics, such as active species temperature and density for a given reactor configuration. Aside from the excitation frequency, the excitation wave pattern (continuous, sinusoidal, and pulsed) also determines the plasma properties. To ignite and sustain plasmas of specific characteristics and energy densities, various types of power supplies, including direct current (DC), alternating current (AC), radio frequency (RF), and microwave frequency (MW) have been employed. An overview of power sources and operating modes is given in Table 1.

Table 1. Overview of the different power sources employed for plasma biomass treatment applications.

Type	Features	Advantages	Limitations	Scalability
Direct Current (DC)	Stable operation; robustness to operating conditions variations	Easy control of the discharge; simple in construction	Reactor's electrode short lifetime due to erosion ⁴⁴ ; low energy efficiency due to unnecessarily extreme operating temperatures, imposed by the spark-to-arc transition; intensive water-cooling of the high voltage electrode; costly AC/DC transformers ⁴⁵	Available at several megawatts and tested at large scale biomass treatment applications
Alternating current (AC)	Sustaining of non-equilibrium plasma conditions; operating at kHz frequencies (high energy inputs)	Extended electrode lifetime due to polarity alternation; no need of complicated and expensive rectifiers for high-power-level applications	Possible malfunctions due to time-dependent electrical parameters	Available for large-scale biomass treatment units
Radiofrequency (RF)	Operating frequencies (1-100 MHz)>>AC; inductive/capacitive coupling; compact	High energy density; electrodeless	Use of inherently low-efficiency oscillator electronics impacting the energy efficiency; difficult tuning of the plasma properties (e.g., the flux of ions, reactive species, and heat) ⁴⁶ ; operating in vacuum (0.01–1 kPa) ⁴⁷	Prevalent for industrial applications ⁴⁸
Microwave (MW)	Operating frequencies 300 MHz<f<300 GHz generated by magnetrons (2.45 GHz or 915 MHz); operating pressure from a few mbar to ambient; input powers up to 100 kW	Wide operating window (feed flow rates, operating temperatures and power densities); electrodeless	Complicated plasma reactor design for solid organic material ⁴⁰	Versatile for biomass valorization
Pulsed power	Sustaining non-equilibrium plasma conditions at high energy inputs; high reduced electric field; generation of highly energetic electrons	Prevention of plasma arcing; overcoming of high breakdown voltages; high energy efficiency	Electromagnetic radiation and interference with the peripherals; absence of upscaling strategies	Available for demonstration-scale applications

Emphasis has been particularly placed on suppressing the discharge transition to arc to sustain non-equilibrium plasma conditions when operating at high energy inputs, thus, limiting the energy dissipation into gas heating. Proposed solutions include the use of i) pointed electrodes (similar to the ones used for corona discharges) to increase the local electric field; ii) resistive or dielectric barriers to limit the excess energy dissipation, e.g., by feeding gases of high thermal conductivity, and iii)

miniaturization of the discharge region (micro hollow cathode discharges)⁴⁶. Those modifications are necessary when a continuous-wave operation (DC, AC, RF, and MW power supplies) and high energy inputs are applied. Only AC power supplies have recently tackled this issue: a dual-frequency operation can suppress plasma arcing and control the plasma temperature.⁴⁹ Unlike other power supplies, pulsed power supplies, and specifically the nanosecond pulsed discharge (NPD), characterized by rapid pulse rise time and narrow pulse width, promotes non-equilibrium plasma conditions at high energy inputs without requiring the above mentioned modifications; the electrons accelerate through extremely short and steep voltage pulses to enable electron-molecule collisions maximizing the electric to chemical energy transformation while heavy species move much slower (limiting thermal effects). The shorter streamer propagation time than photoionization renders the discharge more spatially uniform. As compared to AC, they attain higher electron energy and density.⁵⁰

2.3 Integrated systems

Different combinations of reactor configuration and power supply may be adopted, depending on the application. This section discusses the possible reactor-plasma source configurations and depicts the technically feasible ones in Figure 3.

Continuous DC arc is the oldest plasma technology employed for industrial applications that require high bulk gas temperatures rather than a high density of active species. Electrodes are always necessary to ignite and sustain the discharge plasma. Coupling continuous DC sources with electrodeless plasma or electrode-based DBDs is impossible. Electrons and ions accumulate on the dielectric material surface and create a high local electric field due to their charge as a shield against the external electric field, resulting in discharge suppression. Therefore, external voltage alternation is needed to force the accumulated charge in the field direction (voltage increase) or trigger backward discharge ignition (voltage decrease). In the latter case, the local electric field from the accumulated charges surpasses the gas breakdown voltage and reignites the discharge. AC and pulsed DC power supplies work with all electrode-based reactor configurations, including DBDs, but not with electrodeless ones.

DC-driven plasmas in air or noble gases can also operate in a self-pulsing mode. This behavior is usually observed when using a high Ohmic power supply with a limited power output capacity⁴⁶ and transient spark discharges are often sustained.⁵¹ At kHz-range, high-intensity rectangular or sinusoidal voltages, non-spark discharges can also be sustained.⁵²

Pulsed DC plasmas operate at higher power inputs than continuous DC plasmas and offer higher performance controllability.³³ They feature higher currents than the AC-driven ones and achieve a relatively low gas temperature in the entire plasma zone. Consequently, pulsed DC sources are more effective for non-equilibrium plasma operation atmospheric pressure.⁵³ Specifically, pulsed DC DBDs are an ideal discharge mode at atmospheric pressure;⁵⁴ the plasma, in this case, comprises multiple overlapping non-equilibrium plasma streamers almost uniformly distributed over the discharge gap. Unlike the AC DBDs, which are more filamentary, pulsed DBDs, and in particular the nanosecond ones, can form homogeneous and diffuse discharges.⁵⁵

RF and MW plasmas are triggered by high oscillation alternating voltage rate sources as previously described. RF plasma sources can operate in an electrode-based configuration, including DBDs and low-pressure capacitively coupled plasmas (CCP)⁵⁶ or electrodeless configuration like in inductively

coupled plasmas (ICP). RF CCPs possess a relatively low electron density, contrary to ICPs that attain significantly higher electron density at the same input power.⁴⁸ ICPs are more efficient than CCPs over a wide range of frequencies and pressures.⁴³ Both can operate in pulsed mode to control the plasma temperature.⁵⁷ MW plasma sources can only work with electrodeless plasma reactors. In pulsed mode, they boost non-equilibrium conditions at high energy inputs.

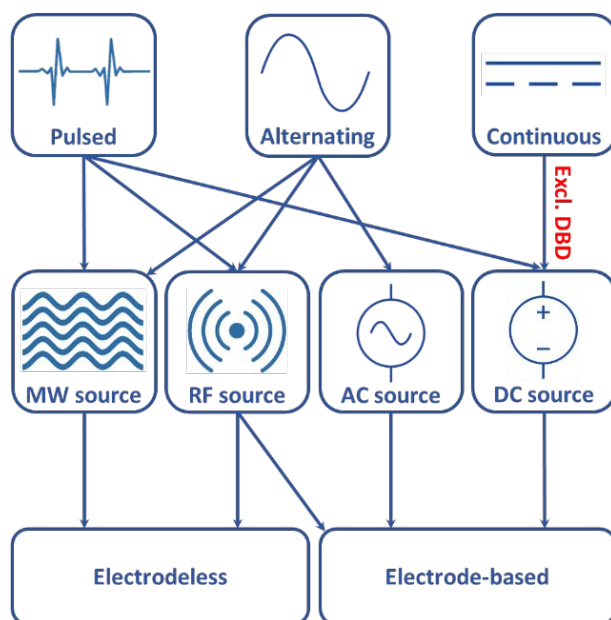


Figure 3: Feasible reactor-plasma source combinations. In red: while discharge ignition in DBD reactors powered by continuous DC plasma sources is achievable, maintaining the discharge for long periods is not possible.

3. Plasma technology for biomass conversion

This section reviews the most significant advances in plasma-driven biomass conversion. We classify processes based on the bulk gas temperature, i.e., low, moderate, high, and very high, and the biomass treatment mode. Advances attained by plasma are compared to conventional processes, i.e., hydrothermal, chemical-based, thermocatalytic, etc. Plasma technology is not compared to peer electrified alternatives.

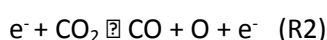
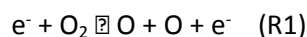
3.1 Low-temperature biomass conversion

3.1.1 Plasma processes and chemistry

Low-temperature plasma treatment of biomass can occur in the plasma-to-solid or the plasma-to-liquid interaction mode. In the former, the plasma-generated reactive species interact with and modify the solid biomass surface (dry treatment). In the latter, the plasma discharge activates the liquid, which interacts with suspended biomass particles. “Hybrid” processes, including the gas-phase conversion of liquid vapors or conversely the liquid phase treatment using gas plasma micro-bubbles, have also been proposed. We describe these interaction modes of biomass with non-thermal plasmas, the most common reactor configurations, and the related chemistries below.

Dry treatment

The dry treatment of biomass entails gas-solid interactions, with the substrate exposed directly or remotely (Figure 4) to plasma-generated reactive species undergoing chemical, morphological, and structural modifications. Atmospheric pressure DBDs are the most common plasma reactors for direct plasma treatment.^{58,59,60,56} In a parallel-plate DBD configuration (Figure 4a), the biomass substrate in the form of powder, pellets, or coating, is placed on the grounded electrode inside the active plasma region. All reactive species, i.e., free radicals, charged species, and UV photons, can participate in the substrate modification, while oxidative gases like O₂, air, and CO₂, and occasionally inert gases, e.g., Ar and N₂, are typically used.⁶¹ Atomic oxygen (O) is a strong oxidant, produced via electron impact dissociation of O₂ or CO₂ in the plasma region:



Atomic oxygen is abundant near the biomass surface in direct mode. Oxygen radicals readily abstract hydrogen, leading to radicals that quickly undergo oxidation by atomic and molecular oxygen and induce surface functionalization manifested as oxygen functional groups (alcohols, carbonyls, and carboxyls), as well as fragmentation through C-C beta bond scission. Other species, e.g., ions and metastables, can acquire substantial energy causing C-H bond activation (highly dependent on the process conditions). Ozone (O₃), reactive nitrogen species (e.g., NO_x in air plasmas), and UV-photons can also induce chemical and structural modification to the biomass molecules.

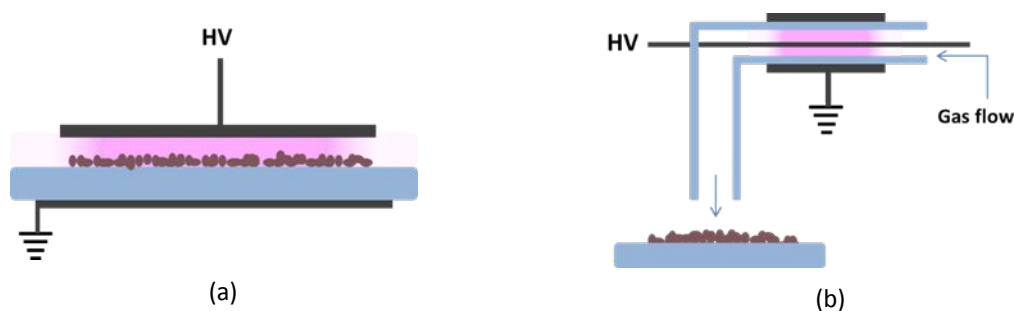
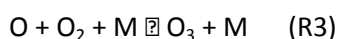


Figure 4: Schematics of reactor designs for dry treatment of biomass substrates by non-thermal plasmas: (a) Direct treatment in a parallel-plate dielectric barrier discharge (DBD) where all the reactive species (radicals, ions, and UV photons) could modify the biomass. (b) Remote treatment using only the long-lived neutral species generated from the DBD plasma.

In remote plasma treatment, the substrate is away from the active plasma region (Figure 4b). Air and O₂ are the most common process gases and only the long-lived reactive species reach the biomass and launch oxidative interactions. Ozone is among the dominant oxidative species, generated via the three-body interaction of atomic and molecular oxygen:



Here M stands for a third body collider. Ozone has a much longer lifetime than atomic oxygen, which quenches rapidly upon leaving the plasma zone. Despite not being as strong oxidant as atomic oxygen, ozone is widely used, e.g., for the oxidation and degradation of lignin by attacking the double carbon bonds of the chains between the aromatic rings.^{62,63,64}

Liquid treatment

In liquid treatment, the plasma is excited directly inside the liquid (in-liquid plasma), or a gas discharge is facing the liquid surface (above-liquid plasma).⁶⁵ Combinations of these two modes and alternative designs are depicted in Figure 5. The liquid can be a suspension of biomass particulates of lignin, cellulose, etc., or a solution containing biomass-derived model compounds. The solvent is typically water, an aqueous electrolyte solution, an organic solvent, or an ionic liquid. The solvent is critical to the plasma-induced chemical reactions; its chemistry, as well as the chemistry of the gas plasma for above-liquid plasma, determine the interaction of plasma species with the lignocellulose constituents. For biomass conversion, liquid treatment is becoming increasingly popular, mostly due to the enhanced mass transport and homogeneous interaction of biomass particles with secondary plasma-generated oxidative species diffusing in the liquid phase.

To better elucidate the plasma-liquid interaction chemistry, we focus on pure water, as discussed in the plasma-activated water literature.^{66,67,68} The plasma treated water is a highly reactive medium due to the formation of reactive oxygen and nitrogen species (RONS). These include long-lived species, e.g., hydrogen peroxide (H_2O_2), nitrates (NO_3^-), nitrites (NO_2^-), and ozone (O_3), and short-lived species, e.g., hydroxyl radicals ($\cdot\text{OH}$), superoxide ($\text{O}_2^{\cdot-}$), and peroxyxynitrite / peroxyxynitrous acid ($\text{ONOO}^- / \text{ONOOH}$). Being a strong oxidizing, and even acidic medium in many cases, plasma treated water can be a green alternative for biomass conversion. The reactive species concentration depends on the design parameters, such as the electrical power supply and electrical characteristics, plasma source geometry, volume of liquid, treatment time, type of gas, and flow rate. The chemistry is extensively covered in many comprehensive review papers.^{69,70,71,72,73} The reaction chemistry between these two modes of liquid treatment differs substantially and is discussed separately.

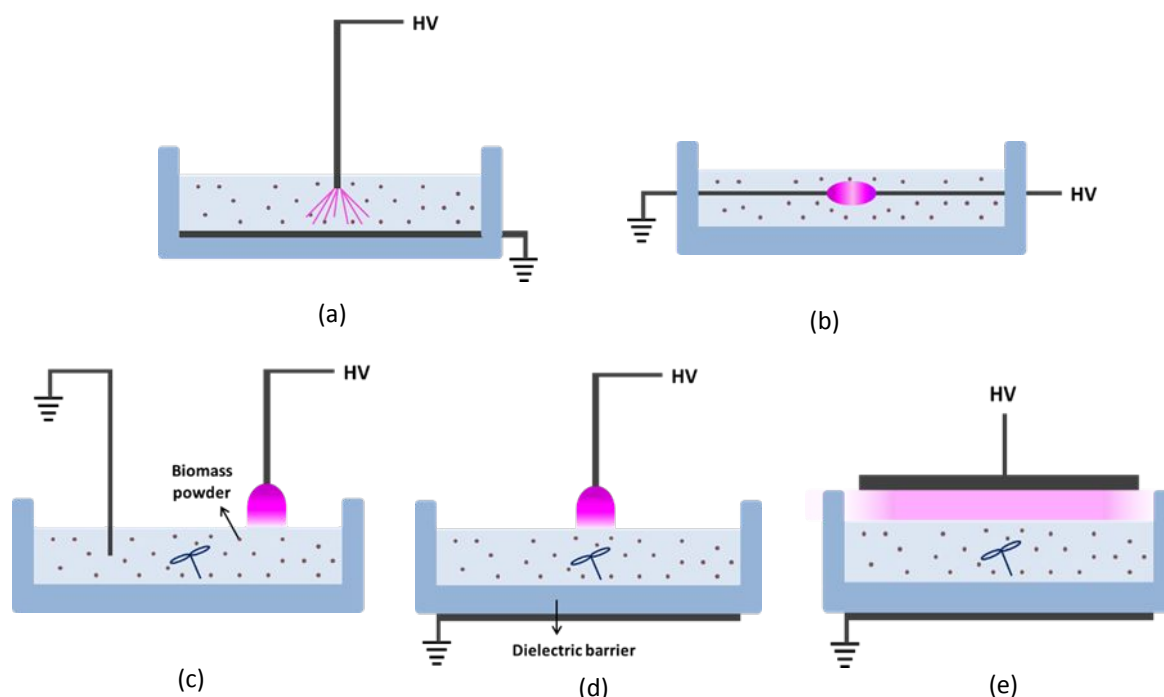
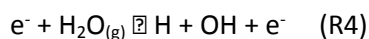


Figure 5: Reactor designs for liquid plasma treatment of biomass substrates: (a), (b) *in-liquid plasma* and (c)-(e) *above-liquid plasma*.

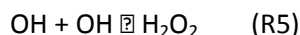
Above-liquid plasma. A plasma in contact with the liquid surface is the most common configuration for liquid-phase oxidation. Typical reactors include plasma jets and DBDs, as well as the plasma-electrolytic

configuration. The plasma treated water chemistry is determined by the gas phase plasma chemistry. The reactive species generated in the gas plasma region are transported to the gas-liquid interface, where they undergo secondary reactions leading to new reactive species penetrating the liquid phase. Herein we consider the most common air-rich discharges above water.

Among the main reactive oxygen species (ROS) in water are H_2O_2 , $\cdot\text{OH}$, and O_3 . The $\cdot\text{OH}$ radicals are produced mainly through gas-phase electron-induced dissociation reactions with water molecules that are introduced to the discharge through evaporation or co-fed in the gas stream.^{70,74,75,76}

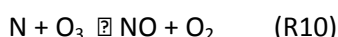
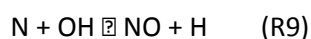
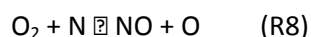
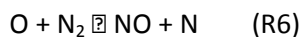


The H_2O_2 forms at the gas-liquid interface by $\cdot\text{OH}$ recombination:



The water downstream of the discharge serves as an H_2O_2 collector and protects it from degradation.⁷⁴ Ozone (O_3) is formed in the gas phase via (R3); its contribution to the liquid phase chemistry remains controversial, mostly due to its relatively low solubility at atmospheric pressure.⁶⁸ However, O_3 cannot be ignored as it can be highly reactive against aromatic compounds.

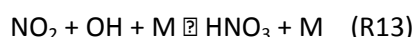
Reactive nitrogen species (RNS) are generated in the gas plasma region, at the plasma-water interface, and in the aqueous phase.^{72,75} The most important ones are the nitrates (NO_3^-), nitrites (NO_2^-), and peroxyxynitrite / peroxyxynitrous acid ($\text{ONOO}^- / \text{ONOOH}$). These secondary RNS species in the liquid phase arise from nitrogen oxides (NO_x) forming in the gas phase from the humid air discharge. Initially, the electron impact dissociative reactions in the gas phase lead to primary reactive species from O_2 , N_2 , and H_2O vapors. Specifically, the gas-phase reactions between neutral particles lead to nitric oxide (NO) through the following reactions:



Compared to the electron impact dissociation of the strong $\text{N}\equiv\text{N}$ bond, (R6) can provide an alternative, more energy-efficient pathway to nitrogen activation through vibrational excitation of N_2 molecules (Zeldovich mechanism).^{77,78} (R6) - (R8) provide the most likely path of NO formation in air, whereas (R9) is also essential in humid air.^{69,72} NO is further oxidized to NO_2 , most likely with atomic oxygen:



Reactions of NO_2 to NO_3 and other nitrogen oxides, e.g., N_2O_5 , are also possible. In humid air, NO and NO_2 react with plasma-generated OH to form nitrous and nitric acid:



N_2O_5 reacts directly with water to form nitric acid. The gas-phase generated acids dissolve readily in water yielding nitrite NO_2^- and nitrate NO_3^- ions. Nitric and nitrous acids also form via liquid-phase reactions between solvated NO_2 and NO_3 and solvent molecules or oxidative radicals (OH or HO_2). Peroxyxynitrous acid (ONOOH) is also reactive, mostly generated from nitrous acid with peroxide under acidic conditions:⁷⁵



For higher pH values, the equilibrium shifts towards peroxyxynitrite ions (ONOO^-). In plasma activated water (PAW), the resulting RONS in the liquid phase react even after the plasma is switched off. Although the reactivity is fading over prolonged storage, the long-lived species, like peroxide and nitrates / nitrites, ensure activity for hours and days after production. A simplified chemistry of the water interaction with air plasma is presented in Figure 6.

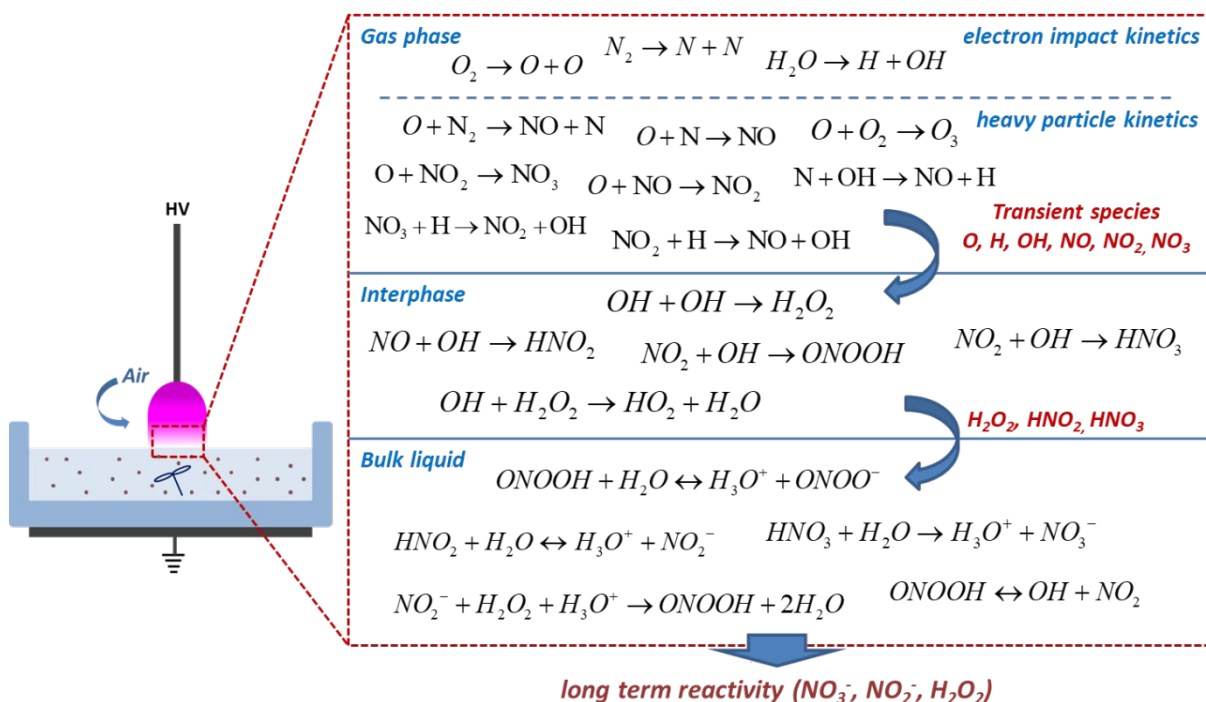


Figure 6: Simplified air plasma-water interaction chemistry for air discharges facing water interfaces.

The phenomena in biomass treatment in aqueous suspensions in contact with air discharges are not fully understood due to the complicated water chemistry and biomass complex structure. Yet, there are two primary types of reactions. First, liquid-phase species, such as OH radicals, solvated O_3 , and H_2O_2 can lead to oxidation, chain cleavage, and ultimately the degradation of organic molecules. Second, the acidification of water, mostly by nitric acid, can cause Bronsted acid catalysis, such as hydrolysis, de-etherification, and dehydration. Oxidation and acid catalysis can act in parallel to break down biomass. A subtle consideration is that acid chemistry in air plasma of dry treatment of biomass powder can be relevant when the powder is not completely dry.

In-liquid plasma. In the in-liquid plasma treatment, the plasma is ignited inside the aqueous medium by breaking down water vapors formed by local heating from the DC current and is promoted by adding an electrolyte to increase the liquid conductivity. The interaction pathways are less complicated as only ROS from water dissociation are implicated in the liquid chemistry. Reactions (R4) and (R5) dominate the formation of short-lived OH radicals and long-lived H_2O_2 . A significant advantage is the enhanced mass transport and reactivity of short-lived radicals forming adjacent to the treated biomass particles. However, underwater discharges are less energy-efficient and cause substantial heating of the liquid.

3.1.2 Plasma pretreatment and delignification

Here, we discuss the least energy-intensive, low-temperature, liquid-phase conversion of lignocellulosic biomass. The lignocellulose is most commonly firstly pretreated to achieve hydrolytically high yields of sugars that are ultimately upgraded to fuels and chemicals via chemical or enzymatic processes.^{79,80} Low-temperature raw biomass pretreatment and delignification for hydrolysis to sugars and functionalization for biopolymer valorization can be plasma-assisted. The heating by the plasma depends strongly on the phase. For dry treatment, the gas temperature, typically estimated spectroscopically, can be a few tens of °C (as in the case of parallel-plate DBDs in inert gas), causing minimal heating on the biomass powder downstream. The solution temperature can rise significantly for in-liquid treatment, depending on the discharge. In the reported works, it is maintained considerably below 100 °C. Acid hydrolysis temperature depends on the substrate and the acid concentration. Hemicellulose is hydrolyzed at 170 °C in dilute acid (DA) process, while in concentrated acid (CA) the temperature can drop to 50 °C.⁸¹ Cellulose hydrolysis requires temperatures from 140 (CA) up to 230°C (DA). Enzymatic hydrolysis runs typically at 37 - 50 °C. The following subsections discuss the plasma pretreatment of the entire raw biomass and then the cellulose and lignin fractions using dry and liquid plasma processing.

3.1.2.1 Raw biomass pretreatment

Lignocellulose pretreatment is necessary to disrupt its highly recalcitrant structure and achieve a high yield of sugar monomers or oligomers via chemical or enzymatic hydrolysis. Pretreatment is typically one of the most expensive processing steps in biomass conversion and imposes challenges for the controlled operation over large scales.^{79,82} It mostly targets the breakdown of lignin, the decrease of cellulose crystallinity, and the increase of biomass surface area, aiming to enhance the contact with acid catalysts or enzymes.^{83,84,85,86} Desirable attributes of practical, green, and economically viable pretreatments include: 1) cost reduction associated with raw material size reduction, 2) low equipment cost, 3) low power consumption, 4) minimal or no use of chemicals and solvents, and 5) minimal waste production.^{79,87} An effective pretreatment should promote accessibility of carbohydrate chains without causing degradation, while facilitating the recovery of ideally intact lignin for subsequent upgrading. Lignin condensation results in a difficult to convert material.

Common pretreatments are mechanical, chemical, electrical, biological and their combinations. Popular techniques include ball-milling, steam explosion, hot water, ozonolysis, and ultrasound. Chemical treatment using dilute acid, lime, and ammonia is among the most cost-effective and promising methods.^{86,88,89,90}

Non-thermal plasma treatment could be a promising, economically viable, and greener biomass pretreatment alternative.⁶¹ It entails only electricity as an energy source, which ideally can be renewable and inexpensive as solar and wind power gradually gets cheaper, low environmental footprint due to the minimal use of chemicals, ambient pressure operation and thus no need for expensive large scale reactors, and custom design and ease of implementation at small-scale, enabling the “scale-out” vision for modern biorefineries.

Both dry and liquid plasma treatments have been proposed, with most reports focusing on delignification efficacy and sugar yield increase in acid or enzymatic hydrolysis. Biomass pretreatment

can also facilitate the extraction of high-value compounds, such as bio-oils or essential oils.^{91,92} The feedstock explored so far is typically lignocellulosic agricultural waste, while food waste can be treated as well. Main literature findings are summarized in Table 2. A detailed description of the experimental activity performed in each cited work follows.

Table 2: Summary of plasma pretreatment of lignocellulosic feedstock.

Substrate	Plasma treatment	Main Results	Ref.
Wheat straw	Dry treatment, parallel-plate DBD, air, AC HV, 20 – 25 KHz, 1.5 min	84% total sugar yield after enzymatic hydrolysis	93
Wheat straw	Dry treatment (remote), coaxial DBD, air and O ₂ , pulsed AC 18.4 kHz, 230 W, 1 – 7 h	95% delignification, 78% glucose yield after enzymatic hydrolysis, 52% ethanol yield	94
Wheat straw	Liquid treatment (above-liquid plasma), DI water, commercial plasma jet, Ar/O ₂ 1%, 20 min	1.8-fold increase in reducing sugar production after enzymatic hydrolysis	95
Sugarcane bagasse	Liquid treatment (above-liquid plasma), Aq. Na ₂ CO ₃ + NaOH, DBD with non-contact electrodes, air, AC HV 3.5 kV, 60 Hz, 2 h	58.5% lignin solubilization at pH 12, 51.3% glucose and 38.5% xylose yields after enzymatic hydrolysis	87
Bagasse	Liquid treatment (above-liquid plasma), Ionic Liquid, plasma jet, He, pulsed DC 3kV, 10 kHz, 4 h	2-fold increase of solubility in [Emim]Oac	96
Japanese cedar	Liquid treatment (above-liquid plasma), Ionic Liquid, plasma jet, He, pulsed DC 3kV, 10 kHz, 4 h	Enhanced solubility of cellulose due to lignin disruption, selective extraction	96
Cornstalk	Dry treatment, parallel-plate DBD, N ₂ /steam, AC HV 3 kV, 2 h	1-step hydrolysis through acidification, 76.65 % conversion, 32.37% sugar selectivity	97
Miscanthus grass	Liquid treatment (microbubbles), DBD, air, AC 16.4 kV _{rms} , 21.2 kHz, 10 % duty cycle, 3 h	0.5% acid-soluble lignin, 26% sugar release (2.5-fold increase) after enzymatic hydrolysis	98
Water hyacinth	Liquid treatment (in-liquid plasma), FeCl ₃ solution, 450 V, 30 min	Lignin reduction from 23.7 to 18.4% crystallinity reduction from 31.2 to 25.1%, 126.5% increase in sugar yield in enzymatic hydrolysis	99
Cassava starch waste (CSW)	Liquid treatment (in-liquid plasma), H ₂ SO ₄ , pulsed 0.4 kV, 30 kHz, 300 min	1-step plasma and hydrolysis, TRS yield 99% and glucose yield 47.9%	100

Spent coffee waste	Dry treatment, parallel-plate DBD, FeCl ₃ , H ₂ SO ₄ , air, AC HV 70 kV, 50 Hz, 2 min	Lignin removal / 0.496 g reducing sugar per g SCW after enzymatic hydrolysis/ 74% fermentation efficiency (2-fold)	101
Brewer spent grain	Liquid treatment (submerged DBD jet), air, AC HV 28 KV, 10 min	2.1-fold increase in reducing sugar yield after enzymatic hydrolysis	102

Shaghaleh *et al.*⁹³ studied the effect of DBD plasma (dry treatment) with air, CO₂, and N₂, on subsequent enzymatic hydrolysis efficiency of wheat straw, an abundant agricultural waste. Optimum conditions included 90 s plasma treatment with air and dry matter in 60% moist environment, giving a sugar yield of 84% via enzymatic hydrolysis. Schultz-Jensen *et al.*^{94,103} used remote atmospheric air or O₂ plasma to pre-treat wheat straw. Ozone preferentially attacks and degrades the lignin, while cellulose and hemicellulose are minimally affected. Lignin degraded up to 95% after 7 h of ozonation, and 78% glucose yield was achieved in enzymatic hydrolysis leading to a 52% yield of ethanol. Sakai *et al.*⁹⁵ pretreated wheat straw water suspensions downstream of an atmospheric pressure Ar/O₂ plasma jet and obtained a 1.8-fold increased production of total reducing-sugars (TRS) via enzymatic hydrolysis.

Bagasse is another popular feedstock. Miranda *et al.*⁸⁷ treated sugarcane bagasse inside aqueous solutions of Na₂CO₃ and NaOH using a DBD with non-contact electrodes. Plasma treatment for 2 h at pH 12 gave a maximum lignin solubility (>50 %) and yields of glucose and xylose of 51.3% and 38.5%, respectively. Kuroda *et al.*⁹⁶ treated Bagasse and Japanese cedar suspensions in an ionic liquid, namely 1-ethyl-3-methylimidazolium acetate ([Emim]OAc), with a He plasma jet. They observed enhanced solubility attributed to the selective extraction of cellulose, enabled by the disruption of the lignin network.

Plasma treatment of other feedstocks has also been reported. Song *et al.*⁹⁷ applied a DBD plasma in N₂ and saturated steam to treat cornstalk powder and achieved an optimum ~77% conversion in 2 h treatment and 32.4% sugar selectivity. Glucose, xylose, mannose, and disaccharides were the main products. The cornstalk conversion was attributed to acid-catalyzed hydrolysis of cellulose and hemicellulose due to the acidification from the N₂/H₂O gas mixture. Wright *et al.*⁹⁸ proposed a plasma microbubble reactor to increase the efficiency of liquid phase biomass pretreatment. The air plasma-generated ozone, nitrogen oxides, and hydroxyl radicals were transferred through microbubbles in liquid suspensions of miscanthus grass and resulted in the release of 0.5 % w/w acid-soluble lignin and 26% of sugars via enzymatic hydrolysis. Gao *et al.*⁹⁹ used plasma electrolysis to treat water hyacinth inside electrolyte solutions. Among several electrolytes tested, FeCl₃ was the most efficient, followed by FeCl₂ and then NaCl and KCl; Fe ions promote hydroxyl radicals through the Fenton chemistry and lead to the oxidative attack of the complex lignocellulose structure. After 30 min of plasma treatment, the lignin content decreased from 23.7 to 18.4%, the crystallinity index fell to 25.1%, and the sugar yield via enzymatic hydrolysis was more than double.

Food waste contains starch and provides an opportunity for plasma processing as well. Prasertsung *et al.*¹⁰⁰ studied the in-liquid plasma treatment of cassava starch waste, which consisted of more than 70% of starch, in dilute H₂SO₄. The plasma pretreatment led to a 5-fold increase in total reducing sugars (TRS) compared to dilute acid hydrolysis. At optimum conditions, the TRS reached 99% yield, while the

glucose yield was 47.9%. The efficient starch hydrolysis was attributed to the oxidative cleavage of ether linkages by hydroxyl radicals formed in the aqueous phase. Ravindran *et al.*¹⁰¹ treated spent coffee waste in presence of iron (III) chloride (FeCl₃) and sulfuric acid using air DBD discharges. The Fenton chemistry facilitated the lignin removal; 0.5 g of reducing sugars per g of feedstock translated to a 2-fold increase of fermentation efficiency to 74%. They applied liquid plasma treatment using a submerged DBD jet to pretreat brewer spent grain in subsequent work¹⁰² and found a more than 2-fold increase in reducing sugar yield via enzymatic hydrolysis.

In the following subsections, we explore plasma treatment's effect on individual components to understand the underlying plasma-biomass interactions.

3.1.2.2 Cellulose

This subsection discusses the plasma treatment of cellulose due to the vast literature and high technological interest in its upgrade. Like raw biomass discussed above, cellulose also requires a pretreatment to enhance its processability and improve process efficiency. Cellulose is typically hydrolyzed by enzymes or acid catalysts to glucose that is then converted to bioethanol, through fermentation by yeast, or to chemicals, such as hydroxymethylfurfural (HMF) and levulinic acid, via chemocatalytic processes.^{104,105,106,107,108} Cellulose pretreatment disrupts its crystalline structure, enhances its solubility, and increases its interface contact area with catalysts or enzymes.^{109,110,111} The objective is to facilitate depolymerization, leading to the highest possible yields of glucose or processable glucans.¹¹² Several pretreatments, such as ball-milling, microwave irradiation, ultrasound, and chemical acid or alkali methods have been applied to cellulose.¹¹⁰

Non-thermal plasma treatment has attracted a lot of attention, mostly due to its environmentally friendly character and ability to produce highly reactive species that interact with cellulose.⁶¹ Plasma - cellulose interaction has been extensively studied through surface modifications of cellulose or cellulose-derived materials, e.g., paper, nanocellulose fibers, textiles, etc., that aim to impart specific functionalities and promote interfacial interactions.^{113,114,115}

Plasmas have been employed in dry and liquid treatment for both amorphous and microcrystalline cellulose. The main literature findings on plasma treatment of cellulose are outlined in Table 3. A description of the experimental activity in each cited work is also given.

Table 3: Summary of literature findings on cellulose plasma treatment for hydrolysis promotion.

Substrate	Plasma treatment	Main Results	Ref.
<i>Plasma pretreatment and acid hydrolysis</i>			
Microcrystalline Cellulose (MCC)	Dry treatment, parallel-plate DBD, air, pulsed HV 11.2 kV, 2 kHz, 3 h	DP from 200 to 120, 22% glucose yield after aqueous acid hydrolysis with A35	116
Amorphous Cellulose (ball-milled MCC)	Dry treatment, parallel-plate DBD, air, pulsed HV 11.2 kV, 2 kHz, 1 h	DP from 200 to 36, 58% glucose yield after aqueous acid hydrolysis with A35	117

Amorphous Cellulose (ball-milled MCC)	Dry treatment, parallel-plate DBD, air, pulsed HV 11 kV, 2.2 kHz, 15 min	Branched glucans, 80% glucose yield (83% conversion) after aqueous acid hydrolysis with H ₂ SO ₄	118
Microcrystalline cellulose (MCC)	Liquid treatment (above-liquid plasma), parallel-plate DBD, Ar and air, AC HV 19-22 kV, 15 kHz, 50 min	DP and crystallinity drop, 93.98% Liq. yield and 41.75 g/L TRS (2-fold increase) after acid hydrolysis with H ₂ SO ₄	119
Microcrystalline cellulose (MCC)	Liquid treatment (above-liquid plasma), DI water, Air, DC 20 mA, 30 min	56% yield (2-fold increase) of cellulose nanocrystals (CNC) after acid-catalyzed hydrolysis with H ₂ SO ₄	120
<i>Single-step plasma acid hydrolysis</i>			
Microcrystalline cellulose (MCC)	Liquid treatment (in-liquid plasma), Aq. solution of H ₂ SO ₄ , pulsed HV 1.6 kV, 15-30 kHz, 5 h	Fenton catalysis from Fe ions, OH radicals 0.7 mM, TRS yield from 7.8 to 27%	121
Microcrystalline cellulose (MCC)	Liquid treatment (above-liquid plasma), parallel-plate DBD, air, 80 W, 3 min	Water acidification (pH down to 1.35), 46% glucose yield in plasma acid at pH 1.42	122
Hemicellulose	Liquid treatment (above-liquid plasma), parallel-plate DBD, air 80 W, 3 min	Water acidification with pH down to 1.35, 38.7% xylose, 9.3% glucose, 3.1% galactose yields hydrolysis at pH 2.81	123
<i>Plasma pretreatment and enzymatic hydrolysis</i>			
α -cellulose	Liquid treatment (microbubbles), DBD, air, AC HV 10.6 kV _{pp} , 29 kHz, 10-60% duty cycle, 2 h	Solubility increases at pH 3 from 17 to 70%, glucose conversion increase from 24 to 51% after enzymatic hydrolysis	124
Carboxymethyl Cellulose (CMC)	Liquid treatment (above-liquid plasma), DI water, commercial plasma jet, Ar/O ₂ 1%, 20 min	Drop of solution viscosity, 1.6-2-fold increase in reducing sugar production through enzymatic hydrolysis	95
Cellulose	Dry treatment, DBD in continuous mode, air, 4.5 kW, 1.5 s	~2-fold increase in O/C ratio, Reduction of crystallinity from 58 to 38.8% / Drop of Mw	125

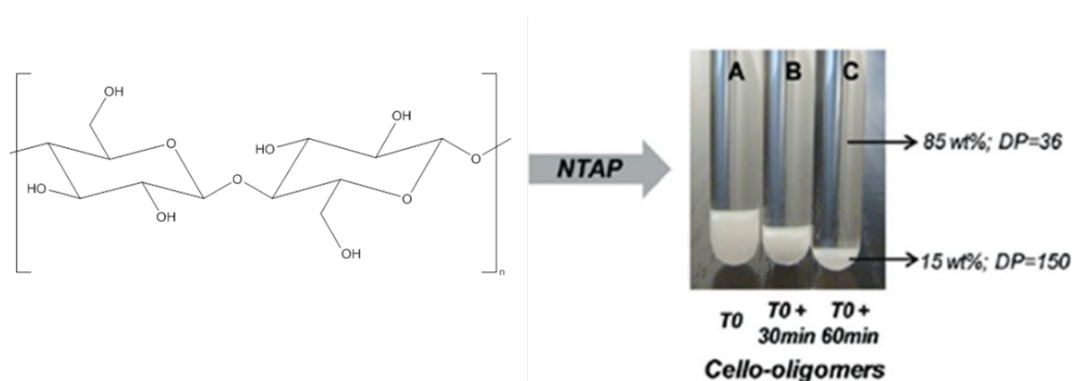
Plasma pretreatment and acid hydrolysis

Benoit *et al.*¹¹⁶ reported on dry plasma treatment of microcrystalline cellulose (MCC) powder using a parallel-plate DBD reactor in air chemistry. The degree of polymerization (DP) decreased from 200 to 120 after 3 h with no further change over longer times. No weight loss was observed, while the particle size and C/O ratio were not altered; however, partial oxidation of cellulose was evidenced by the formation of -CHO and -COOH groups, as deduced from X-Ray Photoelectron Spectroscopy (XPS) measurements. The crystallinity index increased from 78 to 81%, possibly due to the amorphous preferential oxidation over the crystalline phase. Aqueous acid-catalyzed hydrolysis of cellulose with Amberlyst 35 (A35), a sulfonated heterogeneous catalyst, showed that pretreatment resulted in a

glucose yield of 22%, much higher compared to untreated samples (<1%) and ball-milling or ionic liquids (3-14%). In our experience, polymer-based catalysts, such as various Amberlyst catalysts, are not stable at high temperatures of biomass conversion and in regeneration from coke by calcination. Studies on the effect of plasma on these catalysts are also missing but this is not as critical, as catalyst stability issues prevail. A glucose yield of 14% was observed even without an acid catalyst. Plasma treatment successfully depolymerized other polysaccharides like starch and inulin. In follow-up work, the authors used ball-milling treatment of microcrystalline cellulose before exposure to atmospheric plasma.¹¹⁷ That resulted in decrystallization of MCC without affecting its degree of polymerization, increasing the depolymerization efficiency of the subsequent plasma treatment (a DP drop from 200 to 36 after 1 h). The ball-milled and plasma-treated cellulose exhibited an excellent solubility of 84% and 37% in DMSO and water, respectively (Figure 7a). The glucose yield in aqueous acid-catalyzed hydrolysis by A35 was enhanced to 58%.

Ball-milling disrupts the cellulose crystallinity and improves the plasma depolymerization efficiency, as found in recent work.¹¹⁸ The decrease in crystallinity from 80 to <10% via ball-milling promoted the solubility of plasma-treated cellulose in DMSO and water significantly (Figure 7b). This result was attributed to the higher amount of water in the low crystallinity cellulose, but the local cellulose structure, catalyst partitioning, and active plasma species penetration are also important variables that need to be understood. The subsequent acid-catalyzed hydrolysis in dilute H₂SO₄ resulted in an enhanced glucose yield of 80% (Figure 7c). This result is not unexpected given that mechanical treatment of biomass facilitates its deconstruction under most conditions.

Liquid plasma treatments of cellulose suspensions for acid hydrolysis promotion have also been proposed. Huang *et al.*¹¹⁹ applied Ar and air DBD discharges to treat water suspensions of ball-milled MCC (crystallinity 57.4%) for 50 min and found a sharp drop in cellulose DP from 215 to 78, with similar results for air and Ar. The DP drop of MCC without ball-milling treatment was 105, confirming other authors' observations that crystallinity affects the plasma's pretreatment efficiency. The plasma pretreatment of raw MCC, with no prior ball-milling, resulted in a crystallinity drop from 82.8 to 58.9% as well; that result is in contrast to the dry MCC pretreatment discussed above.^{116,117} The acid-catalyzed hydrolysis in H₂SO₄ increased the liquid yield from 68.6 to 94% and the total reducing sugar (TRS) concentration from 22.4 to 41.8 g/L after plasma treatment. Surov *et al.*¹²⁰ used DC plasma discharges in electrolytic configuration to pretreat MCC in water suspension for 30 min and realized an almost 2-fold increase of cellulose nanocrystals yield upon acid hydrolysis in H₂SO₄.



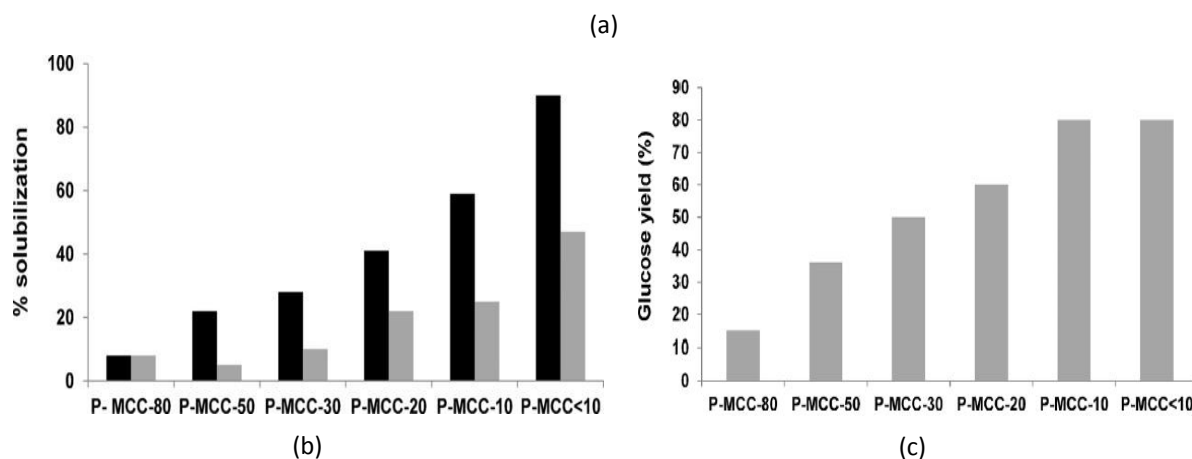


Figure 7: (a) Effect of plasma treatment on the dissolution of ball-milled microcrystalline cellulose (MCC) in DMSO. A) MCC in DMSO, (B) remaining cellulose (53 wt.%) in DMSO after 30 min plasma treatment, and (C) remaining cellulose (15 wt.%) in DMSO after 60 min plasma treatment. Reproduced from ref. 117 with permission from Royal Society of Chemistry, copyright 2012. (b) Effect of ball-milled microcrystalline cellulose (MCC) crystallinity, from 80% (P-MCC-80) to <10% (P-MCC<10), on the dissolution enhancement of plasma-treated samples in DMSO (black columns) and water (gray columns) and (c) the glucose yield of plasma-treated MCC by acid-catalyzed hydrolysis. All samples were treated in an air plasma for 15 min. Reproduced from ref. 118 with permission from Wiley-VCH Verlag GmbH & Co. KGaA, Weinheim, copyright 2016.

Single-step plasma acid hydrolysis

Prasertsung *et al.*¹²¹ studied single-step plasma-acid hydrolysis using in-liquid discharges of MCC suspensions in dilute H₂SO₄. With tungsten or copper electrodes, the plasma slightly increased the TRS yield compared to acid hydrolysis alone. In contrast, the TRS yield increased sharply up to 27% when Fe electrodes were applied. This phenomenon was attributed to the oxidation of Fe electrodes and the release of Fe ions and nanoparticles that act as Fenton catalysts to reduce in-situ formed H₂O₂ to OH. The hydroxyl radicals promote the disruption of cellulose crystallinity by effectively breaking the hydrogen bonds.

Wang *et al.*^{122,123} proposed a plasma-acid-catalyzed hydrolysis process without any external inorganic acid. The concept is based on the acidification of water (Figure 6) when treated with air plasma. Once formed, the “plasma acid” was used for hydrolysis of cellulose (pH = 1.35) and hemicellulose (pH = 2.81), yielding 46% glucose and ~38% xylose, respectively.

Enzymatic hydrolysis

Sakai *et al.*⁹⁵ applied remote atmospheric plasma discharges in an Ar / O₂ mixture to activate carboxymethyl cellulose (CMC) via the enzymatic hydrolysis. Cellulose was treated with plasma in liquid suspensions; the results showed a 2-fold increase in TRS (mainly cellobiose) from radical-pretreated CMC after enzymatic hydrolysis in culture supernatant containing cellulases from the white-rot fungus *Phanerochaete chrysosporium*. The oxygen-radical-pretreatment of CMC also enhanced the TRS using commercial cellobiohydrolases CBHI and CBHII by 1.7- and 1.6-fold, respectively. The cleavage of the cellulose backbone into smaller chains promoted cellulose hydrolysis of reducing- and non-reducing-end cellulases. Wright *et al.*¹²⁴ used a microbubble-enhanced DBD reactor to pretreat α-cellulose in water suspensions. They studied the effect of duty cycle on reactive species generation

and found maximum solubility at high ozone concentrations. Ozone is more effective in attacking the crystalline regions of cellulose than the co-produced reactive nitrogen species. Under optimum pH, duty cycle, and pretreatment time, they obtained a significant increase of cellulose solubility from 17 to 70% and glucose conversion from 24 to 51% via enzymatic hydrolysis.

Plasma-cellulose interactions

Common modifications of cellulose via oxidative plasma treatment include reducing the inter- and intra-molecular chain hydrogen bonding and the homolytic cleavage of the β -1,4 glucosidic bonds with an associated formation of free radicals and an increase in oxygen content. These processes reduce crystallinity, as realized through X-Ray Diffraction (XRD), depolymerize cellulose, as deduced from a significant drop in molecular weight based on Gel Permeation Chromatography (GPC) measurements, and enhance solubility and hydrophilicity of the plasma-treated cellulose.

Cao *et al.*¹²⁵ studied the structural modification of cellulose after treatment with air plasma (dry treatment). XPS, XRD, and GPC showed an almost 2-fold increase of the O/C ratio, a decrease in cellulose crystallinity from 58 to 39%, and a drop in cellulose molecular weight, respectively. They also performed Density Functional Theory (DFT) calculations to gain insight into the cellulose oxidation mechanism, assuming atomic oxygen as the main oxidative species. They revealed that C₄-O bond cleavage is the first step during plasma-induced oxidation due to the lower bond dissociation energy (229.2 kJ/mol) and the second thermodynamically more favorable step is the pyranose ring-breaking reaction.

Delaux *et al.*¹¹⁸ showed that the oxidative plasma treatment in air leads to depolymerization of cellulose to oligomers (cellodextrins) and simultaneously promotes re-polymerization reactions to branched glucans. Contrary to cellodextrins, containing exclusively of β -1,4 glycosidic linkages, these glycosyl units are connected by β -1,6 glucosidic linkages. The authors attributed the oxidative breakdown of cellulose to hydroxyl radicals formed from water present in cellulose. This hypothesis contrasts powder treatment (dry plasma treatment), where mostly O₃ and atomic oxygen are the most reactive and abundant species.

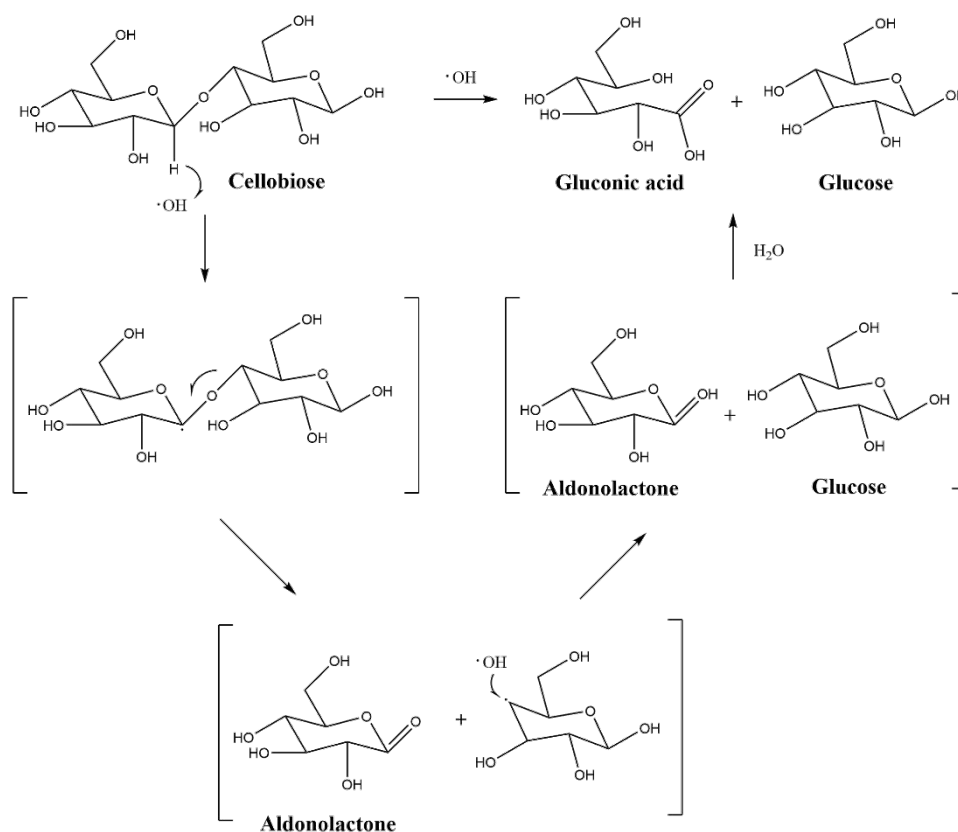


Figure 8: Proposed mechanism for the interaction of hydroxyl radicals with cellulose. Reproduced from ref. 126 with permission from Elsevier, copyright 2020.

While elucidating the underlying plasma-cellulose interactions in dry treatment is challenging due to the abundance of different species, this is more straightforward in liquid plasma treatments. First, acid hydrolysis cleavage of glucosidic bonds is at play due to the plasma acid when air plasma is in contact with water (Figure 6). The second and most dominant is the oxidative cleavage of cellulose bonds by oxidative species (primarily hydroxyl radicals) formed in the liquid phase.

Despite the limited number of investigations of plasma-liquid treatments, one could draw insights from the non-plasma literature. Gu *et al.*¹²⁶ proposed a mechanism for the reaction of hydroxyl radicals with cellobiose. As shown in **Figure 8**, the hydroxyl radicals react readily by abstracting hydrogen from the carbon atoms of the glucosidic C1-O-C4 bond. Pathway A, which begins with abstraction from the C1 carbon, leading to the O-C4 bond's subsequent cleavage, is the most probable according to authors. This conclusion is consistent with the DFT results of Cao *et al.* discussed above. The cleavage of O-C4 bond leads to a carbonylated pyranose ring or, more probably, to ring-opening. This mechanism would rationalize the enhanced O/C content observed by XPS and the abundant C=O functionalities. On the other hand, forming a radical at the C4 position would lead to further breakdown of the cellulose backbone by propagation reactions or further oxidation and recombination or termination, leading to reducing sugars or glucose monomers.

3.1.2.3 Lignin

Lignin is typically considered a low-value by-product in paper mills and bioethanol production plants. In most cases, lignin is incinerated to supply energy. Lignin accounts for up to 30% of the total lignocellulose mass and is the most abundant and renewable source of aromatic compounds; hence, its conversion to value-added products is essential for bio-refinery economic viability. The main strategies for lignin valorization under investigation are:

1) The utilization of lignin in its polymeric form as a phenolic matrix or additive in the fabrication of advanced materials and composites or a renewable resource for carbon fibers used as reinforcements in several composites.^{127,128,129,130,131,132}

2) The breakdown of lignin to its main building blocks, namely p-coumaryl, coniferyl and sinapyl alcohols and their derivatives (**Figure 9**),^{133,134,135} to fabricate copolymers and other materials^{136,137,138} or valuable chemicals.^{139,140} Catalytic conversion of lignin is a core valorization technology to platform chemicals and fuels.^{129,139,140,141,142,143}

Lignin oxidation can enhance its processability for advanced materials¹⁴⁴ or assist its conversion to valuable compounds, such as vanillin and syringaldehyde.^{145,146,147,148,149,150,151,152} In this respect, like ozone or Fenton reagents, plasma processing has also attracted considerable interest. Plasma processing has mostly targeted lignin degradation and lignification (see also the pretreatment of raw lignocellulosic biomass subsection). Still, recent work has also signified plasma's potential for lignin's oxidative breakdown and formation of valuable oxygenates. The plasma-lignin interactions described in the limited number of published studies are summarized in Table 4 and Table 5 for lignin and lignin model compounds, respectively. An extensive description of the experiments of each cited work is also given.

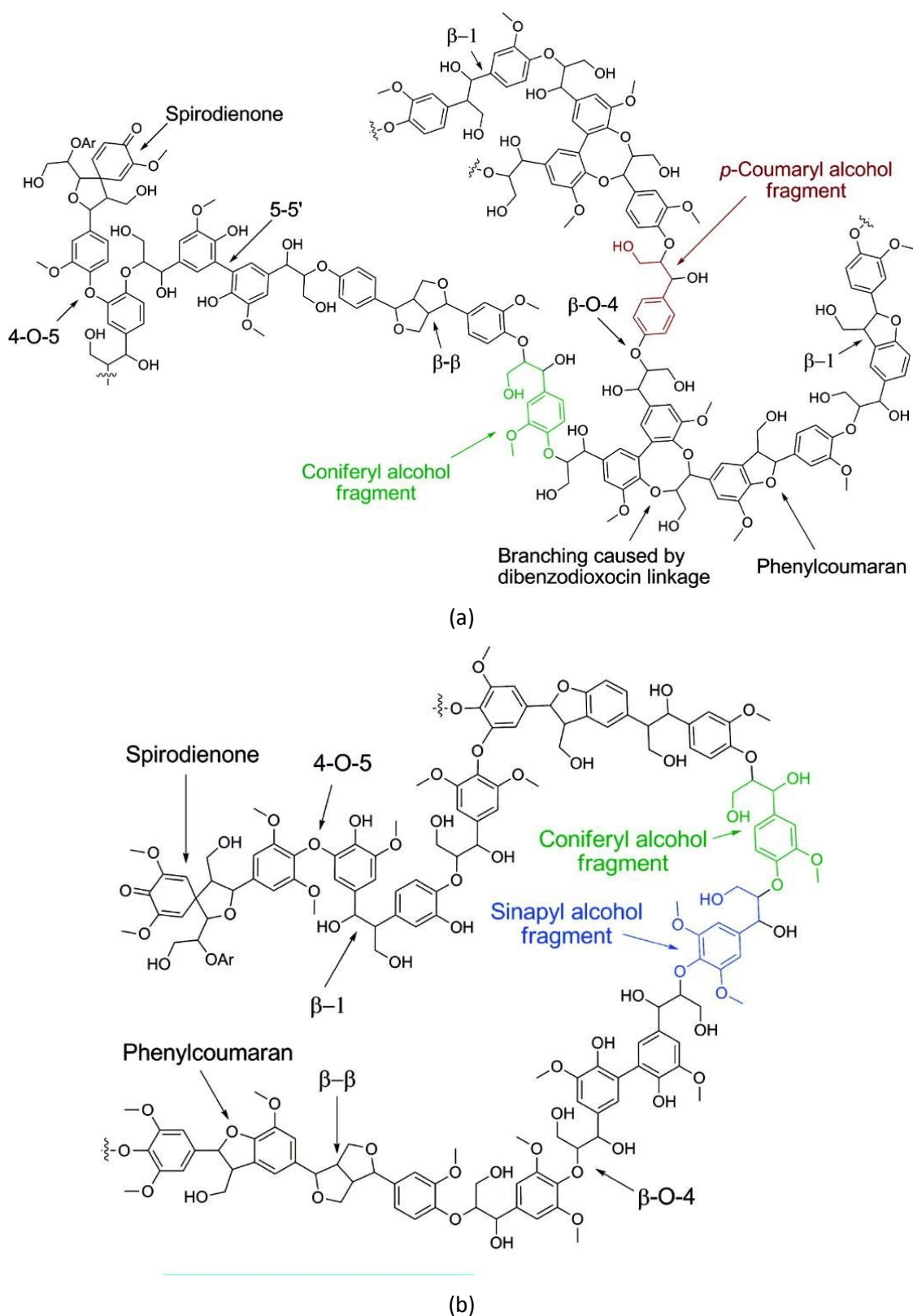


Figure 9: Proposed structure of (a) softwood and (b) hardwood lignin. Reproduced from ref. 133 with permission from American Chemical Society, copyright 2010.

Table 4: Summary of plasma pretreatment of lignin.

Substrate	Plasma treatment	Main Results	Ref.
Cellulolytic enzyme lignin	Liquid treatment (above-liquid plasma), ionic Liquid, plasma jet, He, pulsed DC 3kV, 10 kHz, 4 h	Decrease of lignin Mw	96
Coniferous kraft lignin	Liquid treatment in NaOH solution, Pulsed corona discharges, air, and synthetic O ₂ -N ₂ mixtures, 20 kV, 100 – 840 Hz, 30 min	70% lignin degradation, oxidation to aldehydes (vanillin, syringaldehyde)	153
Kraft lignin	Liquid treatment in NaOH solution, Pulsed corona, air and N ₂ -enriched air, 20 kV, 250W, 840 Hz, 5 - 40 min	Aldehyde formation efficiency increase for higher lignin and lower %O ₂ content, increase of carbonyl groups	154
Lignin	Liquid treatment in MeOH, RF 27.12 MHz, 200 W, 15 min	Production of H ₂ and aromatics (benzene, toluene, phenol)	155
Sugarcane Bagasse Lignin	Dry treatment, microplasma jet, Ar, RF 144 MHz, 20W, 0.5 – 4 h	Lignin breakdown only in the active plasma region / no effect in the afterglow	156
Corn cob lignin	Dry treatment, DBD in continuous mode, air, 4.5 kW, 1.5 s	~2.5-fold increase in O/C ratio, drop of Mw from 12378 to 9357, and β-O-4 linkages from 65.1 to 58.7 per 100 Ar	157
Poplar lignin	Dry treatment, DBD in continuous mode, air, 4.5 kW, 1.5 s	2-fold increase in O content, Mw drop from 10771 to 8364, β-O-4 links drop from 72.5 to 63.8 per 100 Ar	157
Hemp fiber lignin	Inside-liquid treatment, NaOH solution, AC ~ 1 A / 20 min	3-fold increase of solubility in alkali solution	158
Enzymatic hydrolysis lignin	Dry treatment, low pressure, O ₂ , RF 13.56 MHz, 200W, 3 min	O/C ratio increase from 0.25 to 0.4, a decrease of T _g by ~7°C	159
Organosolv lignin	Dry treatment, parallel-plate DBD, synthetic air and Ar, pulsed DC 18 kV, 13 kHz / 2 s	O/C ratio from 0.26 to 0.21 for Ar and 0.49 for air degradation; carbonyl, and carboxyl groups imparted	160
Protobind 2400	Dry treatment, low-pressure CCP, O ₂ , CO ₂ , air and Ar, RF 13.56 MHz, 100 W, 30 min	Alteration of T _g depending on process gas, ~2-fold increase of O/C ratio and decrease in viscosity for CO ₂ and O ₂	161

Compared with cellulose and cellulose-derived materials, the plasma-lignin interactions have hardly been investigated, even for materials applications. One of the first reports on plasma-treated lignin dates back to 2003 when Toriz *et al.*¹⁶² applied a low-pressure plasma using SiCl₄ to implant silicon

atoms and thus modify the lignin surface to strengthen the lignin-polypropylene composites. Plasma-assisted lignin functionalization has also been employed to improve its processability and interaction with other polymers, thus enabling its upgrade to functional materials. Nistor *et al.*¹⁶³ and Chirila *et al.*¹⁶⁴ modified organosolv lignin by carboxylic acids in an RF plasma and improved its hydrophilicity and solubility in aqueous and alkaline solutions, and decreased its particle size. Zhou *et al.*¹⁵⁹ examined the effect of a low-pressure oxygen plasma treatment on the glass transition temperature T_g of enzymatic hydrolysis lignin. They found a decreased T_g and significant oxidation of lignin through XPS analysis.

Kuroda *et al.*⁹⁶ applied a He plasma in contact with [Emim]OAc ionic liquid to treat cellulolytic enzyme lignin and 2-phenoxy-acetophenone, a lignin model compound. They observed a significant drop of lignin molecular weight and the formation of minor amounts of phenol, p-cresol, and syringaldehyde after 4 h treatment. 83% of the model compound decomposed after 90 min. The authors hypothesized that decomposition was due to the cleavage of β -O-4 bonds from imidazolium radicals formed upon reaction with plasma-derived OH radicals.

Amorim *et al.*¹⁵⁶ studied the structural modifications of sugarcane bagasse lignin induced by an Ar atmospheric microplasma jet using FTIR spectroscopy. They concluded that lignin undergoes multiple bond scissions in the active plasma region but no structural changes in the jet's afterglow. Tange *et al.*¹⁵⁵ used RF discharges inside lignin solutions in methanol and produced H_2 , light hydrocarbons, and aromatics (benzene, toluene, and phenol). Titova *et al.*¹⁵⁸ saw a 3-fold increase of lignin solubility by discharges in alkali solutions (NaOH) of hemp fiber lignin. They also studied isoeugenol, a model lignin compound consisting of a guaiacyl group and an unsaturated aliphatic chain.¹⁶⁵ Ring-opening occurred upon subsequent alkali treatment. Panorel *et al.*¹⁵³ used pulsed corona discharges to oxidize kraft lignin in aqueous NaOH solutions and studied the effects of pulse repetition frequency, oxygen content in air mixtures, and initial lignin concentration on the lignin oxidation and aldehyde formation. Pulsed corona discharges were more efficient than conventional ozonation processes, giving an optimum 70% degradation of lignin with low fractions of vanillin and syringaldehyde products. Recent work showed that higher lignin content and lower % O_2 lead to less harsh conditions favoring the aldehyde formation over the ring cleavage and lignin degradation.¹⁵⁴ A high degree of lignin oxidation, inferred by the concentration of carbonyl and carboxyl groups, was also observed. Clearly, understanding plasma-lignin interactions as a function of plasma processing conditions can lead to more controlled product distribution.

Table 5: Summary of plasma treatment of lignin model compounds.

Substrate	Plasma treatment	Main Results	Ref.
2-phenoxy-acetophenone	Liquid treatment ([Emim]OAc suspension), plasma jet, He, pulsed DC 3kV, 10 kHz, 90 min	83% decomposition, cleavage of β -O-4 bond due to the formation of imidazolium radical	96
Isoeugenol	Inside-liquid treatment, NaOH solution, AC \sim 1 A, 20 min	Aromatic structure breakdown in subsequent alkali treatment	165

Coniferyl alcohol	Dry treatment, parallel-plate DBD, synthetic air and Ar, pulsed DC 18 kV, 13 kHz, 2 s	Reduction of O/C ratio with Ar plasma, a decrease of OH groups	160
-------------------	---	---	-----

Plasma – lignin interaction and structural analysis

Due to the complexity of lignin structure and plasma processing, comprehensive characterization is needed to elucidate the plasma-lignin interactions. Klarhofer *et al.*¹⁶⁰ studied the plasma-induced structural modification of organosolv lignin and coniferyl alcohol, a model compound, using XPS, ultraviolet photoelectron spectroscopy (UPS), and metastable impact electron spectroscopy (MIES). They used pulsed DBD plasma in Ar or synthetic air and deposited lignin thin films on an Au substrate. The experiments were performed *in-situ*. The UPS spectra revealed that the peaks assigned to hydroxyl groups decreased. Accordingly, the MIES peaks assigned to hydroxyl groups decreased as well. The oxidation of lignin in air plasma was manifested with a new peak in the UPS spectra at 11.7 eV attributed to carbonyl group. The XPS spectra showed an increase of the peaks C2 (C-O), C3 (C=O or O-C-O) and C4 (O-C=O) and the O/C ratio from 0.26 to 0.49.

Zaitsev *et al.*¹⁶¹ investigated Protobind 2400 lignin's stabilization by low-pressure RF plasma treatment for potential application in renewable carbon fiber fabrication. While they mostly focused on the effect of plasma processing on lignin's T_g , XPS analysis with different process gases showed enhanced oxidation, with a pronounced increase in the O/C ratio in O₂ and CO₂ plasmas. The plasma treatment decreases the lignin viscosity, which promotes its processability and stability during extrusion.

Cao *et al.*¹⁵⁷ studied the structural modification of corncob and poplar lignin by an air plasma. Oxygen radicals oxidize the aliphatic chain (~2-fold increase of the O/C ratio) of the lignin powder but leave intact the phenyl ring. 2D-HSQC NMR revealed a significant drop of the β -O-4 aryl ether linkages with less modification of the other bonds. These findings corroborate with a remarkable reduction in the mean molecular weight of both lignin polymers. The preferential cleavage of ether linkages is vital in the oxidation and degradation of lignin. DFT studies indicate the breakdown of the ether bonds followed by the oxidative cleavage of C _{β} -C _{α} bond in the aliphatic region of lignin is the thermodynamically favorable pathway (**Figure 10**).

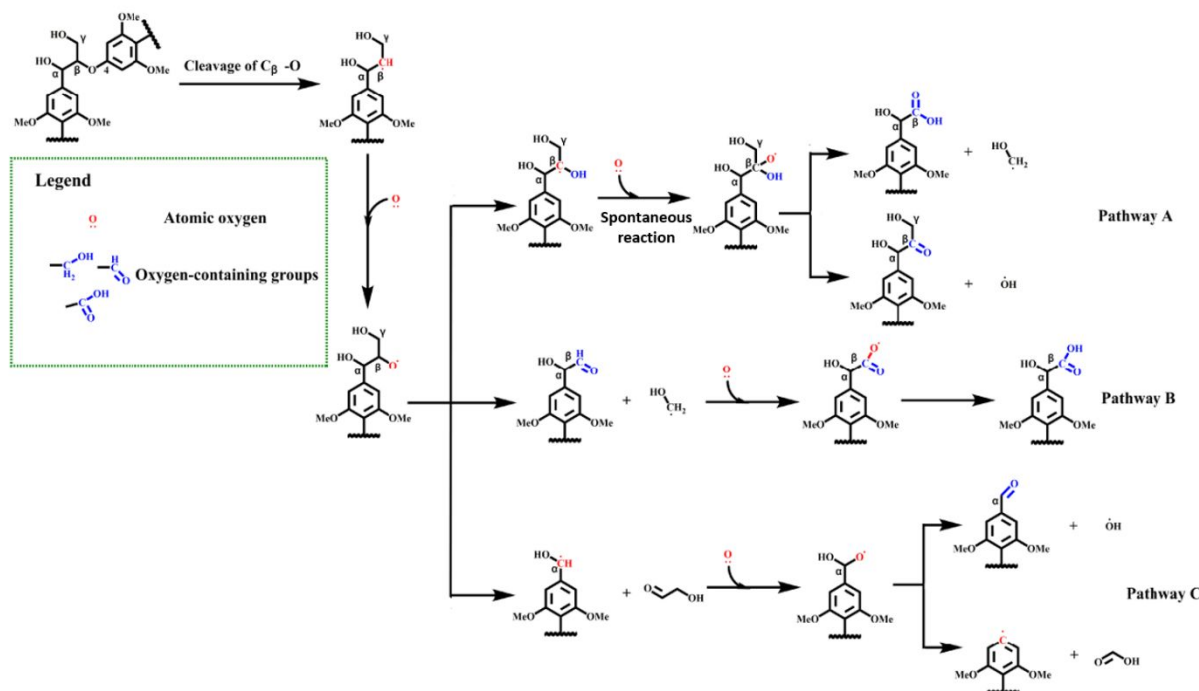


Figure 10: Proposed mechanism for the interaction of plasma-generated atomic oxygen with a lignin model compound consisting of two monomers connected with a β-O-4 aryl ether bond. DFT studies indicate that the initial C_β-O cleavage followed by a C_β-C_α bond scission (Pathway C) are thermodynamically favored. Reproduced from ref. 157 with permission from American Chemical Society, copyright 2020.

3.1.3 Plasma-assisted liquefaction

Liquefaction is the liquid-phase thermochemical conversion of biomass under mild temperatures of 200 - 400 °C¹⁶⁶ in water (hydrothermal liquefaction) or an organic solvent (solvent liquefaction).^{167,168} Water and alcohols are the most common solvents. They are both polar and protic and can be hydrogen donors aiming at bio-oil production with less oxygen.¹⁶⁹ Liquefaction in organic solvent-water mixtures and microwave-assisted liquefaction have also attracted considerable interest.¹⁶⁶ Plasma-assisted liquefaction, based on *in-liquid* discharges, i.e., plasma electrolysis, has been proposed only recently. The studies are summarized in Table 6 and further described in the main text. In all the reports, the authors quantify the 'liquefaction liquid product yield' as:

$$\text{Liquefaction yield (\%)} = 100 - \frac{\text{Mass of solid residue}}{\text{Mass of raw biomass}} 100\% \quad (\text{R15})$$

Table 6: Summary of plasma-assisted liquefaction

Substrate	Plasma treatment	Main Results	Ref.
Bamboo shoot shell (BSS)	In-liquid plasma, PEG / EG mixture and H ₂ SO ₄ , pulsed DC 800 V, 0.1 A, 50% duty cycle, 100 Hz, 3 min	Liquefaction yield 96.7%	170
Pine sawdust	In-liquid plasma electrolysis, PEG / glycerol mixture and H ₂ SO ₄ , pulsed DC 500 V, 50% duty cycle, 100 Hz, 5 min	Liquefaction yield 99.5%	171
Pine sawdust	In-liquid plasma electrolysis, glycerol, 1% H ₂ SO ₄ , pulsed DC 700 V, 50% duty cycle, 100 Hz, 2 min	Liquefaction yield 97.2%	172

Pine sawdust	In-liquid plasma electrolysis, PEG / glycerol mixture, 1.4% NaOH, pulsed DC 752 J/pulse, 8 min	Liquefaction yield 96.7%	173
Corn cob	In-liquid plasma electrolysis, glycerol, 1% H ₂ SO ₄ , pulsed DC 700 V, 50% duty cycle, 100 Hz, 2 min	Liquefaction yield 91.2%	172
Corn cob	In-liquid plasma electrolysis, PEG / glycerol mixture, 2% H ₂ SO ₄ , pulsed DC 700 V, 50% duty cycle, 100 Hz, 5 min	Liquefaction yield 95%	174
Cornstalk	In-liquid plasma electrolysis, glycerol, 1% H ₂ SO ₄ , pulsed DC 740 V, 0.2 A, 50% duty cycle, 100 Hz, 2 min	Liquefaction yield 87.2%	172
Rice straw	In-liquid plasma electrolysis, glycerol, 1% H ₂ SO ₄ , pulsed DC 700V, 50% duty cycle, 100 Hz, 2 min	Liquefaction yield 72.0%	172

Zhou *et al.*¹⁷⁰ studied plasma-assisted liquefaction using in-liquid plasma discharges to treat bamboo shoot shell in a polyethylene glycol (PEG) / ethylene glycol (EG) solvent mixture and an acid catalyst. Liquefaction was faster than the conventional process, giving a liquid product yield of ~97% in 3 min without external heating. Xi *et al.*¹⁷¹ used plasma electrolytic liquefaction (PEL) inside solutions of PEG and glycerol in sulfuric acid and achieved a liquefaction yield up to 99.5% when treating pine sawdust for 5 min. The authors emphasized the crucial role of the high electric field and H⁺ ions on achieving rapid heating. They also compared the catalytic activity of sulfuric acid, p-toluene-sulfonic acid, sodium sulfate, and sodium p-toluenesulfonate¹⁷² on liquefying various feedstocks, such as sawdust, corn cob, corn stalk, and rice straw (Figure 11).

Zhang *et al.*¹⁷³ studied the plasma electrolytic liquefaction (PEL) of sawdust using alkaline solutions. A transition of the discharge from corona to spark was observed with adding sodium hydroxide (NaOH), with a liquefaction yield at optimum conditions reaching 96.7%. They also tested other basic catalysts, such as sodium carbonate (Na₂CO₃) and sodium bicarbonate (NaHCO₃); even though they obtained high liquefaction yields again, the optimum conditions differed for each catalyst due to a change in the liquefaction rate that follows the trend NaOH > Na₂CO₃ > NaHCO₃.

The heating effects in the PEL processing of sawdust were studied by Jiang *et al.*¹⁷⁵ through solution resistance measurements. Electric field heating was dominant in the initial stage of the process, while plasma discharge heating became the primary thermal source for longer processing times and higher power. Thus, solution resistance and discharge heating have a synergistic effect. The mechanism of liquefaction driven by *in-liquid* discharges is even more complex. Zhou *et al.*¹⁷⁶ attempted to elucidate the main pathways governing the plasma-catalytic liquefaction of algae. Despite the non-lignocellulosic structure of algae, which mainly consists of proteins, lipids, and cellulose, a generic mechanism is assumed that involves a) acid-base catalyzed depolymerization, b) heat accumulation and thermal degradation, and c) radical-based oxidation and degradation initiated in the discharge bubbles.

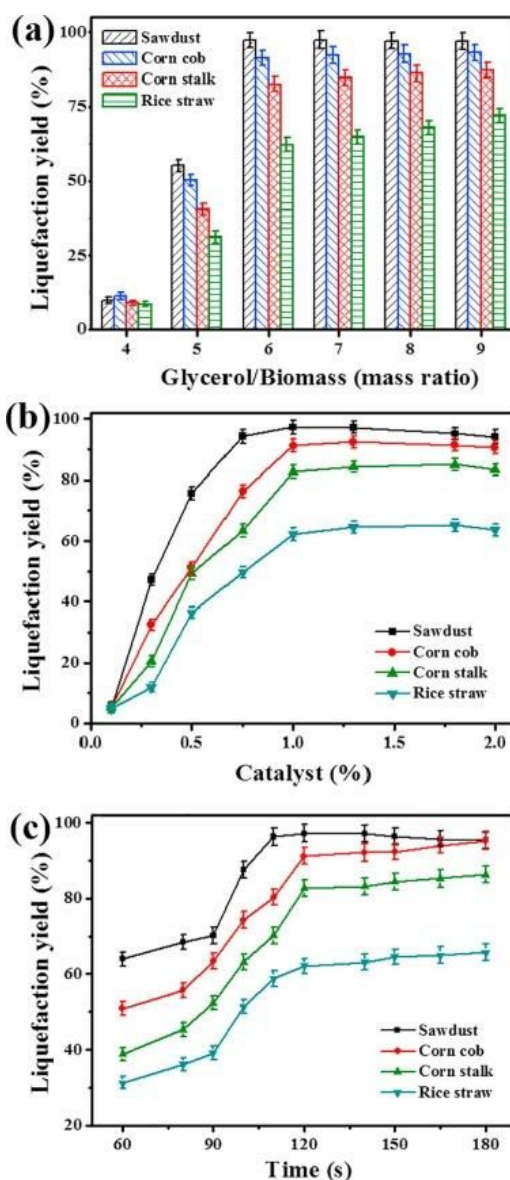


Figure 11: (a) Effect of glycerol to biomass mass ratio on liquefaction yield (biomass 5 g; mass percentage of sulfuric acid 1%, liquefaction time 2 min). (b) Liquefaction yield from four biomass types as a function of the percentage of catalyst (biomass 5 g; mass ratio of glycerol/biomass 6:1; liquefaction time 2 min). (c) Liquefaction yield of four lignocellulosic sources vs. time (biomass 5 g; mass ratio of glycerol/biomass 6:1; mass percentage of sulfuric acid 1%). Reproduced from ref. 172 with permission from Elsevier, copyright 2018.

The analysis of the plasma-assisted liquefaction products is involved. Typically, liquid products are identified using gas chromatography-mass spectrometry (GC-MS). The liquid (bio-oil) product and the solid residue are characterized using elemental analysis and infrared spectroscopy (FTIR). While the main bands in the IR spectra are retained in the liquid and solid products, the relative contribution of each peak differs. The elemental analysis shows a lower carbon content and a higher oxygen content in the solid residue. In contrast, the liquid exhibits a higher carbon content and less oxygenated products, translating to an increase in the high heating value (HHV) compared to the native biomass feedstock.^{173,174,177}

Most plasma-assisted liquefaction studies compare their results to those of other liquefaction technologies that use either conventional heating (oil bath, autoclave, etc.) or non-conventional methods based on microwaves and ultrasound. Plasma electrolytic liquefaction showed remarkably higher energy efficiency compared to all the other technologies, as shown in Table 7.^{173,174,177} Considering the much higher liquefaction rates, the possibility of running in alkaline solutions, and the applicability to several biomass feedstocks, plasma-assisted liquefaction is an up-and-coming biomass conversion technology. However, it is imperative to investigate further the interplay among the plasma heating effects, the electric field, the ion mobility, and the radical contribution to the reactions with the complex biomass molecules. Moreover, hardware should be considerably improved to address current shortcomings, such as the erosion and release of metal ions from the discharge electrodes.

Table 7: Comparison of energy consumption in different liquefaction methods as discussed by Tang et al.¹⁷⁴ Plasma electrolysis shows an order of magnitude less energy consumption for the liquefaction of 5 g biomass than the microwave system; conventional heating shows much higher values.

	Biomass (g)	Time (min)	Liquefaction yield (%)	Energy consumption (kWh ⁻¹)
Oil bath	10	120	91.4	1.6
Autoclave reactor	10	112	95	1.87
Microwave	5	10	99	0.08
Plasma electrolysis	5	5	99.1	0.006

3.1.4 Plasma-assisted torrefaction

The biomass quality by means of heterogeneity, energy density, hydrophobicity, and grindability can be upgraded before thermochemical conversion via torrefaction, a low temperature (pre)treatment. This process differs from conventional drying since the chemical transformation of biomass is also enabled besides moisture removal.¹⁷⁸ It is also considered a mild form of pyrolysis running at 200-300°C under inert and reduced conditions. Devolatilization, depolymerization, and carbonization reactions are enabled in this temperature range, forming a brownish uniform solid, as well as condensable (water, organics, and lipids) and non-condensable (CO₂, CO, and CH₄) gaseous products.¹⁷⁹ Due to the low operating temperatures and high moisture content of biomass, which may impose severe disturbances and fluctuations to the discharge, plasma has hardly been used in this process. Shuangning *et al.*¹⁸⁰ utilized an Ar plasma as a heat source in a laminar entrained-flow reactor to enable devolatilization reactions at a slightly higher temperature. Wheat straw, coconut shell, rice husk, and cotton stalk were used. They concluded that the yield of volatile products depends both on the operating temperature and residence time while the devolatilization process becomes increasingly faster with increasing the operating temperature. Importantly, they reported an 84% total sugar yield in enzymatic hydrolysis upon applying plasma torrefaction. This high yield, which was ascribed to the high operating temperatures (direct and effective heating) and short residence times (high heating rates imply shorter residence times suppressing secondary reactions), is a promising result, but further studies are needed to fully exploit the potential of plasma for torrefaction applications.

3.2 High and very high-temperature biomass conversion

Unlike low-temperature plasma treatment, high and very high-temperature biomass plasma treatment is only performed in the dry, plasma-to-solid interaction mode. DBDs are not suitable since high temperatures cannot be attained; however, the working principle is similar to the one described for low-temperature dry treatment (Section 3.1.1). The primary difference lies in the reactions enabled in each process due to variation of temperatures and plasma agents: in pyrolysis, a mild temperature biomass treatment process in the absence of an oxidizing agent, hydrogen abstraction reactions dominate the chemistry; in gasification, a high-temperature biomass treatment in the presence of an oxidizing agent, (partial) oxidation reactions are enabled and dominate. In tar removal processes, both reactions may be enabled. Herein, we discuss prominent works of the plasma processes mentioned above, underscoring the main findings and mechanistic conclusions. The main findings are organized in tables followed by a detailed description of the experimental approach in each work.

3.2.1 Plasma-assisted pyrolysis

Pyrolysis is a mature thermochemical biomass upgrading process.^{181,182,183} It runs at moderate to high temperatures (500-900°C), with the process gas being either inert, e.g., Ar and N₂, or even reducing like in case of H₂. Biomass is converted into solid (charcoal) and liquid (bio-oil) products at moderate temperatures and gaseous products like syngas, CH₄, CO₂, H₂O, and C₂ at elevated temperatures. The pyrolysis conditions, i.e., reaction temperature, residence times, and heating rates dictate the product yield; in general, low temperatures accompanied by long residence times and low heating rates boost charcoal formation; moderate reaction temperatures and long residence times lead to comparable amounts of liquid, solid, and gas products; moderate reaction temperatures, short residence times, and high heating rates favor liquid formation; and elevated temperatures favor gaseous products.^{24,184} Pyrolysis is typically suggested for liquid product formation rather than gas products. Although high calorific value gases are produced, the gas yield is still low (>40 wt.%) compared to gasification.¹⁸⁵

Entrained flow and bubbling fluidized bed reactors (both fire-heated) are world-widely used for large scale biomass pyrolysis: inert gas flow fluidizes a bed of biomass solids, silica sand and (often) catalyst particles intensifying transport phenomena.¹⁸⁶ Although they feature easy temperature control and efficient heat/mass transfer, the operating cost is high;¹⁸⁶ silica sand and catalyst particles loss are the main cost drivers.¹⁸⁷ In addition, a part of biomass feedstock is burned to meet the pyrolyzer's heat requirements, resulting in significant CO₂ emissions.

The high operating cost can be counterbalanced by increasing the yield and purity of valuable products. Plasma technology has been considered for pyrolytic cracking of biomass since it can overcome major shortcomings of fire-heated pyrolyzers: i) higher energy density promotes much higher operating temperatures (>2773 K¹⁸⁸ vs. maximum 1773 K⁹) that enable cracking reactions of heavy species (i.e., tars) resulting in higher product yields and less by-products (easier purification). In the plasma vicinity, extremely high temperatures may remove contaminants by vitrification (higher purity products). ii) High heating rates (10⁴ K/s¹⁸⁰ vs 10² K/s¹⁸⁹) are applied, giving rise to short residence times (10⁻¹ s¹⁸⁰ vs. 1 s¹⁸⁹); eventually, secondary reactions are inhibited, and product decomposition is prevented

(higher yield per pass). iii) Rapid response to operating conditions variations and quick reach of the new steady-state minimizing material losses (tars formation)¹⁹⁰ caused by a fluctuating temperature profile. Collectively, plasma-assisted pyrolysis achieves higher biomass conversion and lower bio-oil-content than fire-heated pyrolysis; syngas and light hydrocarbons (valuable products) are major products upon fast cooling.^{188,190,191} Further, no biomass feedstock combustion is required. These advantages, however, are partially compromised by the relatively high electricity demand and some technical limitations, including the energy dissipation in the hardware and relatively low electrical-to-chemical energy conversion efficiency, the frequent maintenance, the vulnerability to the high moisture content of biomass (mainly for electrode-based reactors), the limited heat integration, and challenges in upscaling.

Further, plasma is not the only technology with superior features to fire-heated reactors. Solar receivers and concentrators are promising for biomass pyrolysis since they also attain high operating temperatures (~ 2273 K)¹⁸⁹, rapid heating rates ($>10^2$ K/s)¹⁸⁹, and product yields¹⁹². In addition, they are powered solely by renewable electricity. Like plasma, solar receivers and concentrators must overcome technological barriers for widespread implementation. Interested readers in solar technology are referred to a recent report on solar-biomass pyrolysis and relevant concepts.¹⁹³

Given that plasma pyrolysis is the most mature biomass treatment, all the above-mentioned reactor-plasma sources have been exploited, including DC torch,¹⁸⁸ corona,¹⁹⁴ CCP-RF¹⁹⁵ and ICP-RF,¹⁹⁶ and MW plasmas,¹⁹⁷ either in continuous or pulsed mode and hybrid configurations.¹⁹⁸ Products of different state and composition form due to different temperatures activating different reaction paths and the varying biomass composition. The most notable works on plasma pyrolysis of biomass are summarized in Table 8.

Table 8: Overview of plasma pyrolysis of biomass. Feedstock source, operating conditions, and key results are reported. Pyrolysis involves no liquid phase (purely dry treatment).

Substrate	Plasma treatment	Main Results	Ref.
Wood and rice husk	Continuous DC plasma torch, Ar/H ₂ , 270 V, 150 A	Gaseous products: H ₂ , CO, C ₂ H ₂ and CH ₄ , maximum carbon and oxygen conversion of 79% and 72%, respectively, product gas suitable for syngas applications	188
Waste rapeseed oil	AC gliding arc plasma, N ₂ , 1.5 kV, 0.2 A, 0.3 kW	Higher syngas production with better energy efficiency at elevated voltage, lower syngas yield at higher waste oil feed rate and N ₂ flow rate, graphite formation	199
Sunflower-oil cake	Plasmatron, N ₂ , 14-22 kW, ~ 5 min	Short time for sunflower-oil cake pyrolysis, non-leachable vitrified slug/residue	200
Rice straw residue	Plasmatron, N ₂ , ~ 5 kW, 3 min	High heating rate, short heating time, non-leachable vitrified slug/residue, biomass moisture increased H ₂ and CO ₂ amount in the gaseous product	191
Rice straw residue	Continuous CCP-RF, N ₂ , 13.56 MHz, 2 kV, 137-591 W, 1 mbar	Faster heating, higher residues retainment, neither corrosion nor tar formation, short	195,201

		time to steady state, and higher syngas quality than the traditional (electric–thermal) thermolysis	
Fir sawdust	Continuous CCP-RF, N ₂ , 13.56 MHz, 1.6-2 kW, 30-80 mbar	Increased syngas yield, production of char with high porosity for activated carbon after a further upgrade, higher energy efficiency	190,202
Waste wood	Continuous MW, Ar, 2.45 GHz, 1 kW, 200 mbar	Complete pyrolysis, liquid (bio-oil) as the main product, product mean ratio of liquid: solid: gas = 66:20:13 on mass basis	203
Spirulina, rice straw and banyan leaves	Continuous MW, N ₂ , 2.45 GHz, 1 kW, ambient pressure	H ₂ major product, 50% (dry mass basis) of algae hydrogen content converted to hydrogen gas, and an establishment of the operating window for H ₂ productivity enhancement	197,204,205
Water hyacinth	MW-metal interactions induced plasma, He, 2.45 GHz, 0.8 kW, ambient pressure	Bio-oil composition/material of metal coils interaction, significantly lower oxygen and hydrocarbon content than pyrolytic bio-oils, no water content in bio-oil produced by MW-metal interactions induced plasma	206

Zhao *et al.*¹⁸⁸ employed a DC plasma torch consisting of a rod-shaped, tungsten-made cathode and a tube-shaped, water-cooled, copper-made anode to facilitate biomass pyrolytic conversion in an argon/hydrogen plasma to produce H₂, CO, C₂H₂, and CH₄ with up to 79% carbon conversion. Wu *et al.*¹⁹⁹ attempted to convert waste rapeseed oil into valuable chemicals using a rotating AC gliding arc plasma. Higher oil and syngas production and better energy efficiency were attained at an elevated applied voltage. Liquid products consisted of alkanes, cycloalkanes, olefins, and aromatic hydrocarbons.

Shie *et al.*²⁰⁰ conducted a study on plasmatron (the operating mode was unspecified; it can be DC, AC, or CCP-RF) on sunflower-oil cake. Various operating conditions were tested. At 973 K, 14–22 kW input power, and ~5 min residence time, the syngas yield was maximized (CO: H₂: CO₂ = 51.2:48.6: 0.2 on a volumetric basis). More recently, Shie *et al.*¹⁹¹ pyrolyze the residue of rice straw at lower powers (10 kW). CO and H₂ were produced at ~90% of the total volume in 3 min; the inorganics were converted into a non-leachable vitrified and non-hazardous slug.

Tu *et al.*¹⁹⁵ used a CCP-RF plasma thermolysis reactor to pyrolyze rice straw waste and elucidate the effect of key system parameters, i.e., loading power, plateau temperature, and time, on performance. They observed high loading powers resulted in high plateau temperatures, attained in short times, leading to complex compounds (tars) and higher quality syngas. In similar follow-up work,²⁰¹ they reported that high heating rates imposed by RF plasma efficiently boosted the production of H₂, CO, CH₄, and to a less extent of C₂–C₅ hydrocarbons.

Tang and Huang¹⁹⁰ also used a CCP-RF plasma pyrolysis reactor to valorize fir sawdust. They explored the impact of operating pressure (30-80 mbar) and input power (1.6-2 kW) on the yield of gas and char, the gas composition, and the char's quality. The gas yield was maximized, that is 66% of the biomass

feed on a mass basis, at 1.8 kW input power and 50 mbar operating pressure, whereas the total CO and H₂ content in the gas product reached 76% vol. on N₂-free, volumetric basis. The solid product featured a large Brunauer-Emmett-Teller (BET) surface area, a high pore volume with a significant prevalence of micropores. In a follow-up work,²⁰² the impact of additional operating parameters like power input and electrode distance on gas/char yield and quality was explored. The comprehensive energy analysis (**Figure 12**) of the CCP-RF biomass pyrolysis indicates a need for energy efficiency improvement.

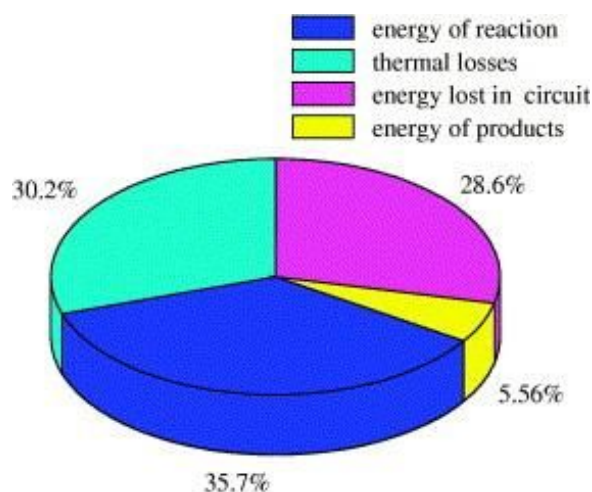


Figure 12: Energy analysis of CCP-RF biomass pyrolysis: energy dissipation and allocation in the different steps involved in RF plasma pyrolysis. Reproduced from ref. 202 with permission from Elsevier, copyright 2005.

Given the limiting energy dissipation in biomass plasma treatment, Lupa *et al.*²⁰³ examined a novel, less energy-intensive microwave plasma source. Waste wood samples were pyrolyzed in Ar plasma, powered by a water-cooled magnetron. Complete pyrolysis was attained; the mean mass ratio of liquid, solid, and gas was 66:20:13.

Hsiao and coworkers^{197,204,205} used a similar MW plasma reactor at atmospheric pressure on various cellulose-based feedstocks, i.e., spirulina, rice straw, and banyan leaves. At elevated microwave power levels associated with high reaction temperatures, H₂ increased while CO₂ and CO decreased. At the absorbed microwave power of 0.8 to 1.0 kW, ~20% to ~50%, respectively, of hydrogen atom mass content in dry algae was converted to hydrogen gas. Using an advanced MW plasma reactor, Bashir *et al.*²⁰⁶ investigated the feasibility of microwave-metal interaction induced plasma for bio-oil production from water hyacinth. The bio-oil composition was strongly affected by the material of metal coils. In contrast, the produced bio-oil oxygen and hydrocarbon content was significantly lower than in conventional pyrolysis.

Finally, Konno *et al.*²⁰⁷ compared the decomposition of cellulose by MW (2.45 GHz) and RF plasma (13.56 MHz) in an Ar plasma. They concluded that the cellulose conversion and syngas amount in the MW plasma was higher than that in RF that produced other gases.

Biomass-derived bio-oils have also been treated in an inert atmosphere and mild temperatures (much lower than the pyrolysis ones) to produce oxygen-free products. In all cases, low energy density discharges were employed,^{208,209} mostly DBDs.^{210–212}

Mechanistic studies on the dissociation-recombination reaction in conventional biomass pyrolysis have been reported. Since cellulose, hemicellulose, and lignin differ in chemical structure and reactions evolve,^{213–215} the reaction mechanism has been studied for individual compounds. Cellulose is primarily cracked in a primary step to light gases like CO and H₂, and organic molecules, such as hydroxyacetaldehyde, hydroxyacetone, pyruvic aldehyde, acetaldehyde, and formaldehyde, which are further broken in a secondary step to syngas.²¹⁶ Lignin dissociates to phenol and styrene and then to CO, CO₂, and CH₄.^{217,218} Hemicellulose forms pentose/hexose and xylose intermediates that dissociate to H₂, H₂O, CO, CO₂, HCHO, CH₃OH, C₂H₅OH, and char.²¹⁹

The biomass reaction mechanism of plasma-assisted pyrolysis is more complicated due to very high heating rates, temperatures, and short residence times. In inert plasmas, i.e., Ar and N₂, heat transfer shall be adequately described to obtain mechanistic insights.²²⁰ In reactive plasmas (H₂), the mechanism is way more complex arising from plasma-driven radical chemistry and heat transfer phenomena. When hydrogen is the plasma agent, high concentrations of hydrogen radicals generated in the plasma zone (Reactions 16 and 17)¹⁸⁸ enable hydrogen abstraction (dehydrogenation) reactions:



Figure 13 overviews the most important reactions.

Cellulose pyrolysis in a hydrogen plasma environment

Cellulose is thermally cracked primarily to hydroxyacetaldehyde and threose via breaking the pyran ring.^{221,222} Threose dehydrates to hydroxyacetone, pyruvic aldehyde, acetaldehyde, formaldehyde, and CO.^{221,223,224} In the secondary pyrolysis step, hydroxyacetaldehyde directly converts to CO, formaldehyde, and hydrogen through consecutive hydrogen abstraction reactions.^{223,225} Hydroxyacetone and pyruvic aldehyde also convert into smaller molecules (formaldehyde and syngas, respectively) through thermal cracking of the C–C around the ketone group²²⁶ followed by hydrogen abstraction.²²³ Acetaldehyde converts into CH₃ radicals and CO in a two-step (hydrogen abstraction and thermal cracking) reaction. CH₃ radicals form C₂ species and CH₄ through C-C coupling, hydrogen abstraction, and hydrogenation,²²⁷ whereas formaldehyde gives syngas.²²⁸ Overall, cellulose pyrolysis in a hydrogen plasma mainly results in syngas and, to a lesser extent, to light olefins. CO primarily results from the carbonyl group and H₂ from hydrogen abstraction reactions.

Lignin cracking in a hydrogen plasma

Lignin is thermally cracked primarily to styrene and phenol.^{229,230} In secondary pyrolysis, styrene gives benzene and acetylene through thermal cracking of the C–C bond between the benzene ring and its side chain.^{229,231} Phenol gives phenyl and phenoxy radicals via thermal cracking of the O–H bond and C–O bond via hydrogen abstraction.²³² Benzene and the phenyl radical finally dissociate to acetylene, hydrogen, and carbon soot via hydrogen abstraction and hydrogenation reactions.²³³ Phenoxy radicals form CO, H₂, and acetylene through thermal cracking and recombination reactions.²³⁴ In summary, CO, H₂, and acetylene are co-produced in a hydrogen plasma of lignin.

Hemicellulose pyrolysis in a hydrogen plasma

Hemicellulose could be considered a mixture of xylose, glucuronoxylan, and o-acetyl xylose.²³⁵ It is primarily converted into smaller molecules via thermal breaking of the pyran ring followed by dehydration, isomerization, and decarbonylation reactions. Due to its complex structure, many liquid

frequent maintenance, and capital cost still merit further improvements.²⁴² Among the plasma technologies, DC²⁴³ and AC^{244,245} arc plasma torches have vastly been used for organic material gasification due to more effortless scalability than other technologies. Nevertheless, RF-²⁴⁶ and MW-²⁴⁷ driven plasmas have also been launched at high capacities, overcoming the limitations of the electrode-based DC/AC plasmas. Moreover, there is a need to develop models to predict and optimize heat transfer and gas-liquid flow patterns. Current reactor designs are almost entirely empirical. The inability to control the degree of ionization and temperature is another limitation. Usually, reactor temperatures are much higher than needed for gasification/pyrolysis. This implies a low energy (and exergy) utilization efficiency (i.e., conversion of excessive electricity to heat), a need for complex heat integration schemes downstream of the reactor, risk of thermal failure of the materials of construction and challenges in insulation to minimize heat losses. It is also challenging to measure temperatures above 2500 K. An overview of biomass plasma gasification is given in Table 9.

Table 9: Overview of plasma gasification of biomass summarizing feedstock source, critical operating conditions, and key results. Gasification involves no liquid phase (purely dry treatment).

Substrate	Plasma treatment	Main Results	Ref.
Crushed wood	Continuous DC plasma torch, Ar/N ₂ /H ₂ O, 210-280V, 250-500 A, 40-133 kW	Syngas production, homogeneous heating, complete destruction of the feedstock, tuning syngas composition via oxygen mass flow/feedstock feed rate	248–254
Rice hull and wood waste	Continuous (transferred and non-transferred) DC plasma torch, air, 50-200 kW	Full decomposition of high-molecular biomass feedstock, high-quality raw material for heat power engineering and chemical industries (up to 90 % of combustible components)	255
Olive pomace charcoal, forest logs residues and energetic plants, crushed wood and glycerol	Continuous DC plasma torch, Ar/H ₂ O (steam), 180-250 V, 140-180 A, 25-45 kW	Production of high-energy syngas, presence of H, OH, and O radical in plasma zone, stable operation	44,256–258
Bio-oil	Continuous DC plasma torch, Ar/H ₂ O (steam), 25 kW	Necessity of injection parameters optimization, avoidance of droplets formation, optimization of plasma power to bio-oil flow-rate ratio	259
Biomass tar (toluene)	Non-thermal pulsed DC plasma, H ₂ O (steam), 4.8 kV, 3.6 mA	Plasma-catalyst synergy: plasma enhanced toluene decomposition; catalyst increased syngas selectivity	260
Glycerol	Pulsed DC (corona) plasma, H ₂ O (feedstock moisture content), 10 kHz, ~6 kV, 7 mA, 20.0-22.8 W	Selectivity >80%, syngas concentration >94%	261

Hard wood shavings residue, PB&MDFB, peach pits, almond hulls, grape pomace, coffee ground	Continuous DC plasma torch, steam with H ₂ /CO, 380 V, 150 A, 22.4-39 kW	Feedstock source flexibility, high H ₂ yields (up to 77% on molar basis)	262
Solid biomass (papermill waste)	Continuous non-transferred thermal DC plasma torch, O ₂ , 340-360 V, 200 A, 80-100 kW	High purity H ₂ (>99.99%) from biomass waste, necessity of process scale-up and H ₂ production cost reduction	263
Corn cob	Non-thermal AC arc plasma, Ar, N ₂ , air and moisture presence, 50 Hz, 200 mA, 10 kV, 25.2 W, 6 min	Increased carbon conversion and CO selectivity with moisture increase, corn cob modifications after the plasma treatment: specific surface area increase, fine protrusions structure, dense tiny pores	264
Wood residue	AC arc plasma, air and moisture, up to 50 kW	High calorific value syngas production, gasification enhancement by plasma input power increase, downdraft with twin-fire scheme (configuration) and air (oxidant) suggested for efficient plasma gasification	265–268
Wood	AC plasma torch, air, and moisture presence, up to 100 kW	Simple process, promising for wood gasification, efficient for high energy content syngas	269
Pyrolytic bio-oil (wood originated)	AC arc plasma, H ₂ O (steam), 50 Hz, 0.9 A, 1 kV, 160 W	Tar and (condensable) vapor cracking, higher gaseous and lower liquid product yields, increased H ₂ /CO ratio (2-9) in final syngas stream	270,271
Wood powder	Non-thermal gliding arc, N ₂ /H ₂ O (steam), ~100 kHz, 0.4-0.7 A, 1-8 kV, ~1 kW	H ₂ production enhancement by water dissociation, carbon conversion and reaction rates enhancement by plasma	272
Municipal solid waste/raw wood mixture	Plasmatron, N ₂ /H ₂ O (steam), 2.5-5.0 kW, ~2 min	Very short time for feedstock gasification, H ₂ increase with steam addition, 0-4.5% wt. non-leachable vitrified slug/residue	273
Distillers grains residue	Plasmatron, N ₂ /H ₂ O (steam), 2-4 kW, <1 min	Syngas yield (mass basis) increase and CO ₂ decrease (via water-shift reaction enhancement) with steam increase	274
Cellulose	Continuous MW, air/N ₂ , 2.45 GHz, 4 kW, ambient pressure	Syngas chemical energy/plasma energy input = 1.84	247

Byproduct from a real industrial fermenter	Continuous MW, air/N ₂ , 2.45 GHz, 6 kW, ambient pressure	High carbon conversion efficiency (89%) and near-equilibrium syngas composition (H ₂ :CO:CO ₂ = 41:53:6 on a molar basis)	40
Biodiesel production byproduct (glycerol)	Continuous MW, N ₂ /O ₂ /H ₂ O (steam), 2.45 GHz, 2 kW, ambient pressure	High gasification efficiency and syngas heating value at elevated MW power, decreased O ₂ /steam flow (O ₂ /fuel = 0.4) and fine droplet size	275

Van Oost *et al.*²⁴⁹ reported the gasification of wood chips in a hybrid argon-water stabilized DC plasma torch (160 kW). Syngas of high caloric value was produced, and a higher H₂ concentration than in the conventional biomass treatment was attained. In a later study, Van Oost *et al.*²⁵⁴ investigated the crushed wood pyrolysis in a similar DC plasma torch, cofeeding water along with argon to stabilize the discharge and promote biomass gasification. The vortex imposed by Ar gas flow shielded the plasma torch and protected the cathode, extending its lifetime. The anode comprised a rotating water-cooled disc, and a water-cooling system kept the wall temperature at 1700 °C. Hydrogen (28–46%), CO (44–68%), CO₂ (2–8%), and Ar (0.2–8%) were detected, whereas longer hydrocarbons and tar were negligible. Using the same setup, Hrabovsky *et al.*^{250,251} observed that the composition of syngas from feeding crushed wood was only slightly influenced by the feedstock feeding rate and power input and was tuned by the ratio of oxygen to the solid flow rates. Hlina *et al.*^{252,253} carried crushed wood gasification experiments with the same setup and confirmed the reactor suitability due to low flow rates and high inner temperatures.

An'shakov *et al.*²⁵⁵ described a plasma-driven gasification system, operating with a non-transferred DC plasma torch along with continuous air supply, as a promising technology for rice hull and wood waste gasification. High-quality syngas containing up to 90% combustibles was produced.

Grigaitiene *et al.*²⁵⁶ developed a water vapor plasma technology using a DC plasma torch with a button-type cathode and step-formed copper anode operating at atmospheric pressure. Spectroscopic analysis revealed that water vapor plasma increased the amount of hydrogen over other gasification processes, and stable operation was achieved. In an entrained bed plasma-chemical reactor powered by the same plasma source, Tamosiunas *et al.* gasified glycerol and crushed wood^{257,258} and olive pomace charcoal⁴⁴ in an argon/water mixture to produce syngas. Guenadou *et al.*²⁵⁹ demonstrated bio-oil gasification, assisted by a thermal DC plasma torch, in the presence of water. The penetration parameters and plasma power input were tuned to allow bio-oil injection inside the plasma core (where the temperature is the highest) for high gasification performance. Tao *et al.*²⁶⁰ evaluated various thermochemical routes namely, direct thermal decomposition, plasma-assisted decomposition, catalytic steam reforming and plasma enhanced catalytic steam reforming of biomass (tar), using toluene as a model compound. Unlike previous works, a non-thermal pulsed DC plasma of negative high voltage was ignited to enhance cracking and recombination reactions. The synergy between plasma and catalyst (Ni/SiO₂) enabled the highest toluene conversion and syngas formation; the plasma accelerated the toluene decomposition while the catalyst selectively promoted syngas reactions formation. A similar pulsed DC corona plasma was also employed by Zhu *et al.*²⁶¹ for glycerol reforming to syngas (selectivity >80%) in the presence of small fractions of water at low temperature and atmospheric pressure, without external heating.

Diaz *et al.*²⁶² implemented a two-stage high-temperature steam plasma system to produce a H₂-rich gaseous product from a diverse feedstock including hard wood shavings residue, particle board and medium density fiber board (PB&MDFB), peach pits, almond hulls, grape pomace, and coffee ground. In the first stage, a glow discharge catalyzed the electrolyte preparation, which consisted of steam and H₂/CO fractions. In the second stage, a continuous DC plasma torch gasified the biomass feedstock in the effluent stream of the first stage. Hydrogen yields of 52-77% on a molar base were obtained.

Byun *et al.*²⁶³ applied thermal plasma gasification to produce high purity H₂ (>99.99%) from solid papermill waste. A continuous non-transferred thermal DC plasma torch was coupled with a H₂ recovery system; the raw syngas produced by plasma gasification was first fed into a water-gas-shift reactor to increase the H₂ content (CO + H₂O → H₂ + CO₂) and then treated using a pressure swing adsorption.

To limit the energy dissipation into gas heating, Du *et al.*²⁶⁴ utilized a non-thermal AC arc plasma to gasify corn cobs. Different plasma agents, namely, argon, nitrogen, and air, were used. Air was beneficial for higher gas yields and CO selectivity than the non-oxidized gases, while moisture improved the gas yield, particularly H₂ formation, carbon conversion, and the H₂/CO molar ratio.

Brattsev *et al.*^{265,266} and Kuznetsov *et al.* worked on wood residue gasification using an AC arc plasma and air as the gasifying agent. They investigated the impact of operating parameters on the syngas quality. High calorific value syngas was produced. The moisture content did not impact syngas quality but decreased syngas yield. Popov *et al.*²⁶⁸ performed equilibrium calculations of the same gasification setup. Compared to previous works,²⁶⁵⁻²⁶⁷ a downdraft design with a twin-fire scheme and air were the most effective plasma configuration and oxidizer for plasma gasification of wood waste.

Further, Rutberg *et al.*²⁶⁹ performed an energy analysis of the syngas produced via plasma-driven wood gasification for heat and power cogeneration. They reported that 8.6 MJ/kg_{wood} of electric energy and 7.5 MJ/kg_{wood} of thermal energy could be cogenerated by the syngas produced by wood (20% moisture) gasification with alternating current (AC) plasma torches.

Luche *et al.*²⁷⁰ examined the improvement of the conventional biomass processing by implementing a plasma booster downstream to destroy tars and aerosols to produce high H₂-content syngas. Indeed, the amount of syngas increased, and the liquid product decreased. Part of condensable vapors and 45% of tars were cracked by the plasma, resulting in a slight H₂ increase from 18 to 20% and CO decrease from 63% to 61%.

Arabi *et al.*²⁷¹ investigated plasma-steam reforming of alcohols/bio-oils/water mixtures and direct plasma treatment of beech wood using the apparatus of Ref.²⁷⁰. They reported that alcohol/bio-oils/water reforming produced high H₂ content syngas with CO and CO₂ concentrations comparable to the conventional thermochemical routes.

Given that plasma enhances reaction rates through free radicals and energy utilization efficiency, Pang *et al.*²⁷² compared conventional gasification to non-thermal plasma-assisted gasification. A non-thermal gliding arc plasma of wood powder in steam increased ~10% the carbon conversion and ~30% the reaction rates over traditional heat sources. The relevant results are presented in Figure 14.

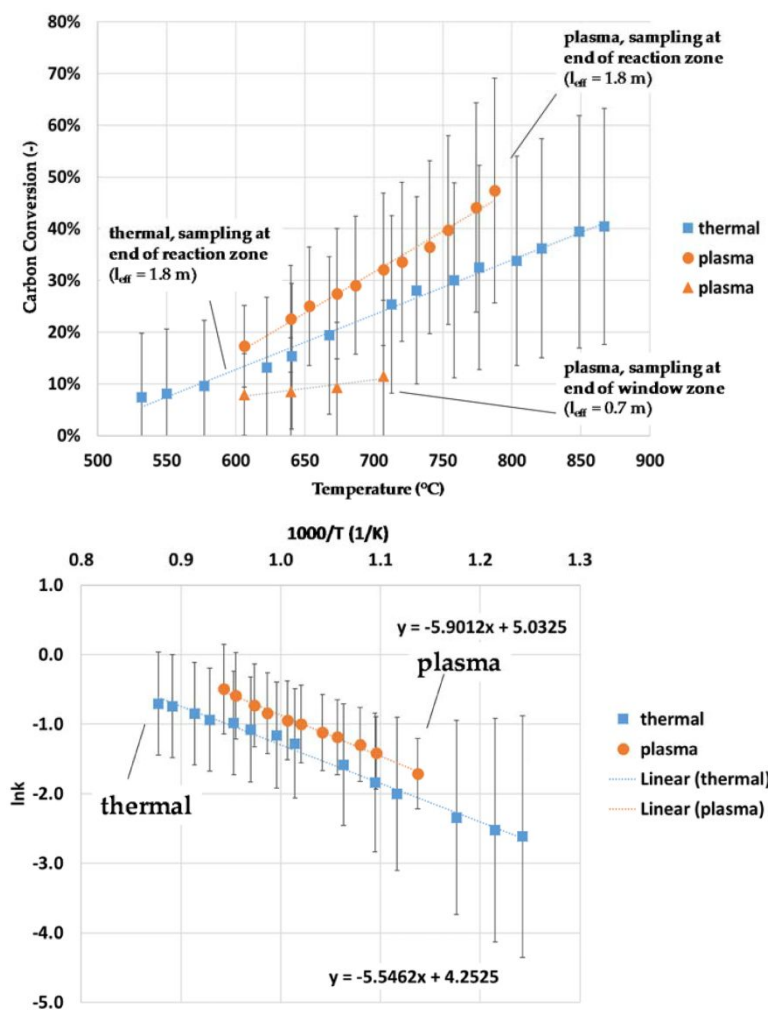


Figure 14: Carbon conversion and reaction kinetics of thermal and plasma wood powder gasification: orange = plasma; blue = thermal.²⁷²

Shie *et al.*²⁷³ evaluated the plasmatron used in pyrolysis^{191,200} for gasification. Municipal solid waste with raw wood and steam were used. About 90% of the gaseous products were produced in 2 min. The syngas yield ranged from 88.6 to 91.8% on a molar basis, assisted by steam methane reforming, hydrogasification, and the Boudouard reactions. Shie *et al.*²⁷⁴ also gasified distillers grains residue to syngas (~95% on a molar basis) in < 1 min.

To avoid severe electrode corrosion, Stefanidis and coworkers²⁴⁷ employed an electrodeless reactor with an external MW-generated plasma energy source to enable cellulose gasification by air at high energy efficiency. Gasification and plasma generation occurred in a unique reactor to enable long residence times in the plasma zone. The produced syngas' heating value exceeded the net microwave energy channeled into the plasma by 84%. Delikonstantis *et al.*⁴⁰ evaluated the suitability of MW-plasma based gasification technology for complex organic biomass valorization. Particularly, air/N₂ gasification experiments of a byproduct stream from a real industrial fermenter were carried out and demonstrated stable and efficient operation with high carbon conversion efficiency and near equilibrium syngas composition, as shown in **Figure 15**.

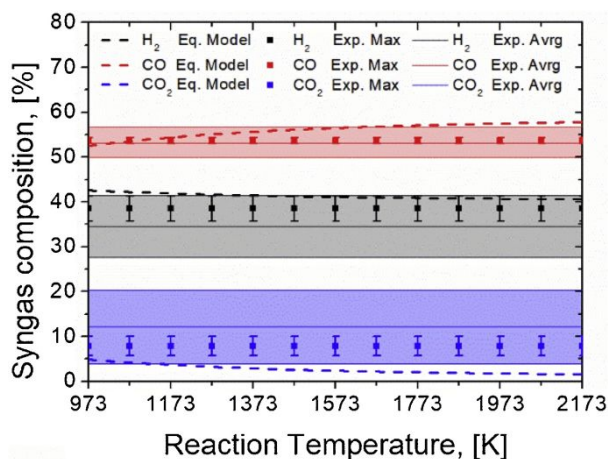
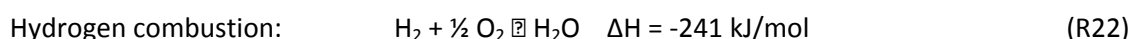
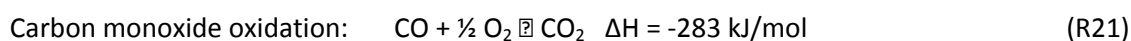
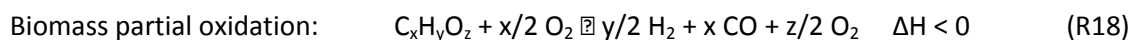


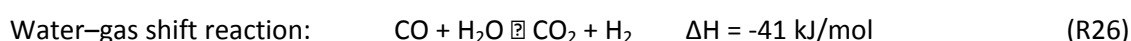
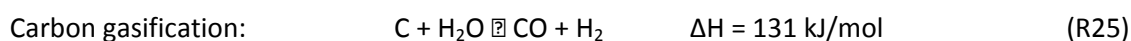
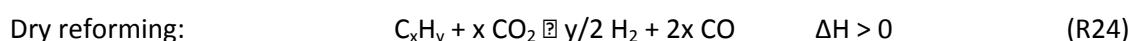
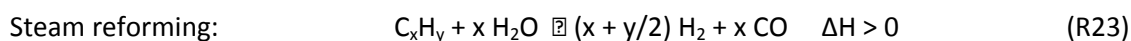
Figure 15: Comparison between experimental and theoretical (based on equilibrium predictions) syngas composition over the temperature range 973–2173 K. Reproduced from ref. 40 with permission from Elsevier, copyright 2019.

Yoon *et al.*²⁷⁵ demonstrated syngas from biodiesel production byproducts (glycerol was used as a model compound) in an MW plasma torch. The input power, gasification agent flow (O_2 and steam), and fuel droplet size were critical to attaining high gaseous product yield and gasification efficiency.

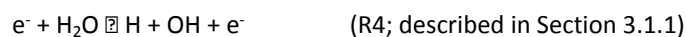
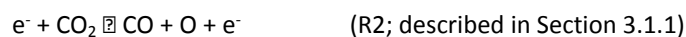
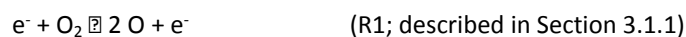
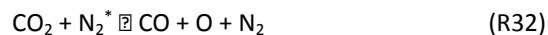
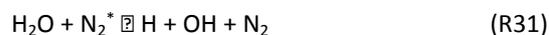
The energy required in pyrolysis to drive the endothermic biomass cracking reactions is externally supplied (allothermal process). In contrast, the energy in gasification is provided by partial oxidation of biomass occurring in the pyrolytic chamber along with other reactions. Overall, the following overall reaction sequence could generally describe the gasification process:²⁴² (Partial) oxidation (exothermic), drying (endothermic), pyrolysis (endothermic), reduction (endothermic), and tar/heavy molecules cracking (endothermic). The oxidation reactions are:



The energy release is channeled into drying and pyrolytic cracking reactions, producing a mixture of CO , CO_2 , and water. When air is used as the oxidizing agent, the product also contains N_2 . In the reduction phase, the products of the pyrolysis and oxidation react to give the final syngas product and tar. The main reactions involved in the reduction phase are:



An oxidizing agent diluted in N_2 gives OH, O and N radicals, enabling additional reaction paths namely, stepwise dehydrogenation and oxidation of molecules produced in primary pyrolysis and tar cracking. Depending on the oxidant, radicals may form via the following reactions:^{67,70,260-262}



OH radicals and, to a less extent, O and N_2^* (mainly nitrogen metastable states $N_2(A^3\Sigma^+)$ and excited states $N_2(a')$ and $N_2(B)$), favor dissociation reactions through H abstraction²⁷⁶⁻²⁷⁸ leading to CO, CO_2 , and H_2O . Reactive intermediates react with O and OH to form stable oxygen-enriched products.²⁷⁶ Water, formed in pyrolysis by OH and O radicals, initiates water-driven equilibrium reactions (R23-26; favored in pyrolysis operating temperatures) through which light hydrocarbons and chars turn into syngas and a certain fraction of CO to CO_2 . Therefore, biomass gasification results in higher syngas yields with higher CO_2/H_2O and lower C_2 /tars than pyrolysis.

3.2.3 Plasma-assisted tar removal

In biomass pyrolysis/gasification, various organic compounds are coproduced that should be removed prior to syngas utilization. Energy-intensive gas cleaning systems, i.e., scrubbers and selective catalytic reformers, are usually placed at the gasifier outlet for this purpose. Alternatively, such compounds (mostly tars) could be removed using plasmas. Plasma application for syngas conditioning by destructing tar and other heavy residues has extensively been discussed in relevant reviews.^{279,280} An overview of literature reports on plasma-assisted tar destruction is presented in Table 10.

Table 10: Overview of plasma-assisted biomass tar destruction, indicating feedstock, key operating conditions, and results.

Substrate	Plasma treatment	Main Results	Ref.
Toluene, naphthalene or mixture of those	Dry treatment, AC gliding arc, N_2/H_2O or N_2/H_2O , 50 Hz, 59.4 W	Tar conversion enhancement by oxidative species (OH and O radicals), simultaneous syngas quality upgrading and tar removal	276-278,281
Surrogate benzene and naphthalene (both mixtures and separately)	Dry treatment, AC gliding arc, N_2/H_2O , up to 1 kHz, 1 A, 15 kV, 15 kW	Benzene decomposition and energy efficiencies: 95% and 120 g/kWh, naphthalene decomposition and energy efficiencies: 79% and 68 g/kWh	282-286

Naphthalene	Dry treatment, DC gliding arc, O ₂ , air, N ₂ , Ar, 0.07-0.1 A, 0.7-2.5 kV, 20-190 W	Highest destruction rate (92.3%) in O ₂ , faster decomposition at higher O ₂ flow, major tar destruction route: naphthalene oxidation	287
Naphthalene/toluene surrogate	Dry treatment, AC gliding arc with forward vortex flow, air/H ₂ O (steam), 50 Hz, 0.3-0.8 A, 0.9-1.6 kV, ~1 kW	>90% naphthalene and toluene conversion	288
Surrogate benzene	Dry treatment, externally oscillated AC gliding arc, N ₂ /H ₂ O (steam), up to 1 kHz, 1 A, 15 kV, 15 kW	Benzene cracking to syngas and light hydrocarbons, 9% higher decomposition and energy yield at external oscillation application	289
Toluene, toluene/naphthalene/phenol mixture	Dry treatment, rotating DC gliding arc, N ₂ , CO ₂ /H ₂ O (steam), 0.3 A, 1.7 kV, 0.4 kW	High (>90%) tar conversion, major gaseous products: H ₂ and acetylene, excited N ₂ , and O, OH radicals can destruct toluene via H abstraction.	290-292
Naphthalene	Dry treatment, two-stage gliding arc, N ₂ , 30 mA, 7 kV, 0.4-2.7 kW	A single-stage plasma reactor 95% tar destruction efficiency for a single-stage treatment, >99% for a two-stage	293
A mixture of benzene, toluene, and 1-methylnaphthalene, benzene in syngas	Dry treatment, continuous MW, N ₂ , N ₂ /H ₂ O (steam), 2.45 GHz, 1.2-1.8 kW, ambient pressure	Acetylene, soot, benzene derivatives, and cyanides were majorly formed in N ₂ flow; CO, CO ₂ , and H ₂ were majorly formed in N ₂ /H ₂ O (steam) flow	294,295
N ₂ , H ₂ O, ethanol, and tar obtained from pine pyrolysis	Dry treatment, continuous MW, N ₂ /Ar, 2.45 GHz, 1 kW, ambient pressure	Complete tar conversion, major CO, O ₂ , solid carbon and (minor) H ₂ formation, unstable plasma in Ar absence	296
Toluene	Dry treatment, microwave-metal interactions induced plasma, Ar, N ₂ /Ar/H ₂ O, 2.45 GHz, 0.9 kW, ambient pressure	>90% toluene destruction efficiency, in-situ coke removal by steam addition	297
Benzene, toluene, furfural, naphthalene, fluorene and pyrene	Dry treatment, AC DBD, Ni/ZSM-5, Ni/SiO ₂ and M _x Al ₃ catalysts with different metal load (M: Ni or Fe, 0:1, 1:3, 1:1, 3:1, 1:0), N ₂ , O ₂ , H ₂ O, CO ₂ , 10 kHz, 30 kV, 60 W	Higher destruction conversion and reduced by-products formation at higher power inputs, enhanced toluene reforming by O and OH radicals, carbon formation suppression by the catalysts, up to 96% tar removal efficiency and 90% CO ₂	298-301
Toluene	Dry treatment, AC DBD, CeO ₂ -MnO _x , air, 14~ kV, up to 24 W	selectivity with Ce ₁ Mn ₁ catalyst, high BET surface area, smaller pore size and crystalline size for combined Ce and Mn	302

Toluene	Dry treatment, AC DBD, Ni/Al ₂ O ₃ , steam, 9 kHz, 30 kV, 35 W	Enhanced H ₂ yield, enhanced tar removal at higher Ni loadings	303
Toluene	Dry treatment, AC DBD, Ni/Al ₂ O ₃ , steam, 1.5 kHz, 20 kV, 40 W	Increased H ₂ production, higher tar content in the product gas at high steam inputs (catalyst saturation)	304
Toluene	Dry treatment, AC DBD, Ni/Al ₂ O ₃ , N ₂ , 9 kHz, 30 kV	Significant toluene removal increase at higher temperatures (associated with power input), 92% toluene conversion in DBD with 5 wt. % Ni/γ-Al ₂ O ₃ , better performance at higher Ni loadings	305
Toluene	Dry treatment, AC DBD, MnO/Al ₂ O ₃ /Ni, N ₂ /O ₂ , 50 Hz, 30 kV	Improvement of toluene destruction rate and carbon dioxide selectivity, byproducts (ozone) suppression, increased stability and activity of the catalyst	306
Benzene, toluene, naphthalene	Dry treatment, AC DBD, N ₂ , H ₂ , CO ₂ , CO ₂ /H ₂ , CO/H ₂ /O ₂ , 20 kHz, up to 40 W	Incomplete tar destruction in absence of H ₂ (as carrier gas)	307–312
Naphthalene (heavy tar) and phenol/toluene (light tar)	Dry treatment, pulsed DC corona, N ₂ , H ₂ , CO ₂ , CO, 1 kHz, 40-100 kV, ~5 kW	Tar removal driven by CO ₂ dissociation, presence of H ₂ , CH ₄ , moisture and air did not affect the process efficiency	194,313
Toluene	Dry treatment, DC corona, air, 2 mA, 6-18 kV	Decomposition of toluene was driven by energy input; CO ₂ , H ₂ O, and polymeric species were majorly produced	314
Naphthalene	Dry treatment, nanosecond pulsed discharge, N ₂ , 250 A, 30 kV	Complete naphthalene destruction at temperatures much lower than the ones required in conventional processes	315

Gliding arc is the most well-tested plasma technology for tar removal. Tu and coworkers studied tar (from biomass gasification) removal by non-thermal plasma, aiming at high-quality syngas. They employed an AC gliding arc discharge with various cracking routes and operating conditions: steam reforming of toluene²⁷⁶ or toluene/naphthalene mixture²⁷⁷ as model tar compound and steam/CO₂ reforming of the same model compounds.^{278,281} A possible reforming mechanism of toluene/naphthalene mixture to syngas is shown in Figure 16. Chun and coworkers developed a similar gliding arc plasma reactor to remove surrogate benzene and naphthalene. They explored benzene,²⁸² naphthalene,²⁸⁴ mixtures,²⁸³ pyrene,²⁸⁵ and a real pyrolysis gas formed in a continuous-screw-type sawdust pyrolyzer.²⁸⁶ Yan *et al.*²⁸⁷ investigated the impact of carrier gases on naphthalene destruction in gliding arc discharges.

Nunnally *et al.*²⁸⁸ investigated tar removal in a gliding arc reactor with forward vortex flow by cofeeding syngas with naphthalene and toluene tar surrogates and air/water vapor as oxidizing agents. Chun *et al.*²⁸⁹ studied surrogate benzene destruction using an externally oscillated gliding arc, which resulted in discharge area expansion. Zhu *et al.* investigated toluene destruction in a novel rotating gliding arc discharge in N₂²⁹⁰ and CO₂/H₂O²⁹² flow. Xu *et al.*²⁹¹ simultaneously investigated toluene, naphthalene,

naphthalene, and others) and cyanides formed as major compounds; however, their amounts were significantly mitigated in favor of CO, CO₂, and H₂ when steam was added. In a complementary work, Jamroz and Wnukowski²⁹⁵ studied the effect of MW plasma on a simulated biomass syngas stream containing benzene as a model tar compound under identical conditions (Ref.²⁹⁴). The high temperature of the plasma and the presence of reactive species result in a significant increase in CO and H₂. O, OH, and H radicals generated in the plasma zone enhance benzene conversion. Elliott *et al.*²⁹⁶ also evaluated the feasibility of MW plasma systems for tar destruction/reforming at atmospheric pressure. N₂, H₂O, and ethanol were cofed, to simulate the gasifier's gases, with tar obtained from pine pyrolysis. N₂ and Ar were the carrier gases. Complete tar destruction was attained; CO and solid carbon were majorly formed. Sun *et al.*²⁹⁷ employed electrical discharges triggered by MW-metal interactions for tar destruction, using toluene as a tar model compound and Ar as the carrier gas. They demonstrated that MW-tungsten discharges effectively cracked toluene into useful gases (H₂, C₂H_x and CH₄) and solid carbon. The solid products were effectively removed by steam co-fed into the discharge. Although high tar destruction efficiencies are obtained in gliding arc and MW plasma, the selectivity to value-added products may be improved. To this end, catalysts can be placed either inside or downstream of the plasma zone to boost syngas selectivity. However, high energy density plasmas, such as gliding arc and MW, are not suitable due to the energetic plasma species and high bulk gas temperatures destroying the catalyst.³¹⁶ Therefore, plasmas of low energy density and bulk gas temperature are necessary for plasma/catalyst coupling.

Sun and coworkers investigated plasma-catalyst synergy for selective destruction of tar to syngas. They employed a DBD reactor to perform plasma-assisted catalytic oxidation of toluene on Ni/ZSM-5 catalyst,²⁹⁸ plasma-assisted steam reforming of different model tar compounds including benzene, toluene, furfural, naphthalene, fluorene, and pyrene on SiO₂ and ZSM-5-supported Ni-based catalysts,²⁹⁹ as well as on M₁Al₃ catalysts with different metal load (M: Ni or Fe, 0:1, 1:3, 1:1, 3:1, 1:0).³⁰⁰ Moreover, they studied biomass tar destruction via plasma (alone) dry reforming.³⁰¹ With comparable plasma-catalytic reactor concepts, Wang *et al.*³⁰² focused on toluene destruction in a DBD reactor coupled with CeO₂-MnO_x catalysts, Liu *et al.*³⁰³ and Blanquet *et al.*³⁰⁴ performed steam reforming of toluene utilizing Ni/Al₂O₃ catalyst, and Xu *et al.*³⁰⁵ tested N₂ flow instead of steam. Guo *et al.*³⁰⁶ evaluated the efficiency of toluene decomposition in a wire-plate DBD reactor equipped with manganese oxide/alumina/nickel foam catalyst in the discharge area at room temperature and atmospheric pressure. Saleem *et al.* also studied the decomposition of biomass tars in DBD using different gas carriers, such as N₂,³⁰⁷ H₂,^{308,309} CO₂,³¹⁰ CO₂ diluted in H₂,³¹¹ and synthetic product gas (H₂, CO, and CO₂).³¹²

The relatively high energy cost and the complications from using a catalyst led to pulsed corona discharges for tar removal. Drinkenburg and coworkers^{194,313} employed corona discharges for tar removal from a biomass-derived fuel in the presence of N₂, H₂, CO₂, and CO. They found that tar removal was enhanced by O radicals formed via plasma-induced dissociation of CO₂. Moreover, H₂, methane, moisture, and air had no effect on the process efficiency at the tested operating conditions. As opposed to Drinkenburg and his coworkers, Mista and Kacprzyk³¹⁴ employed a DC corona for toluene destruction in air plasma and room temperature; the major byproducts were CO₂, H₂O and polymeric species. Gomez-Rueda *et al.*³¹⁵ recently employed a nanosecond pulsed discharge for tar removal in N₂ flow, attaining total naphthalene destruction at much lower temperatures than conventional processes. Unlike biomass pyrolysis/gasification, DC plasmas have barely been used for

biomass tar removal due to the high energy cost and unnecessary elevated operating temperatures. However, DC plasmas have been used for tar removal from syngas produced from wastes,³¹⁷ as high temperatures are required to eliminate the complex tar compounds formed from diverse feedstocks (biomass, plastics, municipal solid wastes, etc.).

3.2.4 Plasma-assisted combustion and vitrification

Low-grade biomass is mainly combusted for electricity generation. However, sustaining a flame is rather challenging due to the feedstock low calorific value. Therefore, an additional energy source is necessary. Plasma can assist flame ignition and propagation since i) the overall temperature is higher, enabling oxidation reactions; ii) abundant chemically active species like O, OH, and H radicals contribute to mechanism intensification; iii) electron-molecule collisions affect the combustion kinetics and iv) electromagnetic forces intensify transport.³¹⁸ Plasma-assisted combustion overcomes conventional combustion limitations, such as tuning of flame temperature, instant dynamic response, flexibility toward operating conditions (inert, reduced, or oxidized). Moreover, the energy channeled by the plasma does not exceed 5% of the flame energy.³¹⁹

Continuous DC transferred plasmas with tungsten-based electrodes for plasma-assisted combustion^{320,321} (not particularly for biomass combustion) suffers from limited electrode lifetime and reliability, water cooling demand, and implementation of AC/DC transformers associated with high energy losses as well as the capital and operating costs. Fulcheri and coworkers^{318,319} launched a novel three-phase AC plasma system utilizing natural gas as active thermochemical gas sheathing for graphite-based electrode erosion suppression. The rig was successfully tested for biomass plasma-assisted combustion. Low-temperature plasmas can also be integrated with conventional biomass combustors to improve overall efficiency. Only recently, Lim and Lea-Langton³²² developed such a conventional biomass combustion furnace integrated with a DBD to provide ozone and oxygen radicals and intensify combustion of leaner fuel-air mixtures. The active species and absence of tungsten-based electrodes contributed to a stable and efficient operation.

Vitrification is a very high temperature (post)treatment process used to treat toxic and hazardous biomass wastes or residues, such as fly ash, from municipal wastes incinerators. The very high operating temperatures (up to 10,000 °C)^{323,324} attained at inert conditions (Ar or N₂ used as plasma agents) promote inorganic material melting, resulting in hazardous metals binding into a non-leaching ceramic matrix (silicate).²⁴⁰ The stabilized and immobilized hazardous substances, including heavy metals and dioxins, are safely landfilled or used as construction material.³²⁵ Plasma-assisted vitrification could be an alternative melting technology to conventional high-temperature systems e.g., microwave melting furnaces and swirling-flow oil furnaces. Due to the very high operating temperatures, the technology is compact and effective in eliminating hazardous compounds, forming contaminants-free and non-leachable slugs. Given the very high vitrification temperatures, only continuous DC transferred plasmas have been employed.^{326–328} Besides, a DC double anode plasma torch has been specifically designed for vitrification.^{324,329} This novel configuration enhanced the plasma aerodynamic stability and jet elongation and allowed for high energy density plasmas ignition at relatively low current intensities.³²⁹ The use of a DC double anode possibly extended the reactor lifetime. Vitrification has hardly been applied for raw biomass residue treatment, due to the absence

of considerable toxic and hazardous compounds load. Only Huang *et al.*³²⁴ mixed biomass ashes with municipal solid waste (MSW) to control the melting and reduce the vitrification energy cost.

Highlights of representative works on plasma combustion and vitrification are presented in Table 11.

Table 11: Overview of plasma combustion and vitrification, including feedstock source, key operating conditions and results.

Substrate	Plasma treatment	Main Results	Ref.
Wood chips	Three-phase AC plasma torch, air, 80 Hz, 150-400 A, 100 kW	Almost complete combustion at high feeding rates, CO ₂ major product and low H ₂ production, negligible CO formation	318,319
Sawdust	Pulsed DBD integrated with a furnace, 36 kHz, 16-20 kV,	Decrease of dry flue gas losses with DBD power input increase, alkanes, alkynes and aromatics ozonolysis (imposed by DBD) mitigated dry flue gas losses	322
Rice husk and wood waste ash mixed with MSW	DC double-arc plasma, Ar, first arc: 20–30 V/100 A, second arc: 50–60 V/100 A, 15 kWh/kg _{feed}	Reduction of melting temperature and heat of MSW fly ash with biomass ash addition	324

4. Scale-up, economic considerations, and technology benchmarking

Commercially available plasma-assisted systems for large-scale biomass utilization have been extensively reported elsewhere.^{70,239,330} Only thermal plasmas have been employed, whereas non-thermal plasma reactors are still in development, with only lab- or pilot-scale installations launched. Therefore, literature data for biomass utilization using non-thermal plasma is relatively scarce. Overall, the following aspects constitute the fundamental challenges toward upscaling and industrialization of the plasma technology in biomass valorization applications – these challenges are more pressing for non-thermal plasmas where non-equilibrium conditions should also be sustained besides reactor performance optimization: i) ignition and sustenance of high volume and energy density discharges for treatment of high biomass flow rates; to this end, high discharge gaps and, consequently, strong electric fields are required. Subsequently, higher breakdown voltages should be applied, but the existing industrial power units are limited to a couple of hundreds of kV; ii) multi-parametric optimization of the flow pattern to maximize the residence time of biomass particles in the hot plasma zone and, concurrently, minimize expensive plasma agent use (i.e., Ar or He) and auxiliary agents (i.e., swirl agents) needed to intensify the plasma stability; iii) higher carbon conversion and cold gas efficiency to boost the process economics. Overcoming the above mentioned challenges along with minimizing heat losses in the hardware and through the reactor walls could significantly improve the energetic footprint of the technology which is the cost driver; iv) regular replacement of the electrodes due to severe erosion, affecting process operation and economics; v) suitable process safety measures should be taken due to the high voltage and high current applied, rendering plasma-assisted systems potentially hazardous.

Thermal plasma-based gasifiers, in particular, have been advanced to higher technology readiness levels (TRL 8: Actual System Completed and TRL9: Actual System Proven in Operational Environment) and upscaled to high capacities (expressed in oven-dried ton/day; $\text{odt}_{\text{biomass}}/\text{d}$) and finally tested industrially. To mention some representative examples: i) Westinghouse Plasma Corp developed a hybrid moving bed-plasma gasifier of 105 odt/d , equipped with plasma torches located at the bottom of the gasifier to facilitate cracking of the organic load and concurrently, the vitrification of the inorganic contaminants; ii) the Plasco Energy Group Inc. built a plasma gasifier of 70 odt/d which comprises a refractory-lined structure and a plasma torch and requires low flows of a gasification agent; iii) the Startech Environmental Corporation launched a 75 odt/d modular plasma gasifier in which the feedstock is initially shredded it into smaller particles into an auger and is subsequently delivered into the plasma chamber to be converted into valuable products; iv) the Solena Group realized the highest capacity plasma gasifiers, reaching throughputs of 480 odt/d . For scale up, three plasma torches were placed at the bottom of the gasifier, while carbon-based catalysts were utilized along with oxygen-enriched air to enhance the cracking reactions in the bed above the torches. Other manufacturers have launched plasma gasifiers at a smaller scale; for instance, InEnTec has built several batch plasma gasifiers treating 10-25 odt/d . Others, such as the Startech Environmental Corporation and Solena Group, can treat up to 1500 odt/d and 1125 odt/d , respectively, by operating several modular units.³³¹ An overview of the capacity range attained at industrial scale by plasma and conventional gasifiers is given in Figure 17.

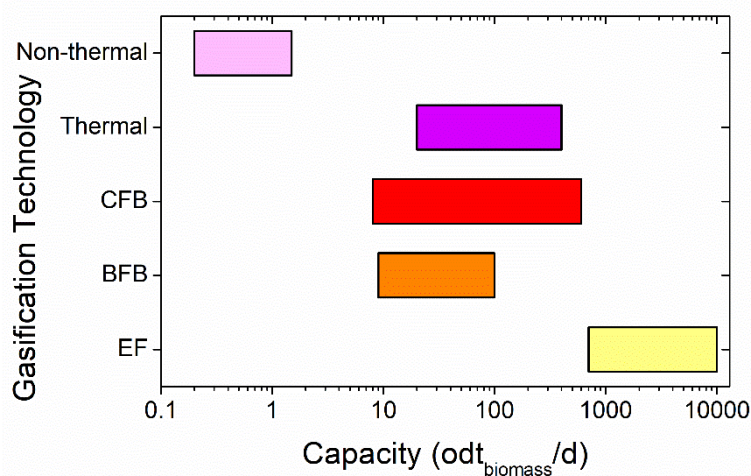


Figure 17: Capacity range (expressed in oven-dried $\text{ton}_{\text{biomass}}/\text{day}$; $\text{odt}_{\text{biomass}}/\text{d}$) achieved at an industrial scale by different gasification technologies. Thermal plasma gasifiers attain comparable capacity as the circulating fluidized bed (CFB) and bubbling fluidized bed (BFB) gasifiers but still lower than the conventional entrained flow (EF) gasifiers. Non-thermal plasma gasifiers are still in development stage (the term thermal plasma implies thermal equilibrium among all species present in the plasma).

In general, technoeconomic data for either thermal or non-thermal plasma-assisted biomass valorization processes are unavailable in the literature. The reported economic data are sourced by existing applications that may differ from case to case due to reactor configuration and capacity variation. Further, fair benchmarking with conventional gasifiers is difficult since different feedstock processing, product distribution, and energy integration schemes are applied. In biomass to liquids processing, the cost considerably varies depending on the final product and other indirect costs. The uncertainty in the cost estimation may be $>\pm 30\%$, since it is always based on quotes from past projects

at a different scale. A detailed analysis of a well-defined plasma system, including upstream and downstream processes, energy efficiency, and product composition, could give an accurate cost estimate. Considering the above-mentioned limitations, we attempted to derive a general cost estimation equation for a plasma gasifier, as shown in Figure 18. The quoted CAPEX values of thermal plasma gasifiers involved in similar gasification process synthesis and product distribution were used³³¹ to correlate the capital expenditure (CAPEX) of a plasma gasifier (employing plasma torches) to its capacity. The trendline can approximately depict the correlation of plasma gasifier CAPEX to its capacity. Feedstock pre-treatment considerably affects CAPEX as well. In particular, offsite treatment (palletization and torrefaction) could lead to a 36% higher CAPEX while onsite treatment (drying chipping/grinding and handling) to 16-22%.³³¹ based on the performance of the non-thermal plasma gasifier developed by Uhm et al.,³³² i.e., 150 kW output power demand per 1.5 odt_{biomass}/d, and the report by Stefanidis and coworkers³³³ that illustrates the microwave plasma equipment capital cost as a function of the output plasma power, i.e., 2k€/kW at output power >100 kW, the CAPEX of a non-thermal plasma gasifier can be as high as 200 k€/odt_{biomass}/d, equivalent to 225 k\$/odt_{biomass}/d. The estimated non-thermal plasma gasifier CAPEX includes only microwave plasma-related hardware.³³³ At the same time, the CAPEX of thermal plasma gasifiers also includes the cost of units needed to convert biomass into electricity. The trend line depicted in Figure 18 is more representative for thermal plasma gasifiers since it has been based on industrial-scale data of thermal plasma biomass gasification plants and is suitable for preliminary CAPEX order of magnitude estimation.

To put the scale in context, a typical 600 acres corn Midwest farm in the US can produce about 2.5 metric tons of hydroxymethylfurfural (HMF) per day from corn stover, the major agricultural waste.¹⁰⁵ Given that biomass contains a significant amount of water, a transportation radius of ~50 miles is economically rational. For the typical 3-4.5 dry tons of corn stover/acre produced within a radius of 50 miles, a total of 24,000-35,000 dry tons of corn stover is annually available. This can be processed within days by a single of the largest scale-reported gasifiers or within a few weeks by a handful of mid-size gasifiers (sizes per Figure 17), a time imposed by the degradation of waste with time. Given the 1997-2000 US corn production average, ~110 million dry tons of corn stover could be available. This will require ~3,500 large gasifiers of 10,000 odt/d (using the largest reported in Figure 17), each within a radius of 50 miles. These are achievable scales. Gasification makes lower value products, and thus, we do not expect implementation of this concept. However, the scales discussed define the problem we need to handle even for value-added products processed via plasma technology.

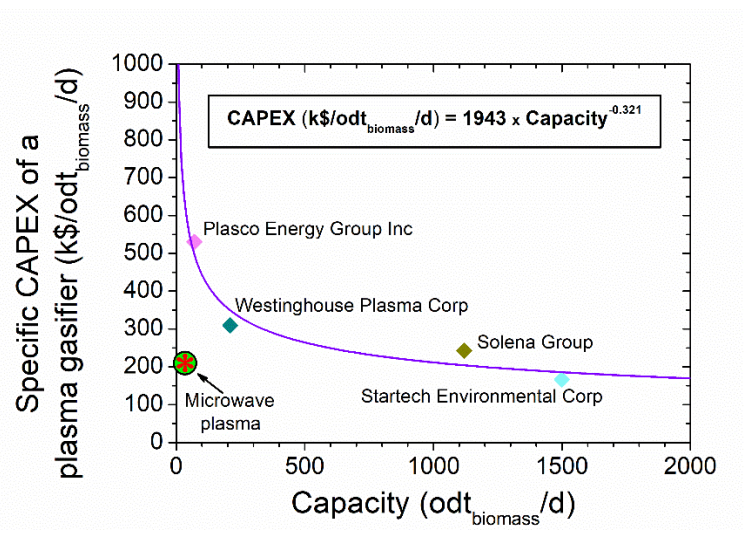


Figure 18: Quoted thermal plasma gasifiers CAPEX for different capacities and similar gasification processes. The trendline correlates plasma gasifier CAPEX to its capacity (expressed in oven-dried $\text{ton}_{\text{biomass}}/\text{day}$; $\text{odt}_{\text{biomass}}/\text{d}$).

The operating expenditure (OPEX) estimation is even more challenging than the CAPEX due to the lack of relevant data. However, the annual OPEX for conventional gasification plants is estimated to be 3-6% of the CAPEX, excluding feedstock (biomass) cost.³³¹ This range varies according to specific labor and other materials costs (e.g., chemicals, bed materials etc.). Imported oxidant utilization instead of onsite production majorly impacts OPEX, increasing it well above the given range. Moreover, clean-up and conditioning of the gasification products (i.e. dust and particle filtering, scrubbing or catalytic absorption of contaminants such as sulfur, nitrogen, and fluoride compounds, adjustment of the produced syngas $\text{H}_2:\text{CO}$ ratio via the water-gas-shift reaction and CO_2 removal to match the Fischer-Tropsch process specifications) also contribute to OPEX rise. Finally, the biomass feedstock cost should also be taken into account.

Given that the annual OPEX of a plasma gasifier is foreseen to be higher than its conventional counterpart due to the regular electrode replacement, one needs real plant data. In passing, we should mention that in the technoeconomic analysis of thermochemical biomass conversion processes, the cost of biomass and utilities typically dominates. This may still be the case for plasma-assisted processes. Table 12 presents some economic data of a pilot (Plasco Energy Group Inc) and a standard plasma plant (InEnTec) for municipal solid waste valorization to electricity. More specific information can be found in ref ³⁰. To the best of our knowledge, no economic data for non-thermal plasma applications are available in the literature so far.

Table 12. Economic data of thermal plasma plants for municipal solid waste valorization to electricity.³⁰

	Plasco Energy Group Inc	InEnTec
<i>Plant features</i>		
Capacity (ton/d)	75	300
Scale	Pilot	Large
Year of realization	2008	2014
<i>Operating expenditures (USD/ton)</i>		
Depreciation ¹	96	77
Operation and maintenance ²	53	53
Subtotal	149	129
<i>Revenues (USD/ton)</i>		
Gate fee ³	65	65
Electricity to grid	53	87
Recovered metals ⁴	2	2
Subtotal	120	154

¹ Depreciation is relative to CAPEX; 10% (10 years life time) payment of the capital cost per year is assumed.

- ² Operation and maintenance include the labor, administration, operator profit, parts and supplies, electricity, fuel, chemicals, insurance, services, and others expenditures.
- ³ Gate fee equals the fee paid by a third party (e.g., community, municipality, etc.) for the waste management service; 65 USD/ton is assumed.
- ⁴ Recovered metals refer to ferrous/non-ferrous metals reclaimed out of waste valorization and sold; a value of 50 USD/ton is assumed.

For a fair interpretation of the economic data, one should carefully consider all the above considerations. As clarified in Ref. ³⁰, the Plasco Energy Group Inc. process is not economically viable since the economics was based on a pilot-scale facility. It is stressed that CAPEX and, subsequently, the high depreciation cost are expected to decrease with technology upscaling. In addition, feedstock of high-moisture content (30%) was treated. Therefore, an upstream drying process was employed, significantly increasing the cost associated with electricity. According to Ref.³⁰, the InEnTec process is economically favorable since the economics was calculated for a standard plasma plant. Depreciation was mitigated due to the economies of scale, and the process output (electricity production) increased due to higher waste volume treatment. Notably, the attractive profit margin is generated by the service supply (waste management) and the electricity sales.

Overall, plasma gasification systems constitute a promising alternative technology to conventional thermally driven gasifiers for efficient conversion of biomass to value-added chemicals. The high plasma temperature and active plasma species enable reactions that are hardly activated in the conventional gasification process, resulting in full cracking of heavy species, impurities melt, and inorganic fraction vitrification. Consequently, higher purity syngas forms and less oxidizing agent is needed. Besides, plasma gasifiers feature instant start-up/shut-down and allow for utilization of intermittent and fluctuating renewable energy. Among other plasma gasifiers, MW plasma systems feature potential for high-quality syngas production. Compared to large-scale DC plasma torches, lower CAPEX and OPEX are foreseen while attaining higher energy efficiencies and being more economically viable at smaller scales for decentralized biomass processing. Yet, MW plasma gasifiers are still in a developing phase; therefore, definitive quantitative performance comparison with commercially available conventional gasifiers and DC plasma torch gasifiers cannot be made at present. Instead, a qualitative performance comparison is possible, as shown in Table 13.

Table 13: Gasification technology benchmarking: qualitative overview of conventional thermally driven, thermal plasma (DC plasma torch) and MW plasma gasifiers.

Gasification system	Conventional (no plasma)	Thermal plasma	Microwave plasma
Feedstock flexibility	Low; can handle a moderate range of material characteristics (moisture <15%, ash, particle size=1-150 mm)	High; the chemistry is driven by both the heat and plasma; can handle heterogeneity, but this affects syngas quality	High; the chemistry is driven by both the heat and plasma; deals only with tiny particles (powder<1 mm)

Syngas quality	Oxygen-rich streams give best results; biofuels production: extensive product cleaning (+ water-gas-shift) required	High temperatures result in low tar levels and high H ₂ and CO levels; biofuels production: extensive product cleaning (+ water-gas-shift) required	High temperatures result in low tar levels and high H ₂ and CO levels; biofuels production: extensive product cleaning (+ water-gas-shift) required
Development status	Industrial applications for heat and power generation; demo projects for biomass to liquid fuels	Industrial applications for heat and power generation; R&D projects for biomass to liquid fuels	Currently no industrial applications; R&D projects for biomass to high-quality syngas
Scale-up potential	Huge scale possible	Small to medium scale possible, modular systems	Challenging magnetron upscaling (>100 kW, the current limit), robust reactor design needed
Costs	Economy of scales; costs distribution (pretreatment, gasification, cleaning) depends on the type of system	High CAPEX and OPEX (expensive equipment, high parasitic load, electrode erosion); lower gas cleaning costs due to reduced product gas dilution compared to conventional gasification	Lower CAPEX and OPEX compared to thermal plasma; no economies of scale but more economically viable at a smaller scale than thermal plasma
Remarks	Problem for large scale plants: feedstock logistics/ large amounts of biomass should be available; biomass pretreatment into an intermediate product to reduce transportation costs	Preferred option to treat hazardous feedstock (vitrification into non-leaching slag)	Limited to lab-scale/pilot projects at present; powdered feedstock (simple components: lignin)

5. Summary and perspectives

The production of materials, chemicals, and fuels from lignocellulosic biomass is essential, as biomass is abundant, renewable, and CO₂-neutral. It is the most energy-efficient way to capture CO₂ from the atmosphere and partially reduce it to carbohydrates and lignin. Green energy from electricity can substitute conventional thermal energy in converting biomass, enabling the transition to small-scale, economically viable, electrified biorefineries. Converting CO₂ from the atmosphere into solid products and long-lived chemicals can even result in negative carbon emissions. The development of biomass conversion technologies has focused nearly exclusively on introducing suitable catalysts and discovering new products without much attention to processing. Electrification of the future biorefinery can eliminate or reduce CO₂ in the production of renewable chemicals and mitigate the environmental footprint of future manufacturing. We believe this is a critical next step and plasma technologies could be a pillar in the electrification of future biorefineries.

In the low-temperature conversion of lignocellulosic biomass, atmospheric pressure plasma technology has been proposed mainly as a pretreatment method to enable delignification and promote the subsequent acid-catalyzed or enzyme hydrolysis toward enhanced production of sugars. Non-equilibrium dielectric barrier discharges (DBDs) are the most popular plasma pretreatment reactors. Raw biomass powder is treated using oxidative plasma chemistry in the gas phase or aqueous suspensions. Reactive species can break down lignin, disrupt the cellulose crystalline structure, enhance the accessibility to catalysts and enzymes, and cleave the ether bonds in all biopolymers, leading to lower molecular weight processable products. In air plasma treatment, the interaction of nitrogen oxides with water leads to acidification, which in turn intensifies acid-catalyzed hydrolysis. Despite significant efforts, there is an imperative need for in-depth studies on the complex plasma-biomass interactions to advance the field. Work on model compounds in archetypical plasma configurations could be instrumental. Moreover, since lignin is the least utilized fraction of biomass, plasma processing could be valuable for lignin breakdown and functionalization. Other waste streams of biorefineries should also be exploited. In-liquid plasma electrolytic treatments enable biomass liquefaction to bio-oil of higher energy density at shorter treatment times than conventional (heating) or non-conventional (microwave, ultrasound, etc.). A drawback of this technique is the “harsh” environment, evidenced by utilizing acids and liquid heating by DC discharges. Unraveling the critical aspects of the process is challenging. Future studies are needed to understand and assess the technology better.

Unlike the above processes, plasma for high and very high-temperature cracking of biomass, either in an inert (pyrolysis) or oxidizing (gasification) environment, produces oils and syngas and has been used extensively. Key traits of thermal plasma over conventional thermal cracking include its high reactivity and energy density, rapid heating rates, and short residence times. These traits promote higher syngas and light hydrocarbon yields and lower tar formation, rendering plasma a superior technology for converting complex and diverse biomass feedstock. Nevertheless, the energy dissipation in the hardware, frequent maintenance due to electrode erosion, limited heat integration, and challenges associated with upscaling are considerable technical challenges. High energy pulsed discharges, preferably of nanosecond time duration, maybe a promising alternative to traditional thermal plasmas. By applying short electrical pulses, the electric energy is channeled mainly into electrons to initiate electron-induced reactions. Overall, the electric to chemical energy conversion is maximized and heat dissipation into gas is reduced.

Plasma technologies could prove valuable for biomass valorization. However, not only are fundamental studies required but technical challenges should also be overcome to realize their integration in modern biorefineries. Critical technical limitations that should be further addressed include i) the energy losses in the hardware (e.g., electrical circuits) that undermine the overall electrical-to-chemical energy conversion efficiency, ii) the inability to control the degree of ionization and temperature levels which are usually much higher than needed for the biomass processing, which implies high exergy losses, need for complex heat integration schemes and risk for thermal failure of the materials, iii) the lack of detailed reactor models that can predict and optimize heat transfer and gas-liquid flows, and iv) the plasma reactor upscaling. Even though the electrified plasma processes are compatible with “scale-out” strategies toward small-to-medium scale biorefineries, the transition from lab-scale to commercial-scale plasma reactors is challenging, as is the case for plasma reactors in several other research fields.

This review's goal was to bridge the gap between the plasma and the biomass conversion fields and communities, i.e., aiming to stimulate interaction among them and lay down the foundations for the future advancement of this multidisciplinary field.

Conflicts of interest

There are no conflicts to declare.

Acknowledgments

This work was supported as part of the Catalysis Center for Energy Innovation, an Energy Frontier Research Center funded by the US Dept. of Energy, Office of Science, Office of Basic Energy Sciences under award number DE-SC0001004.

References

- 1 T. D. Beuchelt and M. Nassl, *Sustain.*, 2019, **11**, 10–12.
- 2 D. Gielen, F. Boshell, D. Saygin, M. D. Bazilian, N. Wagner and R. Gorini, *Energy Strateg. Rev.*, 2019, **24**, 38–50.
- 3 C. B. Field, J. E. Campbell and D. B. Lobell, *Trends Ecol. Evol.*, 2008, **23**, 65–72.
- 4 L. A. Pfaltzgraff, M. De Bruyn, E. C. Cooper, V. Budarin and J. H. Clark, *Green Chem.*, 2013, **15**, 307–314.
- 5 Y. Román-Leshkov, C. J. Barrett, Z. Y. Liu and J. A. Dumesic, *Nature*, 2007, **447**, 982–985.
- 6 G. W. Huber and A. Corma, *Angew. Chemie - Int. Ed.*, 2007, **46**, 7184–7201.
- 7 R. C. Saxena, D. K. Adhikari and H. B. Goyal, *Renew. Sustain. Energy Rev.*, 2009, **13**, 167–178.
- 8 F. Cherubini, *Energy Convers. Manag.*, 2010, **51**, 1412–1421.
- 9 A. Bosmans, I. Vanderreydt, D. Geysen and L. Helsen, *J. Clean. Prod.*, 2013, **55**, 10–23.
- 10 Y. C. Lin and G. W. Huber, *Energy Environ. Sci.*, 2009, **2**, 68–80.
- 11 J. C. Serrano-Ruiz and J. A. Dumesic, *Energy Environ. Sci.*, 2011, **4**, 83–99.
- 12 J. N. Chheda, G. W. Huber and J. A. Dumesic, *Angew. Chemie - Int. Ed.*, 2007, **46**, 7164–7183.
- 13 D. M. Alonso, S. G. Wettstein and J. A. Dumesic, *Chem. Soc. Rev.*, 2012, **41**, 8075–8098.
- 14 D. M. Alonso, J. Q. Bond and J. A. Dumesic, *Green Chem.*, 2010, **12**, 1493–1513.
- 15 S. Van Den Bosch, W. Schutyser, R. Vanholme, T. Driessen, S. F. Koelewijn, T. Renders, B. De Meester, W. J. J. Huijgen, W. Dehaen, C. M. Courtin, B. Lagrain, W. Boerjan and B. F. Sels, *Energy Environ. Sci.*, 2015, **8**, 1748–1763.
- 16 X. Luo, Y. Li, N. K. Gupta, B. Sels, J. Ralph and L. Shuai, *Angew. Chemie - Int. Ed.*, 2020, **59**, 11704–11716.
- 17 N. Puač, M. Gherardi and M. Shiratani, *Plasma Process. Polym.*, 2018, **15**, 1–5.
- 18 K. Takaki, N. Hayashi, D. Wang and T. Ohshima, *J. Phys. D. Appl. Phys.*, DOI:10.1088/1361-6463/ab2e2d.
- 19 N. Puač, N. Škoro, K. Spasić, S. Živković, M. Milutinović, G. Malović and Z. L. Petrović, *Plasma Process. Polym.*, 2018, **15**, 1–12.
- 20 L. K. Randeniya and G. J. J. B. De Groot, *Plasma Process. Polym.*, 2015, **12**, 608–623.
- 21 B. A. Niemira, *Annu. Rev. Food Sci. Technol.*, 2012, **3**, 125–142.
- 22 M. Giannoglou, P. Stergiou, P. Dimitrakellis, E. Gogolides, N. G. Stoforos and G. Katsaros,

- Innov. Food Sci. Emerg. Technol.*, 2020, **66**, 102502.
- 23 P. Bourke, D. Ziuzina, D. Boehm, P. J. Cullen and K. Keener, *Trends Biotechnol.*, 2018, **36**, 615–626.
- 24 V. S. Sikarwar, M. Zhao, P. Clough, J. Yao, X. Zhong, M. Z. Memon, N. Shah, E. J. Anthony and P. S. Fennell, *Energy Environ. Sci.*, 2016, **9**, 2939–2977.
- 25 Y. Wen, C. Shen, Y. Ni, S. Tong and F. Yu, *J. Hazard. Mater.*, 2012, **201–202**, 162–169.
- 26 R. Zhou, R. Zhou, S. Wang, U. G. Mihiri Ekanayake, Z. Fang, P. J. Cullen, K. Bazaka and K. (Ken) Ostrikov, *Bioresour. Technol.*, 2020, **318**, 123917.
- 27 L. D. T. Prola, E. Acayanka, E. C. Lima, C. S. Umpierrez, J. C. P. Vaggetti, W. O. Santos, S. Laminsi and P. T. Djifon, *Ind. Crops Prod.*, 2013, **46**, 328–340.
- 28 R. Zhou, R. Zhou, Y. Xian, Z. Fang, X. Lu, K. Bazaka, A. Bogaerts and K. (Ken) Ostrikov, *Chem. Eng. J.*, 2020, **382**, 122745.
- 29 M. Rajasekhar, N. V. Rao, G. C. Rao, G. Priyadarshini and N. J. Kumar, in *Procedia Materials Science*, Elsevier B.V., 2015, vol. 10, pp. 513–518.
- 30 A. Ramos and A. Rouboa, in *AIP Conference Proceedings*, 2018, vol. 1968.
- 31 M. Danthurebandara, S. Van Passel, I. Vanderreydt and K. Van Acker, *Waste Manag.*, 2015, **45**, 458–467.
- 32 B. Annemie, E. Neyts, R. Gijbels and J. Van der Mullen, *Spectrochim. Acta Part B*, 2002, **57**, 609–658.
- 33 H. Conrads and M. Schmidt, *Plasma Sources Sci. Technol.*, 2000, **9**, 441–454.
- 34 D. Pappas, *J. Vac. Sci. Technol. A Vacuum, Surfaces, Film.*, 2011, **29**, 020801.
- 35 P. J. Bruggeman, F. Iza and R. Brandenburg, *Plasma Sources Sci. Technol.*, , DOI:10.1088/1361-6595/aa97af.
- 36 L. Bárdos and H. Baránková, *Thin Solid Films*, 2010, **518**, 6705–6713.
- 37 N. Venkatramani, *Curr. Sci.*, 2002, **83**, 254–262.
- 38 S. J. Yoon and J. Goo Lee, *Energy and Fuels*, 2012, **26**, 524–529.
- 39 G. Bonizzoni and E. Vassallo, *Vacuum*, 2002, **64**, 327–336.
- 40 E. Delikonstantis, G. Sturm, A. I. Stankiewicz, A. Bosmans, M. Scapinello, C. Dreiser, O. Lade, S. Brand and G. D. Stefanidis, *Chem. Eng. Process. - Process Intensif.*, , DOI:10.1016/j.cep.2019.107538.
- 41 A. Fridman, 2008.
- 42 D. Czyrkowski, B. Hrycak, M. Jasiński, M. Dors and J. Mizeraczyk, *Energy*, 2016, **113**, 653–661.
- 43 L. Vinet and A. Zhedanov, *J. Phys. A Math. Theor.*, 2011, **44**, A399.
- 44 A. Tamošiunas, A. Chouchène, P. Valatkevičius, D. Gimžauskaite, M. Aikas, R. Uscila, M. Ghorbel and M. Jeguirim, *Energies*, 2017, **10**, 1–14.
- 45 Ö. Yazicioğlu and T. Y. Katircioğlu, *Kirklareli Univ. J. Eng. Sci.*, 2017, **3**, 18–44.
- 46 J. Winter, R. Brandenburg and K. D. Weltmann, *Plasma Sources Sci. Technol.*, , DOI:10.1088/0963-0252/24/6/064001.
- 47 J. Hopwood and F. Iza, *J. Anal. At. Spectrom.*, 2004, **19**, 1145–1150.
- 48 E. Kral'kina, *Uspekhi Fiz. Nauk. Russ. Acad. Sci.*, 2008, **51**, 493–512.
- 49 Y. J. Zhou, Q. H. Yuan, F. Li, X. M. Wang, G. Q. Yin and C. Z. Dong, *Phys. Plasmas*, 2013, **20**, 14–20.
- 50 T. Shao, R. Wang, C. Zhang and P. Yan, *High Volt.*, 2018, **3**, 14–20.
- 51 T. Gerling, T. Hoder, R. Bussiahn, R. Brandenburg and K. D. Weltmann, *Plasma Sources Sci. Technol.*, , DOI:10.1088/0963-0252/22/6/065012.

- 52 X. Pei, X. Lu, J. Liu, D. Liu, Y. Yang, K. Ostrikov, P. K. Chu and Y. Pan, *J. Phys. D. Appl. Phys.*, , DOI:10.1088/0022-3727/45/16/165205.
- 53 Q. Xiong, X. P. Lu, K. Ostrikov, Y. Xian, C. Zou, Z. Xiong and Y. Pan, *Phys. Plasmas*, , DOI:10.1063/1.3381132.
- 54 S. Tao, Z. Cheng, N. Zheng, Y. Ping, V. F. Tarasenko, E. K. Baksht, A. G. Burahenko and Y. V. Shut'ko, *Appl. Phys. Lett.*, 2011, **98**, 1–4.
- 55 H. Jiang, T. Shao, C. Zhang, Z. Niu, Y. Yu, P. Yan and Y. Zhou, *IEEE Trans. Plasma Sci.*, 2011, **39**, 2076–2077.
- 56 P. Dimitrakellis, A. Zeniou, Y. Stratakos and E. Gogolides, *Plasma Sources Sci. Technol.*, 2016, **25**, 25015.
- 57 T. von Woedtke, S. Reuter, K. Masur and K. D. Weltmann, *Phys. Rep.*, 2013, **530**, 291–320.
- 58 R. Brandenburg, *Plasma Sources Sci. Technol.*, , DOI:10.1088/1361-6595/aaced9.
- 59 H. E. Wagner, R. Brandenburg, K. V. Kozlov, A. Sonnenfeld, P. Michel and J. F. Behnke, *Vacuum*, 2003, **71**, 417–436.
- 60 X. Xu, *Thin Solid Films*, 2001, **390**, 237–242.
- 61 J. Vanneste, T. Ennaert, A. Vanhulsel and B. Sels, *ChemSusChem*, 2017, **10**, 14–31.
- 62 J. R. Silverman, A. M. Danby and B. Subramaniam, *React. Chem. Eng.*, 2019, **4**, 1421–1430.
- 63 I. Barrera-Martínez, N. Guzmán, E. Peña, T. Vázquez, R. Cerón-Camacho, J. Folch, J. A. Honorato Salazar and J. Aburto, *Biomass and Bioenergy*, 2016, **94**, 167–172.
- 64 C. J. Chuck, H. J. Parker, R. W. Jenkins and J. Donnelly, *Bioresour. Technol.*, 2013, **143**, 549–554.
- 65 A. Choukourou, *Izv. Vyss. Uchebnykh Zaved. Seriya Khimiya i Khimicheskaya Tekhnologiya*, 2019, **62**, 4–30.
- 66 D. B. Graves, *J. Phys. D. Appl. Phys.*, , DOI:10.1088/0022-3727/45/26/263001.
- 67 R. Thirumdas, A. Kothakota, U. Annapure, K. Siliveru, R. Blundell, R. Gatt and V. P. Valdramidis, *Trends Food Sci. Technol.*, 2018, **77**, 21–31.
- 68 R. Zhou, R. Zhou, K. Prasad, Z. Fang, R. Speight, K. Bazaka and K. Ostrikov, *Green Chem.*, 2018, **20**, 5276–5284.
- 69 J. L. Brisset and J. Pawlat, *Plasma Chem. Plasma Process.*, 2016, **36**, 355–381.
- 70 P. Bruggeman and C. Leys, *J. Phys. D. Appl. Phys.*, , DOI:10.1088/0022-3727/42/5/053001.
- 71 Kostya (ken) Ostrikov, R. Zhou, R. Zhou, P. Wang, Y. Xian, A. Mai-Prochnow, X. Lu, P. J. Cullen, K. (Ken) Ostrikov and K. Bazaka, *J. Phys. D. Appl. Phys.*, , DOI:10.1088/1361-6463/ab81cf.
- 72 S. Ž. Corina Bradu, Kinga Kutasi, Monica Magureanu, Nevena Puac, *J. Phys. D. Appl. Phys.*
- 73 P. J. Bruggeman, M. J. Kushner, B. R. Locke, J. G. E. Gardeniers, W. G. Graham, D. B. Graves, R. C. H. M. Hofman-Caris, D. Maric, J. P. Reid, E. Ceriani, D. Fernandez Rivas, J. E. Foster, S. C. Garrick, Y. Gorbanev, S. Hamaguchi, F. Iza, H. Jablonowski, E. Klimova, J. Kolb, F. Krcma, P. Lukes, Z. MacHala, I. Marinov, D. Mariotti, S. Mededovic Thagard, D. Minakata, E. C. Neyts, J. Pawlat, Z. L. Petrovic, R. Pflieger, S. Reuter, D. C. Schram, S. Schröter, M. Shiraiwa, B. Tarabová, P. A. Tsai, J. R. R. Verlet, T. Von Woedtke, K. R. Wilson, K. Yasui and G. Zvereva, *Plasma Sources Sci. Technol.*, , DOI:10.1088/0963-0252/25/5/053002.
- 74 B. R. Locke and K. Y. Shih, *Plasma Sources Sci. Technol.*, , DOI:10.1088/0963-0252/20/3/034006.
- 75 P. Lukes, E. Dolezalova, I. Sisrova and M. Clupek, *Plasma Sources Sci. Technol.*, , DOI:10.1088/0963-0252/23/1/015019.
- 76 Y. Gorbanev, D. O'Connell and V. Chechik, *Chem. - A Eur. J.*, 2016, **22**, 3496–3505.
- 77 W. Wang, B. Patil, S. Heijkers, V. Hessel and A. Bogaerts, *ChemSusChem*, 2017, **10**, 2145–2157.

- 78 S. Li, J. A. Medrano, V. Hessel and F. Gallucci, *Processes*, , DOI:10.3390/pr6120248.
- 79 G. W. Huber, S. Iborra and A. Corma, *Chem. Rev.*, 2006, **106**, 4044–4098.
- 80 A. T. W. M. Hendriks and G. Zeeman, *Bioresour. Technol.*, 2009, **100**, 10–18.
- 81 S. Sadula, A. Athaley, W. Zheng, M. Ierapetritou and B. Saha, *ChemSusChem*, 2017, **10**, 2566–2572.
- 82 T. Eggeman and R. T. Elander, *Bioresour. Technol.*, 2005, **96**, 2019–2025.
- 83 N. Mosier, C. Wyman, B. Dale, R. Elander, Y. Y. Lee, M. Holtzapple and M. Ladisch, *Bioresour. Technol.*, 2005, **96**, 673–686.
- 84 W. Y. Cheah, R. Sankaran, P. L. Show, T. N. B. T. Ibrahim, K. W. Chew, A. Culaba and J. S. Chang, *Biofuel Res. J.*, 2020, **7**, 1115–1127.
- 85 K. Karimi and M. J. Taherzadeh, *Bioresour. Technol.*, 2016, **203**, 348–356.
- 86 M. J. Taherzadeh and K. Karimi, *Pretreatment of lignocellulosic wastes to improve ethanol and biogas production: A review*, 2008, vol. 9.
- 87 F. S. Miranda, S. C. Rabelo, J. G. C. Pradella, C. Di Carli, G. Petraconi, H. S. Maciel, R. S. Pessoa and L. Vieira, *Waste and Biomass Valorization*, 2020, **11**, 4921–4931.
- 88 P. Kumar, D. M. Barrett, M. J. Delwiche and P. Stroeve, *Ind. Eng. Chem. Res.*, 2009, **48**, 3713–3729.
- 89 H. Chen, J. Liu, X. Chang, D. Chen, Y. Xue, P. Liu, H. Lin and S. Han, *Fuel Process. Technol.*, 2017, **160**, 196–206.
- 90 L. Capolupo and V. Faraco, *Appl. Microbiol. Biotechnol.*, 2016, **100**, 9451–9467.
- 91 J. M. Carbonell-Capella, J. Šic Žlabur, S. Rimac Brnčić, F. J. Barba, N. Grimi, M. Koubaa, M. Brnčić and E. Vorobiev, *J. Food Process. Preserv.*, 2017, **41**, 1–8.
- 92 H. N. Rajha, N. Boussetta, N. Louka, R. G. Maroun and E. Vorobiev, *Innov. Food Sci. Emerg. Technol.*, 2015, **31**, 60–66.
- 93 H. Shaghaleh, X. Xu, H. Liu, S. Wang, Y. Alhaj Hamoud, F. Dong and J. Luo, *Energy*, 2019, **176**, 195–210.
- 94 N. Schultz-Jensen, Z. Kádár, A. B. Thomsen, H. Bindslev and F. Leipold, *Appl. Biochem. Biotechnol.*, 2011, **165**, 1010–1023.
- 95 K. Sakai, S. Kojiya, J. Kamijo, Y. Tanaka, K. Tanaka, M. Maebayashi, J. S. Oh, M. Ito, M. Hori, M. Shimizu and M. Kato, *Biotechnol. Biofuels*, 2017, **10**, 1–11.
- 96 K. Kuroda, K. Shimomura, T. Ishijima, K. Takada, K. Ninomiya and K. Takahashi, *Aust. J. Chem.*, 2017, **70**, 731–734.
- 97 C. L. Song, Z. T. Zhang, W. Y. Chen and C. Liu, *IEEE Trans. Plasma Sci.*, 2009, **37**, 1817–1824.
- 98 A. Wright, H. Bandulasena, C. Ibenegbu, D. Leak, T. Holmes, W. Zimmerman, A. Shaw and F. Iza, *AIChE J.*, 2018, **64**, 3803–3816.
- 99 J. Gao, L. Chen, J. Zhang and Z. Yan, *Bioresour. Technol.*, 2014, **171**, 469–471.
- 100 I. Prasertsung, K. Aroonraj, K. Kamwilaisak, N. Saito and S. Damrongsakkul, *Carbohydr. Polym.*, 2019, **205**, 472–479.
- 101 R. Ravindran, C. Sarangapani, S. Jaiswal, P. J. Cullen and A. K. Jaiswal, *Bioresour. Technol.*, 2017, **243**, 327–334.
- 102 R. Ravindran, C. Sarangapani, S. Jaiswal, P. Lu, P. J. Cullen, P. Bourke and A. K. Jaiswal, *Bioresour. Technol.*, 2019, **282**, 520–524.
- 103 N. Schultz-Jensen, F. Leipold, H. Bindslev and A. B. Thomsen, *Appl. Biochem. Biotechnol.*, 2011, **163**, 558–572.
- 104 D. M. Alonso, S. G. Wettstein, M. A. Mellmer, E. I. Gurbuz and J. A. Dumesic, *Energy Environ. Sci.*, 2013, **6**, 76–80.

- 105 R. Weingarten, W. C. Conner and G. W. Huber, *Energy Environ. Sci.*, 2012, **5**, 7559–7574.
- 106 P. Desir, B. Saha and D. G. Vlachos, *Energy Environ. Sci.*, 2019, **12**, 2463–2475.
- 107 V. Choudhary, S. H. Mushrif, C. Ho, A. Anderko, V. Nikolakis, N. S. Marinkovic, A. I. Frenkel, S. I. Sandler and D. G. Vlachos, *J. Am. Chem. Soc.*, 2013, **135**, 3997–4006.
- 108 L. Yang, G. Tsilomelekis, S. Caratzoulas and D. G. Vlachos, *ChemSusChem*, 2015, **8**, 1334–1341.
- 109 F. Guo, Z. Fang, C. C. Xu and R. L. Smith, *Prog. Energy Combust. Sci.*, 2012, **38**, 672–690.
- 110 Y. Liao, B. O. de Beeck, K. Thielemans, T. Ennaert, J. Snelders, M. Dusselier, C. M. Courtin and B. F. Sels, *Mol. Catal.*, 2020, **487**, 110883.
- 111 L. Hu, L. Lin, Z. Wu, S. Zhou and S. Liu, *Appl. Catal. B Environ.*, 2015, **174–175**, 225–243.
- 112 F. Jérôme, G. Chatel and K. De Oliveira Vigier, *Green Chem.*, 2016, **18**, 3903–3913.
- 113 P. Dimitrakellis, A. Travlos, V. P. Psycharis and E. Gogolides, *Plasma Process. Polym.*, 2017, **14**, 1–8.
- 114 Z. Matouk, R. Rincón, B. Torriss, A. Mirzaei, J. Margot, A. Dorris, S. Beck, R. M. Berry and M. Chaker, *Cellulose*, 2021, **28**, 6239–6252.
- 115 M. Fazeli, J. P. Florez and R. A. Simão, *Compos. Part B Eng.*, 2019, **163**, 207–216.
- 116 M. Benoit, A. Rodrigues, Q. Zhang, E. Fourré, K. De Oliveira Vigier, J. M. Tatibouët and F. Jérôme, *Angew. Chemie - Int. Ed.*, 2011, **50**, 8964–8967.
- 117 M. Benoit, A. Rodrigues, K. De Oliveira Vigier, E. Fourré, J. Barrault, J. M. Tatibouët and F. Jérôme, *Green Chem.*, 2012, **14**, 2212–2215.
- 118 J. Delaux, C. Ortiz Mellet, C. Canaff, E. Fourré, C. Gaillard, A. Barakat, J. M. García Fernández, J. M. Tatibouët and F. Jérôme, *Chem. - A Eur. J.*, 2016, **22**, 16522–16530.
- 119 F. Huang, Z. Long, S. Liu and Z. Qin, *Plasma Sci. Technol.*, 2017, **19**, 0–7.
- 120 O. V. Surov, M. I. Voronova, N. V. Rubleva, L. A. Kuzmicheva, D. Nikitin, A. Choukourov, V. A. Titov and A. G. Zakharov, *Cellulose*, 2018, **25**, 5035–5048.
- 121 I. Prasertsung, P. Chutinate, A. Watthanaphanit, N. Saito and S. Damrongsakkul, *Carbohydr. Polym.*, 2017, **172**, 230–236.
- 122 Y. Wang, L. Zhang, Y. C. Ji, H. Li, Q. H. Wang and B. Yuan, *J. Macromol. Sci. Part B Phys.*, 2017, **56**, 203–212.
- 123 Y. Wang, B. Yuan, Y. Ji and H. Li, *Carbohydr. Polym.*, 2013, **97**, 518–522.
- 124 A. Wright, A. Marsh, F. Ricciotti, A. Shaw, F. Iza, R. Holdich and H. Bandulasena, *Biomass and Bioenergy*, 2018, **118**, 46–54.
- 125 Y. Cao, H. Hua, P. Yang, M. Chen, W. Chen, S. Wang and X. Zhou, *Carbohydr. Polym.*, 2020, **233**, 115632.
- 126 F. Gu and H. Liu, *Chinese J. Catal.*, 2020, **41**, 1073–1080.
- 127 M. N. Collins, M. Nechifor, F. Tanasă, M. Zănoagă, A. McLoughlin, M. A. Strózyk, M. Culebras and C. A. Teacă, *Int. J. Biol. Macromol.*, 2019, **131**, 828–849.
- 128 F. G. Calvo-Flores and J. A. Dobado, *ChemSusChem*, 2010, **3**, 1227–1235.
- 129 H. Wang, Y. Pu, A. Ragauskas and B. Yang, *Bioresour. Technol.*, 2019, **271**, 449–461.
- 130 V. K. Thakur, M. K. Thakur, P. Raghavan and M. R. Kessler, *ACS Sustain. Chem. Eng.*, 2014, **2**, 1072–1092.
- 131 E. Ten and W. Vermerris, *J. Appl. Polym. Sci.*, 2015, **132**, 1–13.
- 132 D. Stewart, *Ind. Crops Prod.*, 2008, **27**, 202–207.
- 133 J. Zakzeski, P. C. A. Bruijninx, A. L. Jongerius and B. M. Weckhuysen, *Chem. Rev.*, 2010, **110**, 3552–3599.
- 134 R. Rinaldi, R. Jastrzebski, M. T. Clough, J. Ralph, M. Kennema, P. C. A. Bruijninx and B. M.

- Weckhuysen, *Angew. Chemie - Int. Ed.*, 2016, **55**, 8164–8215.
- 135 L. Shuai, M. Talebi Amiri and J. S. Luterbacher, *Curr. Opin. Green Sustain. Chem.*, 2016, **2**, 59–63.
- 136 A. L. Holmberg, K. H. Reno, N. A. Nguyen, R. P. Wool and T. H. Epps, *ACS Macro Lett.*, 2016, **5**, 574–578.
- 137 R. M. O’dea, J. A. Willie and T. H. Epps, *ACS Macro Lett.*, 2020, **9**, 476–493.
- 138 A. F. Ang, Z. Ashaari, S. H. Lee, P. Md Tahir and R. Halis, *Int. J. Adhes. Adhes.*, 2019, **95**, 102408.
- 139 V. F. Wendisch, Y. Kim and J. H. Lee, *Curr. Opin. Green Sustain. Chem.*, 2018, **14**, 33–39.
- 140 W. Schutyser, T. Renders, S. Van Den Bosch, S. F. Koelewijn, G. T. Beckham and B. F. Sels, *Chem. Soc. Rev.*, 2018, **47**, 852–908.
- 141 C. Li, X. Zhao, A. Wang, G. W. Huber and T. Zhang, *Chem. Rev.*, 2015, **115**, 11559–11624.
- 142 A. Das and B. König, *Green Chem.*, 2018, **20**, 4844–4852.
- 143 L. Shuai, M. T. Amiri, Y. M. Questell-Santiago, F. Heroguel, Y. Li, H. Kim, R. Meilan, C. Chapple, J. Ralph and J. S. Luterbacher, *Science (80-.)*, 2016, **354**, 329–334.
- 144 M. S. Kent, J. Zeng, N. Rader, I. C. Avina, C. T. Simoes, C. K. Brenden, M. L. Busse, J. Watt, N. H. Giron, T. M. Alam, M. D. Allendorf, B. A. Simmons, N. S. Bell and K. L. Sale, *Green Chem.*, 2018, **20**, 3024–3037.
- 145 R. Ma, Y. Xu and X. Zhang, *ChemSusChem*, 2015, **8**, 24–51.
- 146 C. Cheng, J. Wang, D. Shen, J. Xue, S. Guan, S. Gu and K. H. Luo, *Polymers (Basel)*, 2017, **9**, 38–50.
- 147 J. Dai, A. F. Patti and K. Saito, *Tetrahedron Lett.*, 2016, **57**, 4945–4951.
- 148 C. Liu, S. Wu, H. Zhang and R. Xiao, *Fuel Process. Technol.*, 2019, **191**, 181–201.
- 149 V. E. Tarabanko and N. Tarabanko, *Int. J. Mol. Sci.*, , DOI:10.3390/ijms18112421.
- 150 T. Vangeel, W. Schutyser, T. Renders and B. F. Sels, *Top. Curr. Chem.*, 2018, **376**, 1–16.
- 151 X. Yu, Z. Wei, Z. Lu, H. Pei and H. Wang, *Bioresour. Technol.*, 2019, **291**, 121885.
- 152 C. Crestini, M. Crucianelli, M. Orlandi and R. Saladino, *Catal. Today*, 2010, **156**, 8–22.
- 153 I. Panorel, L. Kaijanen, I. Kornev, S. Preis, M. Louhi-Kultanen and H. Sirén, *Environ. Technol. (United Kingdom)*, 2014, **35**, 171–176.
- 154 A. Sokolov, L. Lagerquist, P. Eklund and M. Louhi-Kultanen, *Chem. Eng. Process. - Process Intensif.*, 2018, **126**, 141–149.
- 155 K. TANGE, S. NOMURA, S. MUKASA and H. TOYOTA, *J. Japan Inst. Energy*, 2018, **97**, 171–175.
- 156 J. Amorim, C. Oliveira, J. A. Souza-Corrêa and M. A. Ridenti, *Plasma Process. Polym.*, 2013, **10**, 670–678.
- 157 Y. Cao, M. Tang, P. Yang, M. Chen, S. Wang, H. Hua, W. Chen and X. Zhou, *J. Agric. Food Chem.*, 2020, **68**, 451–460.
- 158 Y. V. Titova, V. G. Stokozenko and A. I. Maksimov, *Surf. Eng. Appl. Electrochem.*, 2010, **46**, 127–130.
- 159 X. Zhou, F. Zheng, X. Liu, L. Tang, G. Xue, G. Du, Q. Yong, M. Chen and L. Zhu, *BioResources*, 2012, **7**, 4776–4785.
- 160 L. Klarhöfer, W. Viöl and W. Maus-Friedrichs, *Holzforschung*, 2010, **64**, 331–336.
- 161 A. Zaitsev, S. Moisan and F. Poncin-Epaillard, *Polym. Degrad. Stab.*, 2018, **156**, 202–210.
- 162 G. Toriz, J. Ramos and R. A. Young, *J. Appl. Polym. Sci.*, 2004, **91**, 1920–1926.
- 163 M. T. Nistor, O. Chirila, G. Cazacu, M. I. Totolin and C. Vasile, *Cellul. Chem. Technol.*, 2014, **48**, 855–862.

- 164 O. Chirila, M. Totolin, G. Cazacu, M. Dobromir and C. Vasile, *Ind. Eng. Chem. Res.*, 2013, **52**, 13264–13271.
- 165 Y. V. Titova, V. G. Stokozenko, E. L. Aleksakhina and A. I. Maksimov, *Surf. Eng. Appl. Electrochem.*, 2012, **48**, 355–358.
- 166 J. Y. Kim, H. W. Lee, S. M. Lee, J. Jae and Y. K. Park, *Bioresour. Technol.*, 2019, **279**, 373–384.
- 167 H. J. Huang and X. Z. Yuan, *Prog. Energy Combust. Sci.*, 2015, **49**, 59–80.
- 168 A. Dimitriadis and S. Bezergianni, *Renew. Sustain. Energy Rev.*, 2017, **68**, 113–125.
- 169 K. M. Isa, T. A. T. Abdullah and U. F. M. Ali, *Renew. Sustain. Energy Rev.*, 2018, **81**, 1259–1268.
- 170 R. Zhou, R. Zhou, S. Wang, Z. Lan, X. Zhang, Y. Yin, S. Tu, S. Yang and L. Ye, *Bioresour. Technol.*, 2016, **218**, 1275–1278.
- 171 D. Xi, R. Zhou, R. Zhou, X. Zhang, L. Ye, J. Li, C. Jiang, Q. Chen, G. Sun, Q. Liu and S. Yang, *Bioresour. Technol.*, 2017, **241**, 545–551.
- 172 D. Xi, C. Jiang, R. Zhou, Z. Fang, X. Zhang, Y. Liu, B. Luan, Z. Feng, G. Chen, Z. Chen, Q. Liu and S. ze Yang, *Bioresour. Technol.*, 2018, **268**, 531–538.
- 173 X. Zhang, C. Bo, D. Xi, Z. Fang, Z. Feng and S. ze Yang, *Renew. Energy*, 2021, **165**, 174–181.
- 174 D. Tang, X. Zhang and S. Z. Yang, *Plasma Sci. Technol.*, , DOI:10.1088/2058-6272/aa9563.
- 175 Y. S.-Z. J. C.-C. L. S.-Y. F. Z. F. Z. Z. X.-H. M. D.-H. X. D.-K. L. B.-Y. Wang Xing-Quan, *Chinese Phys. B*, 2019, **28**, 048803.
- 176 R. Zhou, R. Zhou, X. Zhang, Z. Fang, X. Wang, R. Speight, H. Wang, W. Doherty, P. J. Cullen, K. Ostrikov and K. Bazaka, *ChemSusChem*, 2019, **12**, 4976–4985.
- 177 D. Mei, S. Liu, S. Wang, R. Zhou, R. Zhou, Z. Fang, X. Zhang, P. J. Cullen and K. (Ken) Ostrikov, *Renew. Energy*, 2020, **157**, 1061–1071.
- 178 D. Nhuchhen, P. Basu and B. Acharya, *Int. J. Renew. Energy Biofuels*, 2014, **2014**, 1–56.
- 179 J. S. Tumuluru, S. Sokhansanj, J. R. Hess, C. T. Wright and R. D. Boardman, *Ind. Biotechnol.*, 2011, **7**, 384–401.
- 180 X. Shuangning, L. Zhihe, L. Baoming, Y. Weiming and B. Xueyuan, *Fuel*, 2006, **85**, 664–670.
- 181 M. S. Mettler, S. H. Mushrif, A. D. Paulsen, A. D. Javadekar, D. G. Vlachos and P. J. Dauenhauer, *Energy Environ. Sci.*, 2012, **5**, 5414–5424.
- 182 M. S. Mettler, D. G. Vlachos and P. J. Dauenhauer, *Energy Environ. Sci.*, 2012, **5**, 7797–7809.
- 183 M. S. Mettler, A. D. Paulsen, D. G. Vlachos and P. J. Dauenhauer, *Energy Environ. Sci.*, 2012, **5**, 7864–7868.
- 184 A. Demirbaş, *Energy Convers. Manag.*, 2001, **42**, 1357–1378.
- 185 H. Chen, G. J. Andries. Z. Luo, *Pergamon*, 2003, **44**, 1875–1884.
- 186 S. Papari and K. Hawboldt, *Renew. Sustain. Energy Rev.*, 2015, **52**, 1580–1595.
- 187 H. Vu Ly, B. Lee, J. Wook Sim, Q. Khanh Tran, S. S. Kim, J. Kim, B. Brigljević, H. T. Hwang and H. Lim, *Chem. Eng. J.*, , DOI:10.1016/j.cej.2021.130956.
- 188 Z. Zhao, H. Huang, C. Wu, H. Li and Y. Chen, *Eng. Life Sci.*, 2001, **1**, 197.
- 189 T. Y. A. Fahmy, Y. Fahmy, F. Mobarak, M. El-Sakhawy and R. E. Abou-Zeid, *Environ. Dev. Sustain.*, 2020, **22**, 17–32.
- 190 L. Tang and H. Huang, *Energy and Fuels*, 2005, **19**, 1174–1178.
- 191 J. L. Shie, F. J. Tsou, K. L. Lin and C. Y. Chang, *Bioresour. Technol.*, 2010, **101**, 761–768.
- 192 R. Adinberg, M. Epstein and J. Karni, *J. Sol. Energy Eng. Trans. ASME*, 2004, **126**, 850–857.
- 193 M. C. Ndukwu, I. T. Horsfall, E. A. Ubouh, F. N. Orji, I. E. Ekop and N. R. Ezejiolor, *J. King Saud Univ. - Eng. Sci.*, 2021, **33**, 413–423.
- 194 S. A. Nair, A. J. M. Pemen, K. Yan, E. J. M. Van Heesch, K. J. Ptasinski and A. A. H. Drinkenburg,

- Plasma Chem. Plasma Process.*, 2003, **23**, 665–680.
- 195 W. K. Tu, J. L. Shie, C. Y. Chang, C. F. Chang, C. F. Lin, S. Y. Yang, J. T. Kuo, D. G. Shaw and D. J. Leev, *Energy and Fuels*, 2008, **22**, 24–30.
- 196 H. Huang and L. Tang, *Energy Convers. Manag.*, 2007, **48**, 1331–1337.
- 197 K. C. Lin, Y. C. Lin and Y. H. Hsiao, *Energy*, 2014, **64**, 567–574.
- 198 L. Tang, H. Huang, H. Hao and K. Zhao, *J. Electrostat.*, 2013, **71**, 839–847.
- 199 A. Wu, X. Li, L. Chen, F. Zhu, H. Zhang, C. Du and J. Yan, *Int. J. Hydrogen Energy*, 2015, **40**, 9039–9048.
- 200 J. L. Shie, C. Y. Chang, W. K. Tu, Y. C. Yang, J. K. Liao, C. C. Tzeng, H. Y. Li, Y. J. Yu, C. H. Kuo and L. C. Chang, *Energy and Fuels*, 2008, **22**, 75–82.
- 201 W. K. Tu, J. L. Shie, C. Y. Chang, C. F. Chang, C. F. Lin, S. Y. Yang, J. T. Kuo, D. G. Shaw, Y. Der You and D. J. Lee, *Bioresour. Technol.*, 2009, **100**, 2052–2061.
- 202 L. Tang and H. Huang, *Fuel*, 2005, **84**, 2055–2063.
- 203 C. J. Lupa, S. R. Wylie, A. Shaw, A. Al-Shamma’A, A. J. Sweetman and B. M. J. Herbert, *Fuel Process. Technol.*, 2012, **97**, 79–84.
- 204 Y. C. Lin, T. Y. Wu, W. Y. Liu and Y. H. Hsiao, *Fuel*, 2014, **119**, 21–26.
- 205 Y. C. Lin, T. Y. Wu, S. R. Jhang, P. M. Yang and Y. H. Hsiao, *Bioresour. Technol.*, 2014, **161**, 304–309.
- 206 N. Bashir, K. Hussain, Z. Hussain, M. Y. Naz, K. A. Ibrahim and N. M. Abdel-Salam, *Chem. Eng. Process. - Process Intensif.*, 2018, **130**, 140–147.
- 207 K. Konno, H. Onodera, K. Murata, K. Onoe and T. Yamaguchi, *Green Sustain. Chem.*, 2011, **01**, 85–91.
- 208 H. Taghvaei and M. R. Rahimpour, *RSC Adv.*, 2016, **6**, 98369–98380.
- 209 W. Zhao, J. Huang, K. Ni, X. Zhang, Z. Lai, Y. Cai and X. Li, *J. Energy Inst.*, 2018, **91**, 595–604.
- 210 H. Taghvaei and M. R. Rahimpour, *Process Saf. Environ. Prot.*, 2019, **121**, 221–228.
- 211 H. Taghvaei and M. R. Rahimpour, *J. Anal. Appl. Pyrolysis*, 2018, **135**, 422–430.
- 212 M. R. Rahimpour, A. Jahanmiri, P. Rostami, H. Taghvaei and B. C. Gates, *Energy and Fuels*, 2013, **27**, 7424–7431.
- 213 F. X. Collard and J. Blin, *Renew. Sustain. Energy Rev.*, 2014, **38**, 594–608.
- 214 D. Lv, M. Xu, X. Liu, Z. Zhan, Z. Li and H. Yao, *Fuel Process. Technol.*, 2010, **91**, 903–909.
- 215 A. Gani and I. Naruse, *Renew. Energy*, 2007, **32**, 649–661.
- 216 J. Lédé, *J. Anal. Appl. Pyrolysis*, 2012, **94**, 17–32.
- 217 Q. Liu, S. Wang, Y. Zheng, Z. Luo and K. Cen, *J. Anal. Appl. Pyrolysis*, 2008, **82**, 170–177.
- 218 D. K. Shen, S. Gu, K. H. Luo, S. R. Wang and M. X. Fang, *Bioresour. Technol.*, 2010, **101**, 6136–6146.
- 219 X. Zhou, W. Li, R. Mabon and L. J. Broadbelt, *Energy Technol.*, 2017, **5**, 52–79.
- 220 D. L. Tsyganov, N. Bundaleska and E. Tatarova, *Plasma Process. Polym.*, 2017, **14**, 1–8.
- 221 D. K. Shen and S. Gu, *Bioresour. Technol.*, 2009, **100**, 6496–6504.
- 222 J. Huang, C. Liu, S. Wei, X. Huang and H. Li, *J. Mol. Struct. THEOCHEM*, 2010, **958**, 64–70.
- 223 X. Huang, D. G. Cheng, F. Chen and X. Zhan, *Bioresour. Technol.*, 2013, **143**, 447–454.
- 224 K. Norinaga, T. Shoji, S. Kudo and J. I. Hayashi, *Fuel*, 2013, **103**, 141–150.
- 225 Y. Wu, D. Xie and Y. Xue, *J. Comput. Chem.*, 2003, **24**, 931–938.
- 226 Y. Chen, W. Wang and L. Zhu, *J. Phys. Chem. A*, 2000, **104**, 11126–11131.
- 227 M. Scapinello, E. Delikonstantis and G. D. Stefanidis, *Chem. Eng. J.*, 2019, **360**, 64–74.

- 228 J. S. K. Yu and C. H. Yu, *Chem. Phys. Lett.*, 1997, **271**, 259–265.
- 229 M. W. Jarvis, J. W. Daily, H. H. Carstensen, A. M. Dean, S. Sharma, D. C. Dayton, D. J. Robichaud and M. R. Nimlos, *J. Phys. Chem. A*, 2011, **115**, 428–438.
- 230 P. F. Britt, A. C. Buchanan, M. J. Cooney and D. R. Martineau, *J. Org. Chem.*, 2000, **65**, 1376–1389.
- 231 W. Mueller-Markgraf and J. Troe, *J. Phys. Chem.*, 1988, **92**, 4914–4922.
- 232 C. Horn, K. Roy, P. Frank and T. Just, in *27th Symposium (International) on Combustion*, 1998, vol. 27, pp. 321–328.
- 233 X. Huang, D. G. Cheng, F. Chen and X. Zhan, *Int. J. Hydrogen Energy*, 2012, **37**, 18040–18049.
- 234 X. Huang, D. G. Cheng, F. Chen and X. Zhan, *Ind. Eng. Chem. Res.*, 2013, **52**, 14107–14115.
- 235 D. K. Shen, S. Gu and A. V. Bridgwater, *J. Anal. Appl. Pyrolysis*, 2010, **87**, 199–206.
- 236 X. Huang, D. guo Cheng, F. Chen and X. Zhan, *Renew. Energy*, 2016, **96**, 490–497.
- 237 J. A. Ruiz, M. C. Juárez, M. P. Morales, P. Muñoz and M. A. Mendivil, *Renew. Sustain. Energy Rev.*, 2013, **18**, 174–183.
- 238 S. Heidenreich and P. U. Foscolo, *Prog. Energy Combust. Sci.*, 2015, **46**, 72–95.
- 239 F. Fabry, C. Rehmet, V. Rohani and L. Fulcheri, *Waste and Biomass Valorization*, 2013, **4**, 421–439.
- 240 J. Heberlein and A. B. Murphy, *J. Phys. D. Appl. Phys.*, , DOI:10.1088/0022-3727/41/5/053001.
- 241 I. Janajreh, S. S. Raza and A. S. Valmundsson, *Energy Convers. Manag.*, 2013, **65**, 801–809.
- 242 A. Molino, S. Chianese and D. Musmarra, *J. Energy Chem.*, 2016, **25**, 10–25.
- 243 M. Tendler, P. Rutberg and G. Van Oost, *Plasma Phys. Control. Fusion*, , DOI:10.1088/0741-3335/47/5A/016.
- 244 P. G. Rutberg, V. A. Kuznetsov, E. O. Serba, S. D. Popov, A. V. Surov, G. V. Nakonechny and A. V. Nikonov, *Appl. Energy*, 2013, **108**, 505–514.
- 245 A. V. Surov, S. D. Popov, V. E. Popov, D. I. Subbotin, E. O. Serba, V. A. Spodobin, G. V. Nakonechny and A. V. Pavlov, *Fuel*, 2017, **203**, 1007–1014.
- 246 A. Sanlisoy and M. O. Carpinlioglu, *Int. J. Hydrogen Energy*, 2017, **42**, 1361–1365.
- 247 G. S. J. Sturm, A. N. Munoz, P. V. Aravind and G. D. Stefanidis, *IEEE Trans. Plasma Sci.*, 2016, **44**, 670–678.
- 248 M. Hrabovsky, V. Kopecký, V. Sember, T. Kavka, O. Chumak and M. Konrad, *IEEE Trans. Plasma Sci.*, 2006, **34**, 1566–1575.
- 249 G. Van Oost, M. Hrabovsky, V. Kopecky, M. Konrad, M. Hlina, T. Kavka, A. Chumak, E. Beeckman and J. Verstraeten, *Vacuum*, 2006, **80**, 1132–1137.
- 250 M. Hrabovsky, M. Konrad, V. Kopecky, M. Hlina, T. Kavka, G. Van Oost, E. Beeckman and B. Defoort, *Czechoslov. J. Phys.*, 2006, **56**, 1199–1206.
- 251 M. Hrabovsky, V. Kopecky, M. Konrad, M. Hlina, T. Kavka, E. G. van Oost, J. Beeckman, J. Verstraeten, J. Ledecy and E. Balabanova, in *17th Symposium on Physics of Switching Arc*, 2007, pp. 7–16.
- 252 M. Hlina, M. Hrabovsky, T. Kavka and M. Konrad, *Waste Manag.*, 2014, **34**, 63–66.
- 253 M. Hlína, M. Hrabovský, V. Kopecký, M. Konrád, T. Kavka and S. Skoblja, *Czechoslov. J. Phys.*, 2006, **56**, 1179–1184.
- 254 G. Van Oost, M. Hrabovsky, V. Kopecky, M. Konrad, M. Hlina and T. Kavka, *Vacuum*, 2008, **83**, 209–212.
- 255 A. S. An'shakov, V. A. Faleev, A. A. Danilenko, E. K. Urbakh and A. E. Urbakh, *Thermophys. Aeromechanics*, 2007, **14**, 607–616.

- 256 V. Grigaitien, V. Snapkauskien, P. Valatkevičius, A. Tamošinas and V. Valinčius, *Catal. Today*, 2011, **167**, 135–140.
- 257 A. Tamošius, P. Valatkevičius, V. Valinčius and R. Levinskas, *Comptes Rendus Chim.*, 2016, **19**, 433–440.
- 258 A. Tamošius, P. Valatkevičius, V. Grigaitiene, V. Valinčius and N. Striugas, *J. Clean. Prod.*, 2016, **130**, 187–194.
- 259 D. Guénadou, H. Lorcet, S. Poulain and J. Peybernes, in *Ispc_19*, 2009.
- 260 K. Tao, N. Ohta, G. Liu, Y. Yoneyama, T. Wang and N. Tsubaki, *Fuel*, 2013, **104**, 53–57.
- 261 X. Zhu, T. Hoang, L. L. Lobban and R. G. Mallinson, *Chem. Commun.*, 2009, 2908–2910.
- 262 G. Diaz, N. Sharma, E. Leal-Quiros and A. Munoz-Hernandez, *Int. J. Hydrogen Energy*, 2015, **40**, 2091–2098.
- 263 Y. Byun, M. Cho, J. W. Chung, W. Namkung, H. D. Lee, S. D. Jang, Y. S. Kim, J. H. Lee, C. R. Lee and S. M. Hwang, *J. Hazard. Mater.*, 2011, **190**, 317–323.
- 264 C. Du, J. Wu, D. Ma, Y. Liu, P. Qiu, R. Qiu, S. Liao and D. Gao, *Int. J. Hydrogen Energy*, 2015, **40**, 12634–12649.
- 265 A. N. Brattsev, V. A. Kuznetsov, V. E. Popov and A. A. Ufimtsev, *High Temp.*, 2011, **49**, 244–248.
- 266 A. N. Bratsev, V. E. Popov, A. F. Rutberg and S. V. Shtengel, *High Temp.*, 2006, **44**, 823–828.
- 267 V. A. Kuznetsov, A. N. Bratsev, V. B. Kovshechnikov, I. I. Kumkova, V. E. Popov, S. V. Shtengel and A. A. Ufimtsev, *PPPS-2007 - Pulsed Power Plasma Sci. 2007*, 2007, **2**, 1223–1226.
- 268 E. Popov, N. Bratsev, A. Kuznetsov, V. Shtengel, A. Ufimtsev, V. E. Popov, A. N. Bratsev, V. A. Kuznetsov, S. V. Shtengel and A. A. Ufimtsev, *J. Phys. Conf. Ser.*, , DOI:10.1088/1742-6596/275/1/012015.
- 269 P. G. Rutberg, A. N. Bratsev, V. A. Kuznetsov, V. E. Popov, A. A. Ufimtsev and S. V. Shtengel', *Biomass and Bioenergy*, 2011, **35**, 495–504.
- 270 J. Luche, Q. Falcoz, T. Bastien, P. Leninger, K. Arabi, O. Aubry, A. Khacef, M. Cormier and J. Lédé, *IOP Conf. Ser. Mater. Sci. Eng.*, , DOI:10.1088/1757-899X/29/1/012011.
- 271 K. Arabi, O. Aubry, A. Khacef and J. M. Cormier, *J. Phys. Conf. Ser.*, 2012, **406**, 26–28.
- 272 Y. Pang, L. Bahr, P. Fendt, L. Zigan, S. Will, T. Hammer, M. Baldauf, R. Fleck, D. Müller and J. Karl, *Energies*, , DOI:10.3390/en11051302.
- 273 J. L. Shie, L. X. Chen, K. L. Lin and C. Y. Chang, *Energy*, 2014, **66**, 82–89.
- 274 J. L. Shie, F. J. Tsou and K. L. Lin, *Bioresour. Technol.*, 2010, **101**, 5571–5577.
- 275 S. J. Yoon, Y. M. Yun, M. W. Seo, Y. K. Kim, H. W. Ra and J. G. Lee, *Int. J. Hydrogen Energy*, 2013, **38**, 14559–14567.
- 276 S. Liu, D. Mei, L. Wang and X. Tu, *Chem. Eng. J.*, 2017, **307**, 793–802.
- 277 D. Mei, Y. Wang, S. Liu, M. Allati, H. Yang and X. Tu, *Energy Convers. Manag.*, 2019, **195**, 409–419.
- 278 S. Liu, D. Mei, Y. Wang, Y. Ma and X. Tu, *Waste Dispos. Sustain. Energy*, 2019, **1**, 133–141.
- 279 F. Saleem, J. Harris, K. Zhang and A. Harvey, *Chem. Eng. J.*, 2020, **382**, 122761.
- 280 L. Liu, Z. Zhang, S. Das and S. Kawi, *Appl. Catal. B Environ.*, 2019, **250**, 250–272.
- 281 H. Zhang, F. Zhu, X. Li, R. Xu, L. Li, J. Yan and X. Tu, *J. Hazard. Mater.*, 2019, **369**, 244–253.
- 282 Y. N. Chun, S. C. Kim and K. Yoshikawa, *Environ. Prog. Sustain. Energy*, 2014, **33**, 676–680.
- 283 M. S. Lim and Y. N. Chun, *Environ. Eng. Res.*, 2012, **17**, 89–94.
- 284 Y. C. Yang and Y. N. Chun, *Korean J. Chem. Eng.*, 2011, **28**, 539–543.
- 285 Y. N. Chun, S. C. Kim and K. Yoshikawa, *Korean J. Chem. Eng.*, 2011, **28**, 1713–1720.

- 286 S. C. Kim, M. S. Lim and Y. N. Chun, *Int. J. Hydrogen Energy*, 2013, **38**, 14458–14466.
- 287 L. Yu, X. Li, X. Tu, Y. Wang, S. Lu and J. Yan, *J. Phys. Chem. A*, 2010, **114**, 360–368.
- 288 T. Nunnally, A. Tsangaris, A. Rabinovich, G. Nirenberg, I. Chernets and A. Fridman, *Int. J. Hydrogen Energy*, 2014, **39**, 11976–11989.
- 289 Y. N. Chun, S. C. Kim and K. Yoshikawa, *Chem. Eng. Process. Process Intensif.*, 2012, **57–58**, 65–74.
- 290 F. Zhu, X. Li, H. Zhang, A. Wu, J. Yan, M. Ni, H. Zhang and A. Buekens, *Fuel*, 2016, **176**, 78–85.
- 291 R. Xu, F. Zhu, H. Zhang, P. M. Ruya, X. Kong, L. Li and X. Li, *Energy and Fuels*, 2020, **34**, 2045–2054.
- 292 F. Zhu, H. Zhang, H. Yang, J. Yan, X. Li and X. Tu, *Fuel*, 2020, **259**, 1–11.
- 293 N. Tippayawong and P. Inthasan, *Int. J. Chem. React. Eng.*, , DOI:10.2202/1542-6580.2181.
- 294 P. Jamróz, W. Kordylewski and M. Wnukowski, *Fuel Process. Technol.*, 2018, **169**, 1–14.
- 295 M. Wnukowski and P. Jamróz, *Fuel Process. Technol.*, 2018, **173**, 229–242.
- 296 R. M. Elliott, M. F. M. Nogueira, A. S. Silva Sobrinho, B. A. P. Couto, H. S. Maclel and P. T. Lacava, *Energy and Fuels*, 2013, **27**, 1174–1181.
- 297 J. Sun, Q. Wang, W. Wang, Z. Song, X. Zhao, Y. Mao and C. Ma, *Fuel*, 2017, **207**, 121–125.
- 298 Y. Liu, J. Song, X. Diao, L. Liu and Y. Sun, *Sci. Total Environ.*, 2020, **721**, 137671.
- 299 L. Liu, Y. Liu, J. Song, S. Ahmad, J. Liang and Y. Sun, *J. Hazard. Mater.*, 2019, **377**, 24–33.
- 300 L. Liu, Q. Wang, S. Ahmad, X. Yang, M. Ji and Y. Sun, *J. Energy Inst.*, 2018, **91**, 927–939.
- 301 L. Liu, Q. Wang, J. Song, X. Yang and Y. Sun, *Int. J. Hydrogen Energy*, 2018, **43**, 10281–10293.
- 302 B. Wang, C. Chi, M. Xu, C. Wang and D. Meng, *Chem. Eng. J.*, 2017, **322**, 679–692.
- 303 S. Y. Liu, D. H. Mei, M. A. Nahil, S. Gadkari, S. Gu, P. T. Williams and X. Tu, *Fuel Process. Technol.*, 2017, **166**, 269–275.
- 304 E. Blanquet, M. A. Nahil and P. T. Williams, *Catal. Today*, 2019, **337**, 216–224.
- 305 B. Xu, J. Xie, H. Zhan, X. Yin, C. Wu and H. Liu, *Energy and Fuels*, 2018, **32**, 10709–10719.
- 306 Y. F. Guo, D. Q. Ye, K. F. Chen, J. C. He and W. L. Chen, *J. Mol. Catal. A Chem.*, 2006, **245**, 93–100.
- 307 F. Saleem, K. Zhang and A. Harvey, *Energy and Fuels*, 2019, **33**, 389–396.
- 308 F. Saleem, A. Harvey and K. Zhang, *Fuel*, 2019, **248**, 258–261.
- 309 F. Saleem, K. Zhang and A. Harvey, *Chem. Eng. J.*, 2019, **356**, 1062–1069.
- 310 F. Saleem, K. Zhang and A. Harvey, *Energy and Fuels*, 2018, **32**, 5164–5170.
- 311 F. Saleem, K. Zhang and A. P. Harvey, *Chem. Eng. J.*, 2019, **360**, 714–720.
- 312 F. Saleem, K. Zhang and A. Harvey, *Fuel*, 2019, **235**, 1412–1419.
- 313 A. J. M. Pemen, S. A. Nair, K. Yan, E. J. M. Van Heesch, K. J. Ptasinski and A. A. H. Drinkenburg, *Plasmas Polym.*, 2003, **8**, 209–224.
- 314 W. Mista and R. Kacprzyk, *Catal. Today*, 2008, **137**, 345–349.
- 315 Y. Gomez-Rueda, I. N. Zaini, W. Yang and L. Helsen, *Energy Convers. Manag.*, 2020, **208**, 112540.
- 316 E. Delikonstantis, M. Scapinello, S. D. Sklari and G. D. Stefanidis, *Plasma Process. Polym.*, , DOI:10.1002/ppap.201800065.
- 317 M. Materazzi, P. Lettieri, L. Mazzei, R. Taylor and C. Chapman, *Fuel Process. Technol.*, 2015, **137**, 259–268.
- 318 S. Takali, F. Fabry, V. Rohani, F. Cauneau and L. Fulcheri, 2015, 10.
- 319 V. Rohani, S. Takali, G. Gérard, F. Fabry, F. Cauneau and L. Fulcheri, *Waste and Biomass*

- Valorization*, 2017, **8**, 2791–2805.
- 320 and O. A. L. V. E. Messerle, A. B. Ustimenko, in *Proceedings of the 2014 International Conference on Power Systems, Energy, Environment Plasma-assisted*, 2014.
- 321 V. E. Messerle, A. B. Ustimenko and E. I. Karpenko, in *International Plasma Chemistry Society*, 2011, pp. 2–5.
- 322 M. Lim and A. R. Lea-Langton, *Plasma Chem. Plasma Process.*, 2020, **40**, 1465–1483.
- 323 X. Tu, B. G. Chéron, J. H. Yan and K. F. Cen, *Plasma Sources Sci. Technol.*, 2007, **16**, 803–812.
- 324 Q. Huang, X. Cai, M. M. Alhadj-Mallah, C. Du, Y. Chi and J. Yan, *IEEE Trans. Plasma Sci.*, 2014, **42**, 3549–3554.
- 325 O. Ginés, J. M. Chimenos, A. Vizcarro, J. Formosa and J. R. Rosell, *J. Hazard. Mater.*, 2009, **169**, 643–650.
- 326 K. Moustakas, D. Fatta, S. Malamis, K. Haralambous and M. Loizidou, *J. Hazard. Mater.*, 2005, **123**, 120–126.
- 327 T. W. Cheng, C. C. Tu, M. S. Ko and T. H. Ueng, *Ceram. Int.*, 2011, **37**, 2437–2444.
- 328 S. F. Yang, W. T. Chiu, T. M. Wang, C. T. Chen and C. C. Tzeng, *Waste Manag.*, 2014, **34**, 1079–1084.
- 329 Q. Wang, J. Yan, X. Tu, Y. Chi, X. Li, S. Lu and K. Cen, *Fuel*, 2009, **88**, 955–958.
- 330 V. S. Sikarwar, M. Hrabovský, G. Van Oost, M. Pohořelý and M. Jeremiáš, *Prog. Energy Combust. Sci.*, 2020, **81**, 100873.
- 331 E4Tech, *Review of Technologies for Gasification of Biomass and Wastes Final report*, 2009.
- 332 H. S. Uhm, Y. H. Na, Y. C. Hong, D. H. Shin and C. H. Cho, *Int. J. Hydrogen Energy*, 2014, **39**, 4351–4355.
- 333 J. F. de la Fuente, A. A. Kiss, M. T. Radoiu and G. D. Stefanidis, *J. Chem. Technol. Biotechnol.*, 2017, **92**, 2495–2505.